



City Research Online

City, University of London Institutional Repository

Citation: Belschner, J. (2018). Scheduling heuristic for reduced complexity of coordinated beamforming in large multi-carrier heterogeneous wireless networks. (Unpublished Doctoral thesis, City, University of London)

This is the accepted version of the paper.

This version of the publication may differ from the final published version.

Permanent repository link: <https://openaccess.city.ac.uk/id/eprint/21606/>

Link to published version:

Copyright: City Research Online aims to make research outputs of City, University of London available to a wider audience. Copyright and Moral Rights remain with the author(s) and/or copyright holders. URLs from City Research Online may be freely distributed and linked to.

Reuse: Copies of full items can be used for personal research or study, educational, or not-for-profit purposes without prior permission or charge. Provided that the authors, title and full bibliographic details are credited, a hyperlink and/or URL is given for the original metadata page and the content is not changed in any way.

City Research Online:

<http://openaccess.city.ac.uk/>

publications@city.ac.uk

Scheduling Heuristic for Reduced Complexity of
Coordinated Beamforming in Large Multi-Carrier
Heterogeneous Wireless Networks

Jakob Belschner

Submitted for the Degree of Doctor of Philosophy

City, University of London

Department of Electrical & Electronic Engineering

October 2018

Abstract

The research and development of wireless communication systems is often based on relatively simple models of the network topology, the radio channel and the radio propagation. This is considered to be mostly appropriate, as only under these conditions the complex technical problems in this field can be fully solved to their theoretical boundaries. However, it can also be the case that algorithms or concepts created under simplified assumptions perform in a significantly different way, when they are applied in more realistic scenarios.

This Thesis presents research work which can be seen as a step towards extending the existing research on Coordinated Beamforming to a complex network scenario, i.e. to a large-scale heterogeneous multi-carrier network. For this purpose, a complex simulation framework has been developed. This is used to analyse the significant implications the conditions in a complex network can have on the achievable performance gains. In more detail, the out of cluster interference and the number of mobile stations are identified as factors which heavily influence the performance. This knowledge is then used to design a novel scheduling heuristic, designed to be able to adapt to the particular network scenarios and to estimate the extent of the achievable performance gains. Our simulation results show that the new heuristic achieves significant performance gains for a low number of mobile stations (by applying zero forcing precoding) as well as for a high number of mobile stations (by a coordinated resource assignment that intelligently pairs mobile stations when applying maximum ratio transmission). The Thesis also demonstrates that the effect of the out of cluster interference can cause the reduction of the achievable gains. Due to the knowledge of performance limiting factors, the scheduling heuristic is in addition able to realize a trade-off between complexity and performance by excluding transmission parameters from the scheduling process which are not expected to be beneficial.

Contents

List of Figures	6
List of Tables	11
1 Introduction	17
1.1 Motivation and overview	17
1.2 Contribution of the Thesis	18
1.3 Thesis structure	19
2 Coordinated Multipoint Transmission and its Effect on the Capacity of Large Multi-Carrier Heterogeneous Wireless Networks	21
2.1 Network architecture	22
2.2 Mobile network capacity	25
2.3 Heterogeneous networks	27
2.4 Interference mitigation and coordinated multipoint transmission and reception	31
2.5 Multi-antenna techniques	35
2.5.1 Point to point MIMO communication	35
2.5.2 The MIMO interference channel	39
2.5.3 The MIMO broadcast channel	43
2.6 Scheduling and resource allocation through Orthogonal Frequency Division Multiple Access	44
2.7 Research problem	47
3 Methodology	51
3.1 Overview and basic principle of system level simulations	51
3.2 Network layout	53
3.3 Channel model	55

3.4	Simulation process	57
3.5	Key performance indicators	62
3.6	Study of the propagation conditions in a simulation of a heterogeneous network	66
3.7	Calibration	76
3.8	Summary	80
4	Design of a Precoding and Scheduling Algorithm for Coordinated Beamforming in Heterogeneous Networks	82
4.1	Relaxed zero forcing precoding algorithm for heterogeneous networks . .	82
4.1.1	Overview and Introduction	83
4.1.2	Precoder for the Pico Base Station and Receive Combining Vector for the Pico Mobile Station	88
4.1.3	Zero Forcing and Maximum Ratio Transmission Precoder for the Macro Base Station	89
4.1.4	Combination of Maximum Ratio Transmission and Zero Forcing Precoding	92
4.1.5	Example and Visualization	95
4.2	Scheduling	100
4.3	Summary	104
5	Performance limiting factors in HetNet Coordinated Beamforming	105
5.1	Out of cluster interference	106
5.2	Influence of the number of MSs per BS	114
5.3	Summary	119
6	Reduced Complexity Scheduling Heuristic for Coordinated Beamforming	121
6.1	The complexity of scheduling in the case of coordination beamforming .	122
6.2	HetNet RZF scheduling heuristic	125
6.3	Configuration of the threshold parameters and expected performance . . .	128
6.4	Summary	129
7	Performance Analysis	130
7.1	Simulation parameters	131

7.2	Influence of the number of mobile stations in a network with two base stations	133
7.3	Performance analysis for large networks	135
7.4	Complexity	140
7.5	Applicability of the results to other precoding and scheduling algorithms and other traffic models	142
7.6	Summary	144
8	Conclusions and Future Work	146
	Bibliography	149
A	Numerical MIMO Examples	159
A.1	Maximum Ratio Transmission via Singular Value Decomposition	159
A.2	Zero Forcing precoding	162
B	Further Simulation Results	166

List of Figures

2.1	Network Architecture of LTE Advanced	22
2.2	Heterogeneous network with 21 macro and 21 pico base stations	28
2.3	Areas with strong interference in an heterogeneous network. "New CE" represents a new Cell Edge (CE) area, caused by the Pico BSs.	30
2.4	MIMO System Model for two parallel data streams	36
2.5	MIMO System Model for one data stream	37
2.6	Singular Value Decomposition of the Wireless Channel	38
2.7	Singular Value Decomposition of the Wireless Channel with Precoding	39
2.8	The MIMO interference channel	40
2.9	The Multiple Input Multiple Output (MIMO) broadcast channel	43
2.10	OFDM Transmitter and Receiver Chain	45
2.11	Example for a Frequency Selective Channel	45
2.12	OFDMA Radio Resources	46
3.1	Deutsche Telekom System Level Simulator: Example for Network Layout	54
3.2	Deutsche Telekom System Level Simulator: Wrap Around Technique	54
3.3	Spatial Channel Model: The radio propagation is modelled via paths and subpaths between the antennas of the transmitter and the receiver	56
3.4	Output of the Spatial Channel Model in time domain	57
3.5	Deutsche Telekom System Level Simulator: Block diagram	58
3.6	Key Performance Indicators of the Deutsche Telekom System Level Sim- ulator: Example for Cumulative Distribution Function of Mobile Station Throughput	64
3.7	Key Performance Indicators of the Deutsche Telekom System Level Sim- ulator: Example for the Cumulative Distribution Function of the normal- ized Mobile Station Throughput	65

3.8	Line-of-Sight Probabilities in Urban Macro (UMa) and Urban Micro (UMi) Propagation Model	67
3.9	Pathloss for Line of Sight (LoS) and non Line of Sight (nLoS)	68
3.10	Deployment option 1: Pico base stations deployed 125 metres away from the macro base stations	69
3.11	Deployment option 2: Pico base stations deployed 250 metres away from the macro base stations	69
3.12	Received power levels for deployment option 1: Pico base stations deployed 125 metres away from the macro base stations	70
3.13	Received power levels for deployment option 2: Pico base stations deployed 250 metres away from the macro base stations	70
3.14	Assignment for the MSs	71
3.15	Line of Sight Conditions	72
3.16	Example for an assignment of MSs for pico base stations deployed at cell centre of the macro base stations	73
3.17	CDF of the distance between MSs and serving BSs for pico base stations deployed at cell centre of the macro base stations	73
3.18	Example for the assignment of MSs for pico base stations deployed at cell centre of the macro base stations with hotspot distribution of MSs	74
3.19	CDF of the distance between MSs and serving BSs for pico base stations deployed at cell centre of the macro base stations with hotspot distribution of MSs	74
3.20	Example for an assignment of MSs for pico base stations deployed at cell edge of the macro base stations	75
3.21	CDF of the distance between MSs and serving BSs for pico base stations deployed at Cell Edge of the macro base stations	75
3.22	Example for an assignment of MSs for pico base stations deployed at Cell Edge of Macro Base Station (MBS) with hotspot distribution of MSs	76
3.23	CDF of the distance between MSs and serving BSs for pico base stations deployed at Cell Edge of MBS with hotspot distribution of MSs	76
3.24	Simulator Calibration: User Geometry	78
3.25	Simulator Calibration: Distribution of Signal to Interference and Noise Ratio at the Mobile Stations	78
3.26	Simulator Calibration: Spectral Efficiency	79

3.27	Simulator Calibration: Distribution of mobile station throughput divided by the system bandwidth ("Normalized MS throughput" in Third Generation Partnership Project (3GPP) terminology) [bps/Hz]	80
4.1	The interaction between scheduling and precoding including examples for the targets of scheduling and precoding algorithms	84
4.2	Setup for HetNet Relaxed Zero Forcing	86
4.3	Flowchart of Relaxed Zero Forcing for Heterogeneous Networks	88
4.4	Relaxed Zero Forcing for Heterogeneous Networks: Starting situation for the calculation of the Zero Forcing precoder	90
4.5	Calculation of the Zero Forcing Precoder: Modification of the signals such that they sum up to zero	91
4.6	HetNet Relaxed Zero Forcing Example: Visualization of the Zero Forcing and Maximum Ratio Transmission precoders	96
4.7	HetNet Relaxed Zero Forcing Example: Visualization of the full set of precoders	97
4.8	HetNet Relaxed Zero Forcing Example: Power Levels (interfering and intended) at the Pico Mobile Station (PMS) and the Macro Mobile Station (MMS)	99
4.9	HetNet Relaxed Zero Forcing Example: Resulting SINR at the PMS and the MMS	99
4.10	Flowchart for Proportional Fair Scheduling that applies HetNet Relaxed Zero Forcing	103
5.1	Maximum achievable spectral efficiency gain factor for different levels of Out of Cluster Interference	108
5.2	Network Layout with three Base Stations	109
5.3	Geometry and Out of Cluster Interference Ratio of the Pico MS	110
5.4	Interfering Power at the cooperating Pico MS	111
5.5	Useful Power at the cooperating Macro MS	112
5.6	Spectral Efficiency at the cooperating Pico MS	112
5.7	Spectral Efficiency at the cooperating Macro MS	113
5.8	Sum Spectral Efficiency of Pico and Macro MS	114
5.9	Example for the influence of the number of MSs in the system: Interference Level at the PMS when begin simultaneously served with an MMS .	116

5.10	Flowchart of the simulation to evaluate the effect of the number of mobile stations in the system	117
5.11	Simulation result for the effect of the number of Mobile Stations (MSs) on the interference at the PMSs	118
5.12	Simulation result for the effect of the number of MMSs on the interference at the PMS	119
6.1	Example for proportional fair metric values in the case of HetNet RZF. Each figure depicts the proportional fair metrics for the pairs (x-axis) and the PRBs (y-axis)	124
6.2	Flowchart of the HetNet RZF Scheduling Heuristic	127
7.1	Throughput of MS associated to the Pico Base Station (PBS) in a network with two Base Stations (BSs) and 3 MSs	134
7.2	Throughput of MS associated to the PBS in a network with two BSs and 6 MSs	135
7.3	Throughput of MS associated to the PBS in a network with two BSs and 12 MSs	135
7.4	Throughput of MSs associated to the PBS in a network large network with 42 MSs (network from Figure 2.2)	136
7.5	Throughput of MS associated to the PBS in a network large network with 315 MSs (network from Figure 2.2)	137
7.6	Heterogeneous Network with higher Out of Cluster Interference	138
7.7	Throughput of MSs associated to the PBS in a network large network with 42 MSs (network from Figure 7.6)	138
7.8	Throughput of MS associated to the PBS in a network large network with 315 MSs (network from Figure 7.6)	139
7.9	Number of transmission parameters calculated for the case of 42 MSs and the network layout depicted in Figure 2.2	141
7.10	Number of transmission parameters calculated for the case of 315 MSs and the network layout depicted in Figure 2.2	141
7.11	Number of transmission parameters calculated for the case of 42 MSs and the network layout depicted in Figure 7.6	142
7.12	Number of transmission parameters calculated for the case of 315 MSs and the network layout depicted in Figure 7.6	142

A.1	Singular Value Decomposition of the Wireless Channel: Example	161
A.2	Precoding with Coordination: Zero Forcing Example	165
B.1	Throughput of MSs associated to the MBS in a network large network with 42 MSs (network from Figure 2.2)	166
B.2	Throughput of MS associated to the MBS in a network large network with 315 MSs (network from Figure 2.2)	167
B.3	Throughput of MSs associated to the MBS in a network large network with 42 MSs (network from Figure 7.6)	167
B.4	Throughput of MS associated to the MBS in a network large network with 315 MSs (network from Figure 7.6)	168

List of Tables

3.1	Base Station parameters used for the study of the propagation conditions .	67
3.2	Requirements for investigations of large-scale network performance . . .	81
7.1	System level simulation parameters	132

Acronyms

3GPP Third Generation Partnership Project

5G NR 5G New Radio

ACK Acknowledgement

AoA Angle of Arrival

AoD Angle of Departure

AWGN additive white Gaussian noise

BS Base Station

CBF Coordinated Beamforming

CC Cell Centre

CDF Cumulative Distribution Function

CE Cell Edge

cMMS Cooperating Macro Mobile Station

CoMP Coordinated Multi Point

cPMS Cooperating Pico Mobile Station

CRE Cell Range Expansion

CSI Channel State Information

CSIT Channel State Information at the Transmitter

DSL Digital Subscriber Line

DSSS Direct Sequence Spread Spectrum

DT SLS Deutsche Telekom System Level Simulator

eICIC enhanced Inter Cell Interference Coordination

EIRP Equivalent Isotropically Radiated Power

FDD Frequency Division Duplex

FFR Fractional Frequency Reuse

FFT Fast Fourier Transformation

FHSS Frequency Hopping Spread Spectrum

GSM Global System for Mobile Communications

HARQ Hybrid Automatic Repeat Request

HRSH HetNet RZF Scheduling Heuristic

HS HotSpot

HSS Home Subscriber Server

IA Interference Alignment

IC Interference Channel

ICIC Inter Cell Interference Coordination

IEEE Institute of Electrical and Electronics Engineers

IFFT Inverse Fast Fourier Transformation

ISD Inter Site Distance

ITU-R International Telecommunication Union Radiocommunication Sector

KPI Key Performance Indicator

LoS Line of Sight

LTE Long Term Evolution

LTE-A Long Term Evolution Advanced

MBS Macro Base Station

MCS Modulation and Coding Scheme

MHz Megahertz

MIESM Mutual Information Effective SINR Mapping

MIMO Multiple Input Multiple Output

MISO Multiple Input Single Output

MME Mobility Management Entity

MMS Macro Mobile Station

MRC Maximum Ratio Combining

MRT Maximum Ratio Transmission

MS Mobile Station

MU-MIMO Multi User Multiple Input Multiple Output

NACK Negative Acknowledgement

ncMMS Not Cooperating Macro Mobile Station

nLoS non Line of Sight

NP non-deterministic polynomial

OFDM Orthogonal Frequency Division Multiplexing

OFDMA Orthogonal Frequency Division Multiple Access

OOCI Out of Cluster Interference

OOCIR Out of Cluster Interference Ratio

P-GW Packet Data Network Gateway

PBS Pico Base Station

PCRF Policy and Charging Rules Function

PMS Pico Mobile Station

PRB Physical Resource Block

QoS Quality of Service

RAN Radio Access Network

RNTP Relative Narrowband Transmit Power

RRM Radio Resource Management

RSRP Reference Signal Received Power

RZF Relaxed Zero Forcing

S-GW Serving Gateway

SDMA Space Division Multiple Access

SE Spectral Efficiency

SFR Soft Frequency Reuse

SINR Signal to Interference plus Noise Ratio

SIR Signal to Interference Ratio

SISO Single Input Single Output

SLNR Signal to Leakage and Noise Ratio

SLS System Level Simulation

SNR Signal to Noise Ratio

SVD Singular Value Decomposition

TAC Tracking Area Code

TCP Transmission Control Protocol

TDD Time Division Duplex

TTI Time Transmission Interval

VPN Virtual Private Network

WiMAX Worldwide Interoperability for Microwave Access

WLAN Wireless Local Area Network

ZF Zero Forcing

Chapter 1

Introduction

This chapter provides an overview and the motivation of this work (Section 1.1), describes the contribution of the Thesis (Section 1.2) and introduces the structure of the following chapters (Section 1.3).

1.1 Motivation and overview

The recent years have seen a continuously growing demand for mobile data services. This is a trend that is expected to continue in the future [1, 2]. To fulfil this continuous demand, improving the so-called network capacity is critical. Network capacity relates to the volume of data a network is able to transport at maximum in a given time instance. If the user demand exceeds the network capacity, a significant degradation in the user experience such as call drops and slow data transfers can be the consequence.

It is therefore important to develop concepts and methods to ensure the network capacity can keep track with the growing demand. As every base station of a mobile network provides a certain capacity, network densification, i.e. deploying more and more base stations has been widely used to increase the network capacity. In addition to this, heterogeneous networks [3] have been proposed as cost-effective means to further increase network densification. They consist of new base stations with lower transmit power (also called small cells) which are integrated into the existing network of traditional high power base stations.

However, the increase in the density of base stations in a heterogeneous network can cause significant problems, as mobile stations (e.g. the user smartphones) receive not only their intended signals, but also signals dedicated to other mobile stations. Interference can

degrade the received throughput of a mobile station or even cause an outage.

Coordination between base stations, also referred to as Coordinated Multipoint Transmission and Reception (CoMP) can be a solution to this problem of interference. Within the context of CoMP, Coordinated Beamforming [4, 5] is seen as a promising coordination scheme to be applied in heterogeneous networks.

The existing results in the literature for the performance of Coordinated Beamforming are diverging in terms of the achievable gains (for more detail see Section 2.7). In addition, recent work underlines the importance of a correct modelling of the network topology to investigate the performance of coordinated systems [6]. These two aspects together form the main motivation for the research presented in this Thesis.

This Thesis therefore contributes an answer to the question "Under which conditions can Coordinated Beamforming provide substantial performance gains in a large-scale heterogeneous network?". To achieve this contribution, a very detailed simulation is applied. As a result, two factors that determine the potential for performance gains are found and described. In addition to this first contribution, also two new algorithms, named (1) HetNet Relaxed Zero Forcing (RZF) and (2) HetNet RZF Scheduling Heuristic (HRSH) are a contribution of this Thesis.

More specifically, HetNet RZF describes a signal processing technique (so-called precoding) to modify signals at a high power base station, such that it causes a configurable level of interference at a mobile station connected to a low power base station. HRSH is an algorithm for an efficient distribution of radio resources (i.e. the resources required to transfer data to a mobile station), controlling HetNet RZF. HRSH makes use of the results provided in the first contribution.

The simulation results show that Coordinated Beamforming can achieve significant performance gains in terms of throughput at the mobile stations connected to a low power base station, thus improving the network capacity. However, it is also shown that they are subject to the aforementioned factors which limit the available gains. With respect to HRSH, it is shown that this algorithm can realize the achievable gain to a large extent, while limiting the number of computations required.

1.2 Contribution of the Thesis

The contribution of this Thesis is related to the application of Coordinated Beamforming in heterogeneous networks. It is structured into three parts:

1. The first contribution is an answer to the question "Under which conditions can Coordinated Beamforming provide substantial performance gains in a large-scale, Orthogonal Frequency Division Multiple Access (OFDMA) based heterogeneous network?" In this regard, a detailed system level simulation is used. As a result, two performance limiting factors, including the corresponding dependencies, are determined.
2. The second contribution is a new precoding algorithm for Coordinated Beamforming which is based on the specifics of heterogeneous networks, named HetNet Relaxed Zero Forcing (RZF). It is designed such that a corresponding scheduler can configure the amount of interference that a high-power macro base station creates to mobile stations connected to a low-power pico base station.
3. In a third part, the results of the first and second contribution are used to create a novel heuristic to apply HetNet RZF, named HetNet RZF Scheduling Heuristic (HRSH). It realizes the achievable gains close to an exhaustive search with a reduced computational complexity.

1.3 Thesis structure

This document is structured as follows: Chapter 2 introduces the fundamentals of the capacity of wireless networks and describes how the capacity can be extended by means of coordination. This includes also the architecture of 3GPP Long Term Evolution Advanced (LTE-A) as the state-of-the-art mobile communication system, an introduction to heterogeneous wireless networks as well as the definition of the research problem for this work. Chapter 3 describes the methodology to be applied, which mainly consists of a description of the used system level simulation. In Chapter 4 a novel precoding and scheduling algorithm is proposed, which is designed to be applied in heterogeneous wireless networks. Chapter 5 describes how the characteristics of a large network (i.e. the existence of a large number of mobile and base stations) create factors that limit the achievable performance gains from Coordinated Beamforming. This knowledge is then used in Chapter 6 to propose a novel scheduling heuristic with reduced computational complexity. The performance analysis in Chapter 7 contain the simulation results for different network topologies and number of mobile stations before Chapter 8 draws conclusions and gives an outlook to potential future work.

There is a close link between the structure of this Thesis and its contributions: Chapter 5 relates to the first, Chapter 4 to the second and Chapter 6 to the third contribution.

Chapter 2

Coordinated Multipoint Transmission and its Effect on the Capacity of Large Multi-Carrier Heterogeneous Wireless Networks

The underlying challenge of this work is providing a network capacity that can fulfil the growing demand for wireless services. This chapter introduces fundamentals and summarizes work from different areas that are related to the topic.

Section 2.1 starts with an introduction of the network architecture of Long Term Evolution Advanced (LTE-A), a state of the art Orthogonal Frequency Division Multiple Access (OFDMA) based mobile radio technology. Section 2.2 then describes the fundamentals of mobile network capacity. It is shown that there are three options to increase the network capacity, out of which two are considered here and described in more detail: Network densification and interference mitigation (Section 2.4). In this respect also heterogeneous networks are introduced (Section 2.3), which are a recent trend towards a new level of network densification.

Advanced interference mitigation techniques often make use of coordination and multiple antennas at the transmitter and / or the receiver which is well-known under the name Multiple Input Multiple Output (MIMO). Section 2.4 therefore also gives an overview about coordination techniques known under the name Coordinated Multi Point (CoMP). The underlying principles of the advanced CoMP schemes rely on MIMO. Section 2.5 therefore not only introduces MIMO itself, but also how it is used to realize CoMP.

OFDMA is a key technique in mobile communication systems and introduced in Section 2.6. Finally, Section 2.7 describes again, how the topics of this chapter are interrelated, before defining the research problem.

In the following we make use of these mathematical conventions: A^* indicates the complex conjugate transpose of matrix A , A^T the transpose of matrix A , $\|a\|$ the Euclidean norm of vector a and $|a|$ the magnitude of a complex value a .

2.1 Network architecture

LTE-A is today's dominant mobile radio technology for wide area networks. It uses a relatively simple network architecture which is depicted in Figure 2.1.

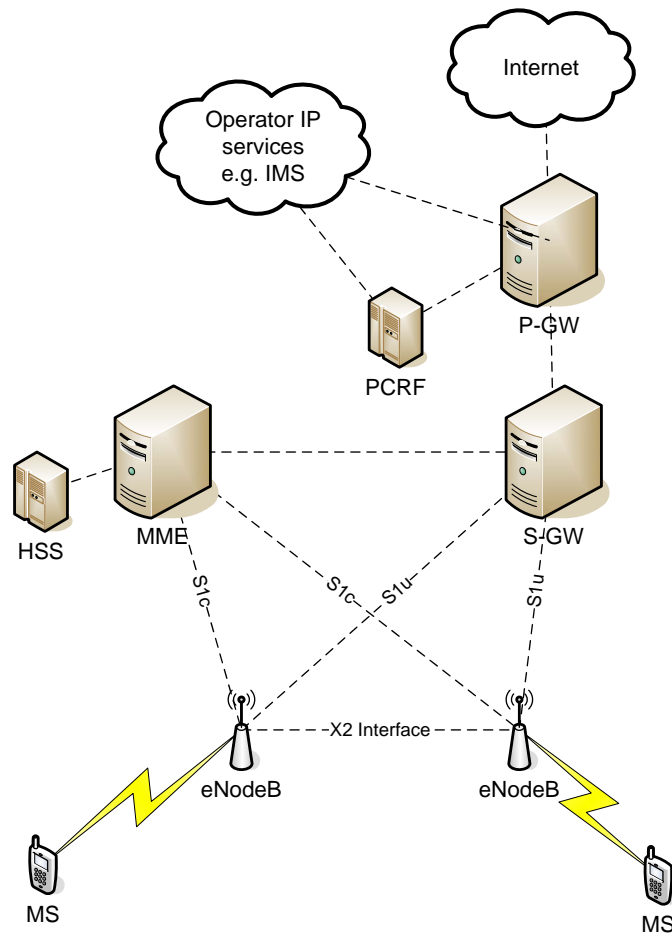


Figure 2.1: Network Architecture of LTE Advanced

The design distinguishes between the user plane which is mainly responsible for transporting the payload data and the control plane, responsible for e.g. authentication and handover. The main network elements of the LTE-A network architecture are:

- *eNodeB*: The eNodeBs form the Radio Access Network (RAN). An eNodeB can be seen as the implementation of a Base Station (BS). More precisely an eNodeB is a logical node. A typical implementation of an eNodeB is a three sector eNodeB at one site [7]. The key functionalities located in the eNodeB are:
 - Radio Resource Management (RRM): The scheduler is located in the eNodeB and controls which OFDMA radio resource is used by which Mobile Station (MS) for up- as well as downlink. More details on OFDMA and scheduling are provided in Section 2.6.
 - Mobility Management: The eNodeB can, in case necessary, request an MS to perform measurements of reference signals transmitted by other eNodeBs in order to detect if a handover is necessary. If this is the case, the currently serving eNodeB (source eNodeB) contacts a target eNodeB and initiates the handover.
 - Encryption of data to and decryption of data from the MS.
- *Mobility Management Entity (MME)*: The MME is the main control plane entity of the network. Among others, it represents the following key functionalities:
 - Idle mode tracking and paging: The MME stores the Tracking Area Code (TAC) of the MS in idle mode. A tracking area typically consists of several eNodeBs. In case a connection to an MS in the idle mode is necessary (e.g. for an incoming call), the MME initiates the paging to trigger the transition of the MS to the connected mode.
 - Authentication: The MME is connected to the *Home Subscriber Server (HSS)* which stores the authentication information of the MSs. Using this information, the MME can authenticate MSs that try to attach to the network.
 - Mobility management: As mentioned, the serving (so-called source) eNodeB initiates a handover and selects a target eNodeB. Subsequently, the target eNodeB contacts the MME to redirect the data flow from the source to the target eNodeB ("path switch request"). The MME then requests the Serving Gateway (S-GW) to redirect the user plane data.
- *Serving Gateway (S-GW)*: The S-GW is a part of the user plane and mainly acts as a router. As described above, it serves as a mobility anchor for user data by switching the data flow from the source to the target eNodeB in the case of handover.

- *Packet Data Network Gateway (P-GW)*: Similar to the S-GW this element mainly acts as a router within the user plane. It provides the connection to public data networks like the Internet and is responsible for IP address allocation of the MSs. Besides, the P-GW enforces the quality of service policies defined by the *Policy and Charging Rules Function (PCRF)*.

The interfaces between nodes that are relevant for the radio access network are also depicted in Figure 2.1, namely:

- The *S1c interface* connects the eNodeBs to the MME. This interface transports all kind of control plane information.
- The counterpart of the S1c interface is the *S1u interface*. It transports the user plane information and connects the eNodeB to the S-GW.
- The *X2 interface* interconnects two eNodeBs. It is used for:
 - *Mobility management*: For handover the source eNodeB contacts the target eNodeB via the X2 interface. After the MS has connected to the target eNodeB, the MME initiates the path switch. Before it has been completed, the source eNodeB forwards the user data to the target eNodeB via the X2 interface.
 - To support *Inter Cell Interference Coordination (ICIC)*, it is possible to exchange messages between eNodeBs via the X2 interface. An example is the Relative Narrowband Transmit Power (RNTP) indicator that enables interference avoidance.
 - *CoMP* requires information exchange between eNodeBs with low latency and high bandwidth. As the X2 interface is the only direct link between two eNodeBs, the X2 interface is also used for CoMP. However, this drastically increases the latency and bandwidth requirements on the X2 interface. It should be noted that the X2 interface is only logically a direct link. Having also a physical direct link often requires high investments for new interconnections (e.g. via fibre or microwave radio). Therefore, it might be the case that the X2 interface is implemented via a central router in the transport network.

2.2 Mobile network capacity

There are two main requirements for a mobile radio network: coverage and capacity. Coverage is achieved by deploying a network that provides a minimum level of received power at any location. This level has to be sufficient to enable communication between the BSs and the MSs in up- and downlink. A basic coverage can often be reached with a limited number of BSs, installed at a high altitude and operating on a low carrier frequency.

The term capacity refers to the amount of data the network is able to transfer at maximum in a given time instance. It is therefore measured (e.g. by means of simulations as they will be used throughout this Thesis) under a full load [8] (i.e. all BSs transmit as much data as possible). The capacity C of a wireless link can be determined via the Shannon-Hartley theorem (Equation 2.1). In it, B is the system bandwidth. S/N describes the Signal to Noise Ratio (SNR) (in uplink at the BS, in downlink at the MS). It compares the received power at the MS with the noise power in the receiver of the MS. A high SNR enables the usage of higher order modulation schemes such that an increase data throughput on the wireless link can be achieved. The capacity C is often also referred to as the Shannon capacity.

$$C = B \cdot \log_2 \left(1 + \frac{S}{N} \right) \quad (2.1)$$

In the case there are multiple MSs attached to a BS, the wireless links from and to the BS share a common capacity by means of a multiple access strategy (more details are described in Section 2.6). To maximize the capacity of a BS, it is possible to serve only the MSs with the highest SNR. However, this would lead to all other MSs not being served at all, which is not acceptable for practical networks. The maximization of the capacity should therefore always be combined with a fairness criterion, such that all MSs are served. More details on this are also described in Section 2.6. As a result of serving multiple MSs via a multiple access strategy, an averaged SNR over multiple MSs arises.

The Shannon Capacity is only valid for additive white Gaussian noise (AWGN) channels. This is especially an issue when interference has to be considered by adding interference power to the noise power. It is only valid under the assumption that the interference power follows a Gaussian distribution which is not necessarily the case. In addition, real systems are not able to achieve the full channel capacity due to practical implementation problems, e.g. channel estimation errors. For these reasons, the Shannon capacity cannot

be used to calculate the exact performance of a wireless system. However, it is a useful and widely used method to estimate the capacity, while the limitation should be kept in mind. Under the assumption that interference is Gaussian distributed, it can be added to the noise power, such that the SNR becomes the Signal to Interference plus Noise Ratio (SINR).

The capacity of a network ($C_{Network}$) consisting of k BSs is described by Equation 2.2, wherein C_{BS_i} denotes the capacity of an individual BS_i .

$$C_{Network} = \sum_{i=1}^k C_{BS_i} \quad (2.2)$$

The fact that it scales with the number of BSs (N_{BS}) has widely been used in the deployment of mobile radio networks: By sectorizing a cell, it is split into multiple independent BSs, increasing the capacity accordingly. In addition, also in areas where the network coverage is sufficient, additional BSs can be installed to increase the network capacity (so-called network densification).

The main disadvantage of a network densification is an increase in inter-cell interference. The smaller the cell sizes become, the more interference the receivers experience. As the SINR decreases, interference reduces the capacity of individual links and therefore limits the achievable gains from densification. Section 2.4 presents techniques to tackle this effect by mitigating interference.

From Equations 2.1 and 2.2 it can be seen, that there are three alternatives to increase the network capacity: An increase of N_{BS} is the target of network densification, as discussed. Interference mitigation increases the SINR and in turn the capacity of the individual BSs. Scaling the system bandwidth B is a third option. In this work, network densification and interference mitigation are used as means to increase network capacity. This is done under the assumption of a fixed system bandwidth. In parallel, increasing the system bandwidth is always a third option to linearly increase the system capacity. Equation 2.1 is based on the assumption that only a single data stream is transmitted. By using MIMO, it is possible to also send multiple data streams using Space Division Multiple Access (SDMA), which also can increase the capacity. MIMO is described in more detail in Section 2.5.

Achieving a high network capacity is most relevant for the downlink, i.e. the data flow from the BSs to the MSs, as this is the dominant type of traffic [9, 10]. This work therefore focusses on the downlink.

2.3 Heterogeneous networks

A recent trend that evolves network densification to a new level is the development towards heterogeneous networks [3]. Previously a denser network was achieved by adding BSs of the same kind and based on the same construction (high antenna altitude) and transmit power. At a certain level of densification (e.g. an inter site distance of a few hundred metres) this is not a viable option for the following reasons: The availability of suitable sites for high power BSs is limited, the installation is expensive due to required construction work and antennas at high locations create more interference than necessary in other cells. A potential solution is using other types of BSs in a heterogeneous network. It is created by adding low power BSs, often called small cells, to an existing network with high power BSs. There are different types of low power BSs such that a heterogeneous network can consist of a mixture of the following network elements [11][12]:

- Macro Base Stations (MBSs) are the basis of today's mobile networks. Their antennas are installed at higher locations (e.g. rooftops). A typical value for the transmit power of an MBS is 43 dBm, plus a maximum antenna gain of typically 14 to 17 dBi, resulting in an Equivalent Isotropically Radiated Power (EIRP) of 60 dBm (1000 Watt). This high transmit power enables a wide-area coverage, including indoor locations. The backhaul link has to provide a high capacity, which is realised by fibre or microwave radio links.
- Pico Base Stations (PBSs) can be seen as a lightweight type of the MBS. Their transmit power is lower (typically 30 to 40 dBm EIRP). Due to their smaller size they can be installed at lamp masts, walls or indoor locations. The capacity required for the backhaul can also be high, meaning that fibre or high speed Digital Subscriber Line (DSL) backhaul is suitable.
- Relay nodes are similar to PBSs with the difference that they are not equipped with a wired backhaul connection. Instead, a wireless connection to an MBS or PBS is used for backhaul.
- Femto BSs are, in contrast to the previous BS types, customer owned and operated devices. They have a low transmit power (a typically 23 dBm EIRP). Their size is comparable to a Wireless Local Area Network (WLAN) access point. It is often assumed that only a closed group of subscribers can connect to a femto BS, which creates special interference conditions [13][11]. As femto BSs are installed

by the customer, their locations are not planned by the network operator. The back-haul connection is often provided by a Virtual Private Network (VPN) connection through the Internet.

MBSs and PBSs as well as relay nodes are normally, in contrast to femto BSs, operated, installed and planned by the operator. A typical case of a heterogeneous network is the densification of an existing network with the help of PBSs. An example for such a network is depicted in Figure 2.2. The network consists of 21 MBSs, where in each of the coverage areas of an MBS (a sector) a PBS (red dot) is placed. In it, the MBSs, due to the low inter site distance of 500 metres (a typical assumption for urban networks [14]), provide a full coverage of the area. For the downlink with its strong transmit power imbalance (e.g. 60 dBm for an MBS compared to 40 dBm for a PBS), the PBSs have to accept strong interference for the MSs they are serving.

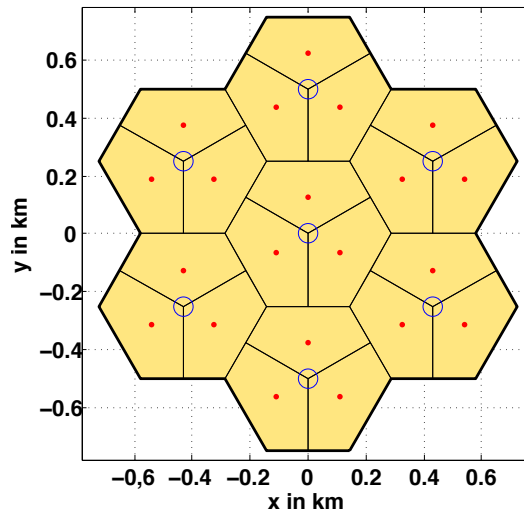


Figure 2.2: Heterogeneous network with 21 macro and 21 pico base stations

In a heterogeneous network the areas where low power BSs are received with a higher signal power than an MBS are relatively small. As the MSs by default attach to the BS received with the strongest received signal power, therefore fewer MSs connect to a low power BSs compared to the MBSs. Due to the low number of MSs that share the radio resources of a low power BS, the MSs attached to these normally achieve a higher throughput compared to the Macro Mobile Stations (MMSs). As a result the heterogeneous network tends to an uneven (potentially unfair) throughput distribution among the MSs and a fluctuating user experience for the MSs: When attached to a low power BS, high data rates are achievable whereas at other times (when connected to an MBS), a lower performance is experienced.

Cell Range Expansion (CRE) proposed for LTE-A [11] [12] is a technique to increase the fairness of a heterogeneous network, especially for networks with MBSs and PBSs, by balancing the load between the different BSs. This is achieved by turning additional MMSs into Pico Mobile Stations (PMSs). To do so, MSs are no longer attached to the BS that is received with the highest signal power at the location of the MS. Instead, a CRE offset (typically 6 to 9 dB) is used. An MS then prefers a PBS to an MBS until the power received from the MBS is more than the CRE offset higher than the one from the PBS. The effects of CRE are:

- The fairness of the network increases as more MMSs turn into PMSs, meaning that:
 - More MS benefit from the presence of PBSs.
 - The throughput of PMSs decreases as more PMSs share the resources to the PBS (this is a negative effect, but it also increases the fairness).
 - The throughput of the MMSs increases as more MSs are offloaded from the MBSs to the PBSs.
- The overall network capacity decreases. This is a result of the new attachment of the MSs: The highest network capacity can be achieved when all MSs are connected to the strongest BS. Due to the introduction of the CRE offset three groups of MS can be defined. In the following the power an MS receives from the strongest PBS is denoted as P_{pico} , the power received from the strongest MBS as P_{macro} , the setting of the CRE offset as B , the sum power of all other BSs as I (interference) and the noise as N .
 - For the group of MSs where $P_{pico} > P_{macro}$, the association (to the PBSs) as well as the SINR does not change.
 - The same holds true for the group of MSs where $P_{macro} - B > P_{pico}$. These MSs remain assigned to the MBS.
 - For the group of MSs where $P_{pico} < P_{macro}$ and $P_{pico} + B > P_{macro}$ the association changes from the macro to the pico BS due to the CRE offset. This means that P_{pico} turns from interference into the desired signal and P_{macro} from the desired signal into interference. The SINR changes from $\frac{P_{macro}}{I+P_{pico}+N}$ to $\frac{P_{pico}}{I+P_{macro}+N}$. As for this group of MSs $P_{pico} < P_{macro}$, the SINR decreases.

- In case the CRE offset is set too high, strong negative effects occur: Many MSs try to connect to the PBS, but fail as the signal received from the PBS is much lower than the one from the MBS. Or in other words the inference situation of such MSs becomes unacceptable. Simulation results show that a reasonable setting for the CRE offset is a few dB or lower [15]. Also, in case of a too high CRE offset, PBSs can get overloaded.

To summarize, CRE offers a possibility to better distribute the performance gains that PBSs offer among the MSs. This is an important functionality as the target of heterogeneous networks should be to provide increased performance everywhere, not only at certain locations. In contrast, CRE also decreases the network capacity, especially at high CRE offset settings and can create conditions with strong interference.

Each PBS creates a new small Cell Edge (CE) area, characterized by strong interference as shown in Figure 2.3. In case CRE is used, the size of this area increases.

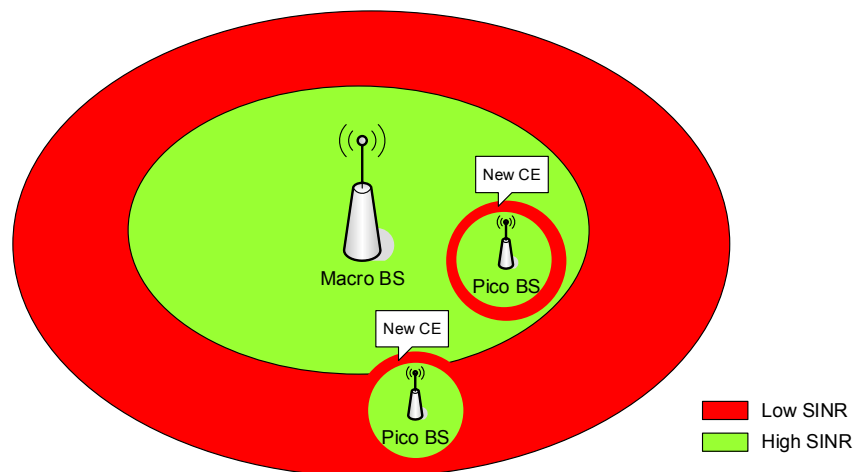


Figure 2.3: Areas with strong interference in a heterogeneous network. "New CE" represents a new Cell Edge (CE) area, caused by the Pico BSs.

Within the expanded area a special interference situation occurs: The serving BS of an MS is no longer the BS received with the highest signal power at the location of the MS. Instead, a very strong interferer (the MBS) is present. This creates an opportunity for any kind of interference mitigation to be employed: If it is possible to reduce or to remove the interference from the MBS in the expanded area, the SINR of the MSs there will increase drastically.

From an implementation point of view, the CRE offset value is a modified handover threshold. The handover decision is executed based on the received power levels biased by the CRE offset.

2.4 Interference mitigation and coordinated multipoint transmission and reception

This section provides an overview about interference mitigation as a means to improve the performance of wireless networks. As it will be shown, interference mitigation is closely related to coordinating BSs - so-called Coordinated Multi Point (CoMP), which will therefore also be introduced in this section. Section 2.5 then describes details on how interference mitigation is achieved by means of coordination and the usage of multiple antennas at the BSs.

Interference mitigation aims at improving the performance of a wireless link by reducing the interference it experiences. There are different approaches to interference mitigation which can be categorized [16] into the three subcategories: interference averaging, interference avoidance and removing interference by means of signal processing (e.g. interference cancellation):

- Interference averaging reduces the probability that single links experience strong interference. This can be achieved by spreading a signal over a larger frequency band [17], for example by means of Frequency Hopping Spread Spectrum (FHSS) [18] or Direct Sequence Spread Spectrum (DSSS) [19].
- Interference avoidance aims at preventing the occurrence of interference by restricting the usage of frequency bands for certain transmitters or limiting their transmit power. The reduced generation of interference improves the performance for neighbouring links. Examples for interference avoidance are:
 - The static frequency reuse factor employed in the Global System for Mobile Communications (GSM) [20]
 - Fractional Frequency Reuse (FFR) [21, 22] used in Long Term Evolution (LTE) and Worldwide Interoperability for Microwave Access (WiMAX) [23], where for a first part of the system bandwidth a reuse factor of one is configured (all BSs can use this band). The second part of the system bandwidth is

divided into subbands and for each subband a frequency reuse factor higher than one is applied. Each BS can use one subband from the second part of the system bandwidth in addition to the first part. In the second part of the system bandwidth interference is avoided, as only limited BSs have access to each subband.

- An advanced version of FFR called Soft Frequency Reuse (SFR) [21, 22] also used in LTE and WiMAX [23]. Here BSs are allowed to transmit also on the subbands from the second part of the system bandwidth (which they have been restricted from in FFR), but with limited transmit power.
- For heterogeneous networks, LTE-A supports a dedicated time domain interference avoidance approach named enhanced Inter Cell Interference Coordination (eICIC) [24, 25, 26]. In it, the MBSs do not transmit at selected time slots, such that PBSs or other low power BSs can serve MSs under a reduced interference.
- Removing interference by means of signal processing refers to algorithms that eliminate interference, executed in the transmitter or the receiver. At the receiver side, this process is referred to as interference cancellation [27]. At the transmitter side, signals can be preprocessed before transmitting them, such that interference at the receivers does not occur or is reduced. This process of preprocessing signals is called precoding [28]. Precoding in most cases relies on using multiple transmit antennas and is in more detail introduced in Section 2.5. Interference Alignment (IA) [29] combines precoding at the transmitter and interference cancellation at the receiver by jointly optimising the processing in the transmitter and in the receiver.

With respect to the network capacity, the interference mitigation approaches have the following effects:

- In interference averaging, the total amount of interference in the system does not change. This approach therefore does not have the potential for a capacity improvement on a system level.
- Interference avoidance can cause significant improvements in terms of the SINR at the receivers [22]. However, it also causes additional restrictions. FFR for example implies that the bandwidth of the individual BSs shrinks, thereby reducing their capacity (see Equation 2.1 in Section 2.2). The overall potential for a capacity

improvement on a system level by means of interference avoidance is therefore low.

- Removing interference by means of signal processing offers a significant potential for improving the network capacity. As an example, the simulation results in [30] show that the throughput of two BSs might be increased by the order of 200%. This work therefore focusses on interference mitigation by means of signal processing.

Interference avoidance as well as precoding is often combined with coordination between BSs [31]. Recent work on coordination is subsumed under the term CoMP and introduced in the following.

Coordination between BSs of a mobile radio network has been under discussion for fourth as well as fifth generation systems [32] [33]. Its main objective is to enable efficient interference mitigation schemes. There is a set of different coordination schemes [32] [34], introduced in this section. To enable coordination, communication interfaces between the BSs have to be established, e.g. using wired interconnections. The schemes presented here especially differ in the amount of data that needs to be exchanged between the BSs [35]. The tighter the cooperation is, the higher the requirements for the communication interface in terms of latency and bandwidth are. Loose schemes only require the exchange of Channel State Information (CSI), i.e. information about the status of the wireless links between the cooperating BSs and the MSs. Tight cooperation also involves data sharing, meaning that data to be transmitted to the MSs must be present at multiple BSs. The following CoMP schemes exist:

- *Transmission point blanking* [36, 37] is a loose cooperation scheme. Here one BS (also called transmission point in the context of CoMP) can be muted (prevented from transmitting data) to reduce the interference of MSs at another BS. Referring to the types of interference mitigation described above, this is an interference avoidance technique, which can be used to improve the performance of individual MSs suffering from a low SINR. Transmission point blanking requires CSI sharing between the BSs.
- *Dynamic transmission point selection* [36, 37] performs a quick switching of a transmission from one BS to another, such that a traditional (relatively slow) handover procedure is avoided. It relies on CSI sharing. Unlike the other schemes, it is not an interference mitigation technique.

- *Coordinated scheduling* [38, 39] targets an optimized assignment of the OFDMA radio resources between BSs, which can result in interference avoidance. OFDMA and the process of scheduling will be introduced in Section 2.6. Coordinated scheduling requires CSI sharing.
- *Coordinated Beamforming (CBF)* [5] relies on using multiple antennas at the BSs and a corresponding coordinated signal processing to remove interference in the process of precoding. Coordinated Beamforming requires CSI sharing. While the data rate required for the exchange of CSI is limited [40], the requirement in terms of latency can be demanding (below 1 ms) [41]. The underlying principles of CBF (precoding for so-called MIMO interference channel) will be described in detail in Section 2.5.2.
- *Joint Transmission*, also called Network MIMO [42], [43] is a tight cooperation scheme that requires CSI and data sharing. Here multiple BSs transmit data jointly, such that an MS can receive a data stream that was transmitted by multiple BSs simultaneously. Individual transmissions by the BSs can sum up constructively, which increases the received power at the MS. This is especially beneficial in areas where two or more BSs provide similar power levels. In addition, interference cancelling precoding schemes (similar to CBF) can be executed in a joint transmission cluster which will be described in detail in Section 2.5.3.

As it can be seen, there are two CoMP schemes related to interference mitigation by means of signal processing, CBF and Joint Transmission, which will be topic of Section 2.5. However, in the literature there is often no clear distinction between both approaches. The name CBF is also used in the context of Joint Transmission. From an architectural perspective there is, however, the huge difference in terms of data sharing (which is required for Joint Transmission, but not for CBF). Within the context of this work, therefore a clear separation is used and all schemes that involve data sharing are called Joint Transmission schemes.

Recent work underlines the importance of a correct modelling of the network topology to investigate the performance of coordinated systems [6]. The coordination takes place within a group of BSs, the so-called cooperation cluster. Suitable algorithms can cancel interference within this cluster. They operate in the BSs of a cooperation cluster or in an overarching controller. However, there is always a level of interference from the BSs outside the cluster (Out of Cluster Interference (OOCI)) which cannot be cancelled.

As shown in [6], this limits the performance of coordinated systems. The performance limit caused by OOCI can also be seen from two different directions in the related work: When simplified networks (e.g. with two cells only) are considered, huge gains from interference cancellation are possible [30] [44]. On the other hand, in realistic, large scale networks, gains are difficult or impossible to obtain [45] [46]. With respect to CBF also [47] points out that it has to be studied under practical network conditions.

2.5 Multi-antenna techniques

This section describes techniques for multi-antenna communication, also known under the name Multiple Input Multiple Output (MIMO). As a basis, a point-to-point MIMO link between a BS and an MS is introduced in Section 2.5.1. The MIMO Interference Channel, which is the basis for CBF, is then described in Section 2.5.2. The MIMO broadcast channel as the basis for Joint Transmission is the topic of Section 2.5.3. As this work is focussed on CBF, the emphasis lies on the MIMO interference channel.

2.5.1 Point to point MIMO communication

State-of-the-art wireless systems make use of MIMO, meaning that transmitters and receivers are equipped with at least two antennas and the corresponding signal processing capabilities. For the purpose of introducing the MIMO principles, a generic MIMO system as depicted in Figure 2.4 is used, which shows a BS transmitting to an MS. The signal s_1 is intended to be sent to MS_1 . It can consist of two parallel data streams (the case of a single data stream is described later). The signal s_1 is now precoded by means of the precoder v_1 . As the lines in below V_1 in Figure 2.4 indicate, the precoding determines, how the signals are forwarded towards the antennas. A precoder $V_1 = \begin{bmatrix} 1 & 0 \\ 0 & 1 \end{bmatrix}$ would as an example mean that the first data stream is transmitted via the first antenna and the second data stream via the second. As a second example, $V_1 = \begin{bmatrix} 0 & 1 \\ 1 & 0 \end{bmatrix}$, would cause the opposite, i.e. the first data stream to be transmitted via the second antenna and the second data stream via the first antenna. More details on how to use the precoder besides these basic examples follow in this section. The transmitted signal then undergoes the radio channel H_{11} and arrives at the antennas of MS_1 . Here it mixes with interference from a simultaneous transmission at another BS that arrives through channel H_{1j} . Before the decoding and

demodulation, the received signal is processed through the receiver combining matrix U_1 . This matrix can be used to compensate the inter-stream interference between the two data streams of s_1 which was caused by H_{11} .

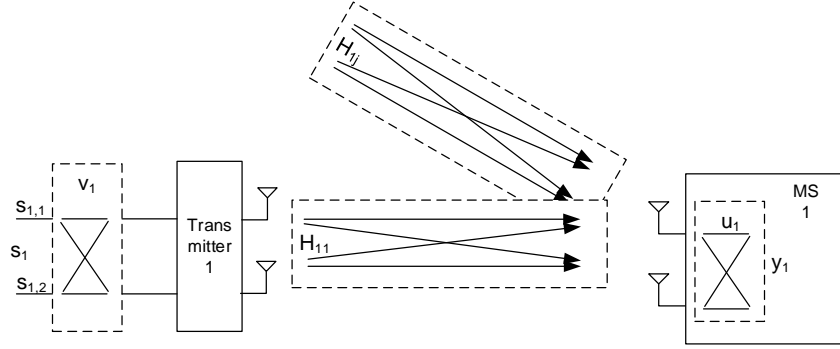


Figure 2.4: MIMO System Model for two parallel data streams

The mathematical and more detailed representation of Figure 2.5 from an MS perspective is given in Equation 2.3.

$$y_i = \underbrace{\sqrt{P_i} \alpha_{ii} u_i H_{ii} v_i s_i}_{\text{Wanted Signal}} + \underbrace{\sum_{\substack{1 \leq j \leq k \\ j \neq i}} \sqrt{P_j} \alpha_{ij} u_i H_{ij} v_j s_j}_{\text{Interference}} + \underbrace{n_i}_{\text{Noise}} \quad (2.3)$$

It describes the received signal at MS_i attached to BS_i . The first part of the received signal ("Wanted Signal") describes the intended data transmission from BS_i to MS_i . It is a product of the following factors:

- $P_i \in \mathbb{R}$ represents the transmit power of BS_i .
- $\alpha_{ii} \in \mathbb{R}$ the pathloss between MS_i and BS_i . It is a scalar that describes the attenuation of the transmitted power.
- $u_i \in \mathbb{C}^{2 \times 2}$ describes the processing in MS_i .
- $H_{ii} \in \mathbb{C}^{2 \times 2}$ is the complex transfer function of the radio channel between MS_i and BS_i .
- $v_i \in \mathbb{C}^{2 \times 2}$ is the precoder selected at BS_i .
- $s_i \in \mathbb{C}^{2 \times 1}$ are the coded symbols to be transmitted by BS_i

More details on the individual components, especially on the precoder, follow below. The second part of Equation 2.3 describes the interference that MS_i experiences. It sums the signals arriving from k other BSs. The third part relates to the noise in the receiver.

Figure 2.5 is equal to the previous MIMO system model with the difference that only one data stream is transmitted per BS. The precoder v_i now consists of only two elements that describe how the signal is distributed over the antennas. Similarly, u_i consist of two elements that describe the combining of the signals in the receiver.

Mathematically this model can also be described by Equation 2.3, with the difference in the dimensions of the following variables:

- $u_i \in \mathbb{C}^{1 \times 2}$ describes the combining in MS_i .
- $v_i \in \mathbb{C}^{2 \times 1}$ is the precoder selected at BS_i that distributes the signal to the antenna ports.
- $s_i \in \mathbb{C}^{1 \times 1}$ the coded symbol to be transmitted by BS_i

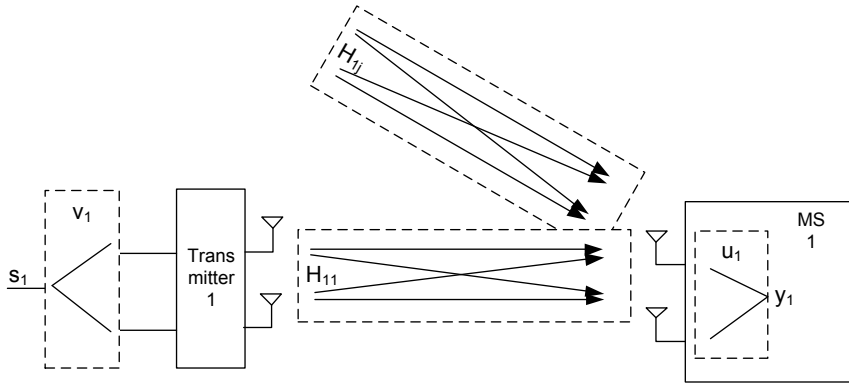


Figure 2.5: MIMO System Model for one data stream

In the following, the precoding process will be introduced in more detail. In general, the term precoding refers to the usage of knowledge about the wireless channel at the transmitter (Channel State Information at the Transmitter (CSIT)) side [48]. It can be divided into linear and non-linear precoding techniques [48, 49]. In the case of linear precoding, the process of precoding at the transmitter is separated from the coding of the data [48, 49]. This also assumed in Equation 2.3 as well as in Figures 2.4 and 2.5, where *coded* data s is the input of the system.

Non-linear precoding techniques make use of the additional advantages from coupling data coding and precoding on the cost of increased complexity [49, 50]. Examples of non-linear precoding are Tomlinson-Harashima Precoding [51] [52] and Dirty Paper Coding [53]. Especially when combined with a large set of MSs to choose from, linear precoding techniques offer a good trade-off between performance and complexity [49, 50]. Linear

precoding is used in LTE-A [7], WiMAX [48] and 5G New Radio (5G NR) [54]. For this reason linear precoding is applied here.

In the case the BSs of a network are not coordinated, precoding can be used to improve the link quality of the MSs it is serving. The precoder which achieves the capacity of the channel can be derived using Singular Value Decomposition (SVD) [55, 56]. To do so, the wireless channel matrix H is decomposed into three parts as described by Equation 2.4 (* indicates the conjugate transpose).

$$H = U\Lambda V^* \quad (2.4)$$

Figure 2.6 visualizes the principle. It relies on the fact that the off-diagonal elements of the matrix Λ are zero such that the original channel is transposed into a set of parallel Single Input Single Output (SISO) channels. The diagonal elements of Λ indicate the gains of these channels and are ordered such that $\lambda_1 \geq \lambda_2 \geq \lambda_n$ (in the case of a system with two receive antennas only two diagonal elements occur, whereas in a more general case also more are possible).

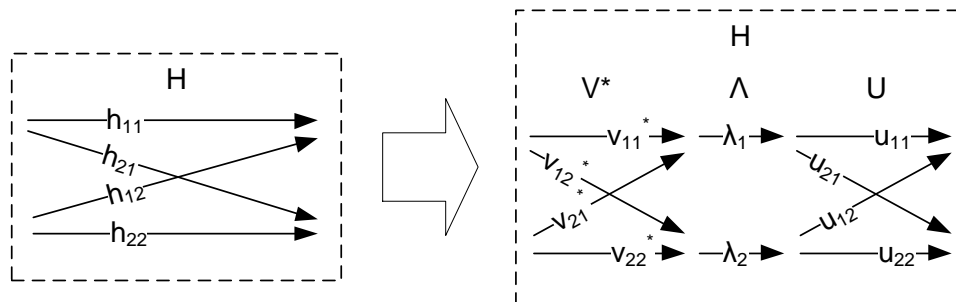


Figure 2.6: Singular Value Decomposition of the Wireless Channel

If there are multiple data streams in parallel to the MS (spatial multiplexing), the parallel SISO channels can be used for it along with corresponding precoding that maps the data streams to the SISO channels.

For a single data stream to be transmitted, it is optimal to allocate the full transmit power to the first channel of Λ (which offers the highest channel gain) [55]. This is achieved by choosing a suitable precoder at the BS as it is depicted in Figure 2.7. The data which is supposed to be sent is indicated by s . It is precoded by means of the vector v_t before sending. It can be seen from Figure 2.7 that the intended data flow towards λ_1 passes through $v_{t1}v_{11}^*$ and $v_{t2}v_{21}^*$. To maximize the amplitude of these two links, v_t has so

be chosen according to Equations 2.5 and 2.6 and u_r according to Equations 2.7 and 2.8.

$$v_{t1} = v_{11} \quad (2.5)$$

$$v_{t2} = v_{21} \quad (2.6)$$

$$u_{r1} = u_{11}^* \quad (2.7)$$

$$u_{r2} = u_{21}^* \quad (2.8)$$

The principle of precoding data such that it is received with a maximal received power is referred to as Maximum Ratio Transmission (MRT) [57]. Section A.1 gives a numerical example on how MRT precoding can be realized with the help of the SVD.

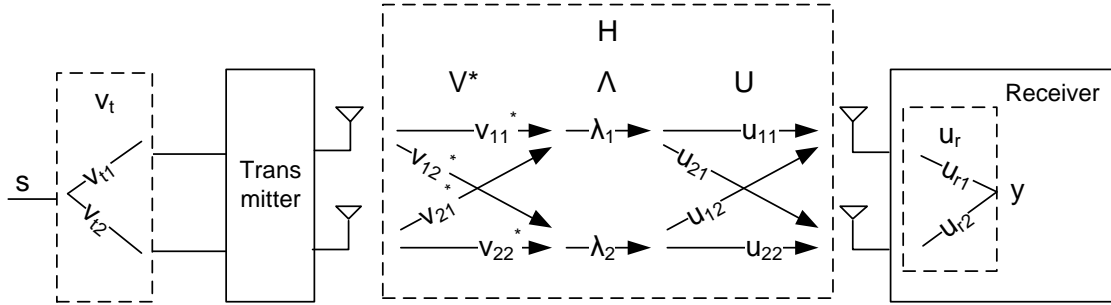


Figure 2.7: Singular Value Decomposition of the Wireless Channel with Precoding

2.5.2 The MIMO interference channel

The MIMO communication discussed up to this point did not involve any coordination between BSs. In this section coordination for the MIMO interference channel will be discussed, which is the basis for CBF and depicted in Figure 2.8. Figure 2.8 shows two BSs which are transmitting data towards two MSs. The first MS is served by the first BS and the second MS by the second BS. It is important to note that in this setup there is no data sharing between the BSs, i.e. the first BS does not have access to s_2 and the second BS does not have access to s_1 . However, both BSs share the CSI, such that both BSs are aware of H_{11} , H_{12} , H_{21} and H_{22} .

The work performed in [58] studies CBF from a computational complexity theory point of view. It is shown that finding an *optimal* solution to CBF is a non-deterministic polynomial (NP) time hard problem. It is therefore at least as hard as an NP-complete optimization problem, for which an efficient way for finding an optimal solution probably does not exist. Nevertheless, there is a set of different approaches to CBF, introduced in the following.

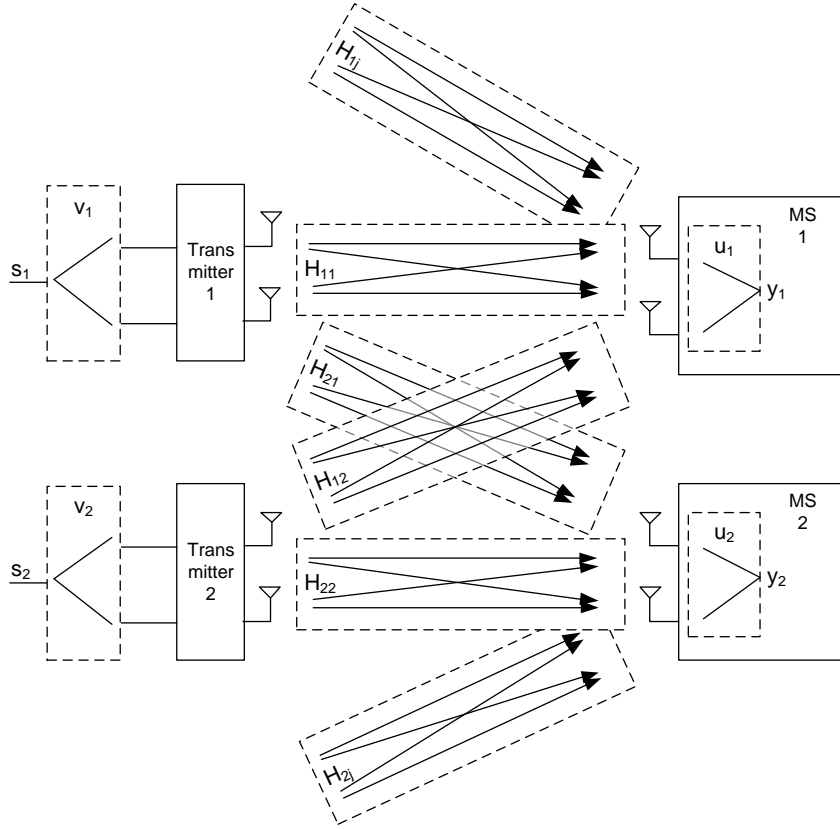


Figure 2.8: The MIMO interference channel

The target of CBF is to jointly design the two precoders v_1 and v_2 to mitigate the interfering channels H_{12} and H_{21} . However, it should be noted that this does not have the potential to mitigate interference from other BSs through H_{1j} and H_{2j} . There are several algorithms for a joint optimization of the precoders v_1 and v_2 which are introduced in the following. As an extreme case, it is possible to fully remove the interference that one BS causes to an MS of the second BS. As interference is forced to be zero, the corresponding principle is called Zero Forcing (ZF) precoding. In ZF precoding, v_1 and v_2 are chosen such that Equations 2.9 and 2.10 are fulfilled

$$u_2 H_{21} v_1 = 0 \quad (2.9)$$

$$u_1 H_{12} v_2 = 0 \quad (2.10)$$

As it can be seen from Equations 2.9 and 2.10, finding the precoding vectors v_1 and v_2 that fulfil this target depends on the receivers (u_1 and u_2). For the case of Maximum Ratio Combining (MRC) combining receivers [55], an algorithm that calculates the ZF precoders is provided in [4]. A numerical example for the ZF precoding algorithm in [4] can be found in Section A.2.

The two precoding schemes that have been described up to now (MRT precoding in Section 2.5.1 and ZF precoding in this section) are the two extremes with respect to the effect they cause: MRT precoding maximizes the received power at the MS to be served, without any consideration of the interference that is created at other MSs. In ZF precoding, the constraint to fully remove interference causes that, depending on the realization of the instantaneous channel, power reductions in the intended signal compared to MRT have to be accepted.

The precoding schemes Signal to Leakage and Noise Ratio (SLNR) precoding [59] and Relaxed Zero Forcing (RZF) [60, 61] target a compromise between MRT and ZF. They define precoders that reduce interference (but not null it out) and increase the intended signal compared to ZF.

SLNR precoding [59] is based on maximizing the ratio of the intended signal power to the sum of noise and generated interference power ("leakage"). The SLNR at BS_i that occurs when serving MS_i is defined by Equation 2.11.

$$SLNR_i = \frac{\|H_{ii}v_i\|^2}{n_i^2 + \sum_{\substack{1 \leq j \leq l \\ j \neq i}} \|H_{ji}v_i\|^2} \quad (2.11)$$

The term $\|H_{ii}v_i\|^2$ represents the intended power towards MS_i . It is divided by the noise power in the receiver of MS_i (n_i^2) and the sum of powers that is transmitted towards the l MSs that are served simultaneously by other BSs.

The work presented in [62] shows how a combination of an MRT and a ZF precoder can be achieved, which was then described as RZF [60, 61]. For the Multiple Input Single Output (MISO) Interference Channel (i.e. with receivers that are equipped with only one antenna) the precoder is defined by Equations 2.12 and 2.13.

$$v_i = \alpha_1 v_{i,MRT} + \alpha_2 v_{i,ZF} \quad (2.12)$$

$$\text{under the condition: } \|v_i\| = 1 \quad (2.13)$$

The parameters α_1 and α_2 can be used to configure the precoding depending on the objective (interference minimization or power maximization). This is an advantage compared to SLNR precoding which practically selects one uncontrolled point in between ZF and MRT [61]. [61] also proposes an extension of RZF to the MIMO Interference Channel. However, the proposed approach is iterative such that it is not possible to compute precoders in a single step which can be unacceptably complex for realistic systems.

In [63] and [64] the trade-off in the design of the precoder is described ("competition versus cooperation"). A BS can act "selfishly" meaning that it maximizes the utility (signal) of its MS (MRT precoding). The opposite is a fully "altruistic" behaviour, such that no interference to the MS of the cooperating BS is created, irrespective of the disadvantage (reduced signal power compared to MRT) for its own MS.

In this section, precoding for the MIMO Interference Channel, which is a processing of data at the BS, was described. The selection of the precoder v at the BS is independent from the receiver, which calculates a receiver processing matrix u . Interference Alignment (IA) [29, 65, 66] is a method that couples both processes such that the precoding vectors and the receiver processing matrices are derived jointly. However, there is only for the high SNR regime a closed form solution to achieve IA [65]. Besides, there is a set of iterative algorithms [67] for IA. As an example, [66] proposes an iterative approach in this regard which operates as follows:

1. The BSs of the network transmit with arbitrary precoders v to the MSs.
2. The receiver processing matrices u of the MSs are calculated such that they suppress interference (for more details on the exact calculation the reader is referred to [66], Section V).
3. A reverse communication (from the MSs to the BSs) takes place, in which the MSs use the receiver processing matrices derived in step 2 as transmit precoders.
4. The BSs calculate interference suppressing receiver processing matrices according the same principle used in step 2.
5. The communication direction is reversed again. The BSs now uses the receiver processing matrices derived in step 4 as precoders.
6. The algorithm continues with step 2 until convergence is reached, which is defined by a point where the so-called weighted leakage interference (for more details see [66], Section V) reaches zero.

Precoding algorithms such as RZF and SLNR as well as IA require detailed information about the characteristics of the radio channels, the so-called CSI [59]. With respect to the scenario depicted in Figure 2.8, this means that information about the complex channel transfer functions H_{11} , H_{21} , H_{12} and H_{22} is required, which in addition has to

be shared between BSs [35]. To obtain full CSI, in Time Division Duplex (TDD) systems, channel reciprocity can be utilized, such that detailed CSI for the downlink can be obtained through uplink channel estimation [59]. In more detail, MS 1 can send out a known channel estimation sequence, that is received at BS 1 and BS 2, such that the channels H_{11} and H_{12} can be measured. The same principle can be used for MS 2 in order to also analyse H_{21} and H_{22} .

For Frequency Division Duplex (FDD) systems, CSI can be obtained through feedback from the MSs, which might be limited, such that the full potential of CBF cannot be exploited. As only under the assumption of this knowledge the full potential of CBF can be exploited, this is also assumed in the following. Section 7.5 discusses how the results obtained for full CSI can be interpreted in the direction of systems with limited CSI.

2.5.3 The MIMO broadcast channel

Figure 2.9 shows the so-called MIMO broadcast channel, which is the basis for CoMP Joint Transmission. For the sake of simplicity, Figure 2.9 does not show the interference from BSs which are not part of the cooperation (H_{1j} and H_{2j} in Figure 2.8), which however still exists.

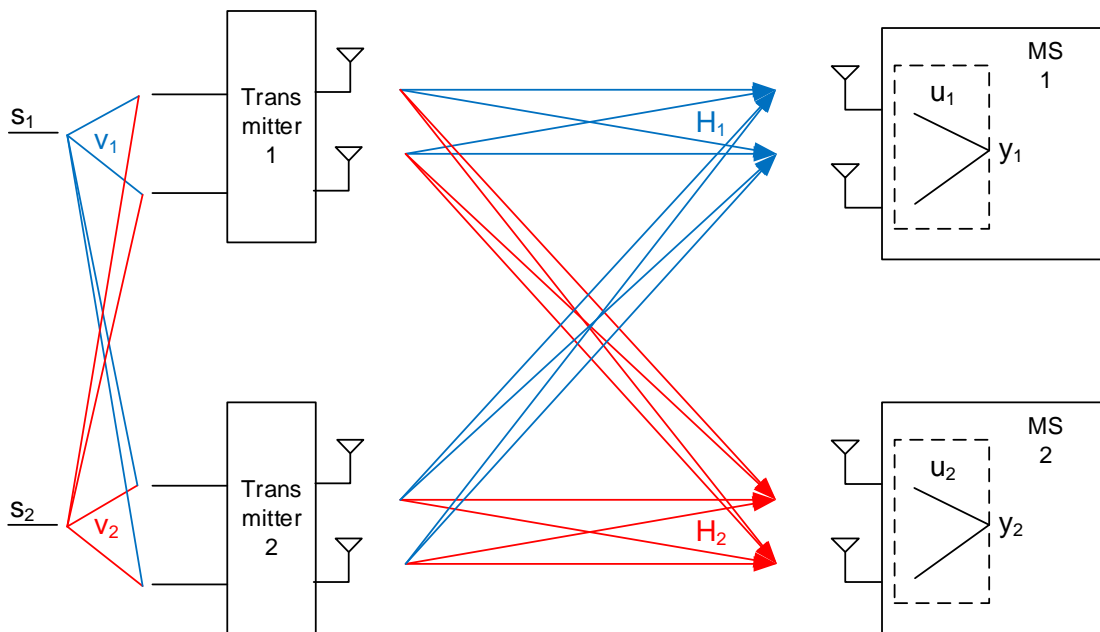


Figure 2.9: The MIMO broadcast channel

As it can be seen from Figure 2.9, the signal s_1 is now not only transmitted via the first BS, but via both BSs, which also explains the name Joint Transmission. Both BSs

therefore not only share CSI as in the case of the MIMO interference channel with CBF, but also the data to be transmitted.

The trade-off between ZF and MRT, as described for the MIMO interference channel also exists for the MIMO broadcast channel [68]. Correspondingly, also the principles to achieve a compromise between MRT and ZF are similar. SLNR precoding [59] can also be applied for the MIMO broadcast channel.

Due to their very tight coupling, both BSs in Figure 2.9 can also be seen as one BS with antennas at different sites [58] in which the principles of Multi User Multiple Input Multiple Output (MU-MIMO) [50] can be applied. In MU-MIMO resource management [69], a Physical Resource Block (PRB) is allocated to more than one MS and the corresponding data streams are separated by means of precoding.

2.6 Scheduling and resource allocation through Orthogonal Frequency Division Multiple Access

Similar to MIMO, Orthogonal Frequency Division Multiplexing (OFDM) [70] is a dominant technique in state-of-the-art wireless systems. It is used in Institute of Electrical and Electronics Engineers (IEEE) WLAN 802.11 a/g/n/ac and in the Third Generation Partnership Project (3GPP) air interface technologies LTE and 5G NR [54]. Figure 2.10 shows the processing chain for an OFDM transmitter and receiver. Instead of transmitting data symbols sequentially, OFDM creates multiple subcarriers to transmit data in parallel. The serial input data is therefore converted into parallel data streams, which can independently be modulated in digital domain (so-called constellation mapping, where I/Q samples are generated). An Inverse Fast Fourier Transformation (IFFT) then creates the time-domain signal. A cyclic prefix is inserted to remove inter-symbol interference (details follow below). After a digital/analogue conversion, the signal is modulated onto the radio frequency carrier and transmitted. An OFDM receiver performs the corresponding reverse operations. The OFDM subcarriers are orthogonal in frequency domain, such that one subcarrier does not create interference to another.

There are two main benefits of OFDM: (1) Its resistance to multipath propagation and (2) the possibility to adapt the modulation and coding to a frequency selective channel. Multipath propagation causes a transmitted symbol to arrive multiple times at the receiver, especially due to reflections. When delayed reflections of a first symbol arrive during the

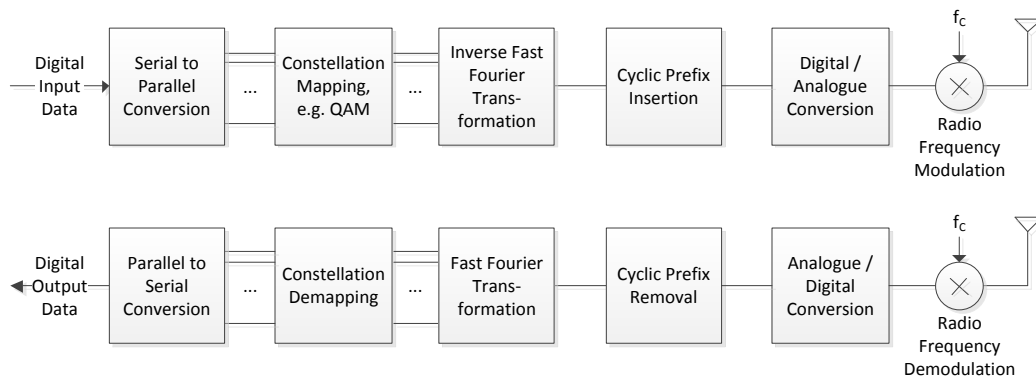


Figure 2.10: OFDM Transmitter and Receiver Chain

reception of a second symbol, this causes so-called inter-symbol interference. OFDM reduces inter-symbol interference, as it converts a serial transmission of short symbols into parallel longer transmissions, such that reflections are received within the duration of the symbol. Remaining inter-symbol interference is removed by the cyclic prefix, a guard period at the beginning of a symbol.

A frequency selective radio channel is also mainly caused by reflections. At the location of the receiver, the reflections can sum up constructively or destructively. This behaviour depends on the carrier frequency, such that the amplitude of the channel transfer function varies over the frequency as depicted in Figure 2.11. In an OFDM system, this fact can be exploited by using a higher order modulation for subcarriers with good channel conditions. With respect to Figure 2.11, good channel conditions refer to a high amplitude, whereas in general good radio conditions refer to a high SINR.

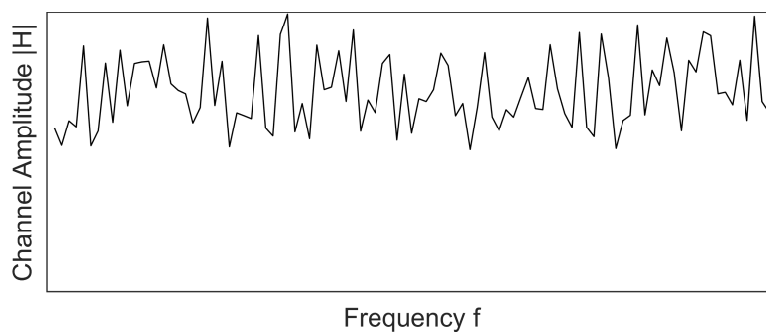


Figure 2.11: Example for a Frequency Selective Channel

With respect to precoding, OFDM has a special role: Linear precoding techniques often assume a frequency-flat channel which is in conflict with the fact that state-of-the-art mobile communication systems use a large system bandwidth (e.g. 20 MHz) where it is unrealistic to assume a flat channel over the full bandwidth. OFDM offers a solution for this as described in [48]: "A *frequency-flat solution, however, can be applied to a*

frequency-selective channel by decomposing the transmission band into multiple narrow, frequency-flat subbands. Specifically, we can apply the solution per subcarrier in systems employing OFDM.” OFDMA is a multiple access method based on OFDM. OFDMA creates time / frequency radio resources as depicted in Figure 2.12. Each radio resource can then be allocated to one user, such that multiple MSs can be served simultaneously. While in theory one radio resource could consist of one subcarrier for the duration of one OFDM symbol, in practice a set of subcarriers for the duration of multiple symbols is allocated to an MS. This is especially important to restrict overhead, as each resource assignment causes signalling to inform the MSs about the current allocation. LTE-A uses OFDMA radio resources of 180 kHz, allocated to the duration of one millisecond, the so-called Physical Resource Blocks (PRBs). Within this work, the terms radio resource and PRB are used interchangeably.

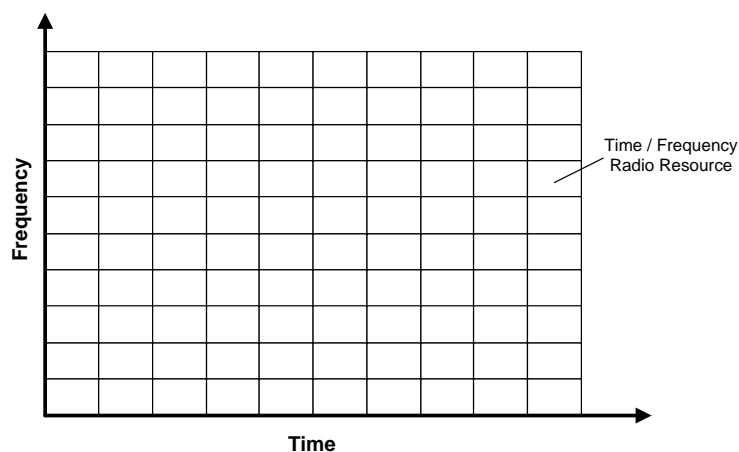


Figure 2.12: OFDMA Radio Resources

The allocation of the OFDMA radio resources to the MSs is the main task of the scheduler, a functionality of the BS [71]. The scheduling process is a complex procedure as the resource assignment has to meet a set of different requirements: It has to fulfil Quality of Service (QoS) requirements of the individual data streams, trade-off between the demand of different users in case there are insufficient radio resources, set the Modulation and Coding Scheme (MCS), MIMO modes and precoders and allocate radio resource for retransmissions of previous transmissions that could not be correctly decoded. The scheduling algorithm is not subject to standardization (e.g. in LTE, 5G NR and WiMAX). As the scheduling impacts the performance of the overall system, manufacturers of mobile communication equipment consider the scheduling algorithm as a trade secret that is not published. Consequently, the scheduling algorithms that are used in commercial systems

are to a large extent unknown. However, there is set of well-known general scheduling strategies [72, 73, 74], such as:

- The round-robin scheduler, in which each MS receives the same amount of PRBs, which is therefore a fair assignment from a resource perspective.
- The max-min scheduler, which maximizes the minimum throughput of the MSs, resulting in high degree of fairness from a throughput perspective.
- The proportional fair scheduler and its application to OFDMA , which achieves a compromise between fairness and throughput maximization.

Proportional fair scheduling and its adaption to OFDMA [75] [76] is used in this work due to its wide adoption and is introduced in more detail in Section 4.2.

2.7 Research problem

To define the research problems of this Thesis, this section first provides a summary of this chapter with the intension of showing how the individual aspects are interrelated:

- Section 2.1 introduced the network architecture of LTE-A as a state-of-the-art mobile radio communication network. It was shown here that in LTE-A systems, each BS by default independently assigns the PRBs to the MSs attached to it.
- Section 2.2 described the fundamentals of mobile network capacity. It was pointed out that the network capacity can be increased by means of network densification and (or in combination with) interference mitigation.
 - In the direction of network densification, heterogeneous networks (Section 2.3) as a strategy for network densification have been introduced.
 - Regarding an increased network capacity by means of interference mitigation, Section 2.4 introduced different approaches to interference mitigation. As described in Section 2.4, interference mitigation often makes use of coordination and Multiple Input Multiple Output (MIMO) (and combinations of it). Section 2.5 correspondingly described the different MIMO techniques in detail.
- Orthogonal Frequency Division Multiple Access (OFDMA) and scheduling, described in Section 2.6, sets the framework for how MIMO and Coordinated Multi

Point (CoMP) are applied. As it has been shown in Section 2.6, all relevant mobile radio networks standards make use of OFDMA, which underlines its importance in the design of new algorithms.

This work is related to applying Coordinated Beamforming (CBF) as one CoMP technique in a heterogeneous network, with a special focus on a detailed modelling of a large-scale multi-carrier network. It has three main objectives:

1. to determine and describe the factors that influence the performance of CBF in terms of increasing the network capacity in a heterogeneous network,
2. designing a linear, non-iterative precoding algorithm for the MIMO interference channel, tailored for the usage in heterogeneous networks and
3. designing a computationally efficient implementation of the scheduling process for CBF in a heterogeneous network.

These individual objectives are motivated as follows:

1. The first objective is based on what has been described in Section 2.4:
 - The work presented in [6] and [47] underlines the effect which the network topology and practical network conditions have on the performance of CoMP schemes. The impact of the network topology on the performance of CBF should therefore be determined.
 - The existing simulation results [30, 44, 45, 46] show huge differences which are caused by different modelling of the network.

Therefore this work is supposed to be executed under a set of important assumptions made for a correct modelling of large-scale multi-carrier networks:

- A frequency selective radio channel
- An OFDMA multi-carrier system
- A multitude of MS, served by time and frequency multiplexing of radio resources by means of scheduling
- A frequency selective scheduling
- A large number of BSs
- Cell Range Expansion (CRE)

- A linear and non-iterative precoding technique that is capable of covering the full range of interference suppression from ZF (full suppression) to MRT (no suppression)
- Proportional fairness among the throughput of MSs has to be achieved

The combination of these assumptions makes an analysis complex. However, a large-scale system is characterized by this set of assumptions and each of them can heavily impact the performance of CBF. This objective will be addressed in Chapters 5 and 7, using a detailed simulation software described in Section 3.

2. With respect to the second objective (designing a precoding algorithm) it was stated above that a linear and non-iterative precoding technique is required. This decision is based on the following background: *Linear* precoding is the basis of all major contemporary mobile radio systems, including LTE-A and 5G NR. Although non-linear precoding could offer additional gains, it is unclear if and when it might reach commercial standards. *Non-iterative* precoding refers to the usage of a precoding algorithm than is able to generate precoders in a non-iterative computation. Under the dynamic conditions described above it considered as unrealistic to execute iterative precoding algorithms until they converge. This objective will be addressed in Chapter 4.
3. As it will be shown in Chapter 6, the scheduling process in the considered scenario can be highly demanding from a computational point of view. The scheduling has to be executed in real-time for the following reasons: Firstly, the radio channels to the MSs fluctuates heavily due to small-scale or also called fast fading [77]. A change in the radio channels requires updating precoders, as e.g. Equation 2.9 shows. Secondly, the scheduling happens on very short-time frames (e.g. one millisecond in the case of LTE-A) especially in order to achieve a low latency and to be able to follow the changing radio channels. As described in Section 2.6, a scheduling decision comprises also the selection of the precoder to be used. As a result, the calculation of a scheduling decision, including the generation of precoders is required within one millisecond. This motives the third objective, which will be addressed in Chapter 6.

This work is performed under the assumption of perfect channel knowledge and link adaptation, for the following reason: Imperfect or limited channel knowledge and correspond-

ing errors in the link adaptation can be an impairment to CoMP [78]. However, channel estimation is implementation dependent and fundamentally different for TDD compared to FDD systems [79]. Using for example only the limited information available in LTE-A FDD systems [32], might affect the performance, such that other performance influencing factors cannot be determined any more.

Chapter 3

Methodology

To investigate the influence of a technology such as Coordinated Beamforming on the capacity of a mobile communication network there are three different options:

1. A field trial: Using a realistic (e.g. prototypical) implementation under defined test cases with and without Coordinated Beamforming (CBF) in order to compare the differences.
2. An analytic model: In case a mathematical description of the complete system can be defined, the impact of CBF can be calculated using this model.
3. Computer simulations: By simulating the behaviour of real networks in computer software, CBF can be investigated similarly to a field trial but with reduced effort.

Out of these options number one is in-feasible because of the high effort that it would require. Defining an analytic model that covers the whole complexity of a full mobile communication system is expected to be extremely difficult. Computer simulations offer a reduced complexity and effort compared to both other solutions and were therefore chosen here. This chapter describes computer simulations in detail.

3.1 Overview and basic principle of system level simulations

This section describes computer simulations of mobile communication systems. After introducing the principle of simulations the subsequent subsections give details about the System Level Simulations (SLSs) used for the work presented here.

Simulations of mobile communication networks can be classified into four groups [80]. Link-level simulations (Class IV in [80]) concentrate on the detailed simulation of one single link e.g. between a BS and an MS. SLSs (Class III) simulate multiple Base Stations (BSs) and multiple Mobile Stations (MSs) with detailed radio channel models but simplifications on link level (e.g. the performance of modulation and coding schemes is not simulated but obtained from look-up tables). MSs in this case are normally placed at static locations. Dynamic SLSs (Class II) use more simplifications in order to be able to simulate longer time scales which are necessary for using non-static MSs. Protocol Level Simulations (Class I) finally require even more simplifications on lower levels (e.g. frequency flat radio channels) to be able to simulate the time frames necessary for the analysis of a higher layer protocol, e.g. Transmission Control Protocol (TCP), performance.

As the performance of CBF highly depends on the characteristics of the radio channel, an investigation requires a detailed modelling of it. Additionally, a detailed modelling of the network topology in a multi-cell environment is required. Out of this combination, SLSs (Class III in [80]) are a suitable tool in this context.

SLSs are mainly used to determine the capacity of a network. Capacity in this context is defined as the total amount of data the network can transport under full load and is also called "system throughput" in [80]. For the work presented here, an Long Term Evolution Advanced (LTE-A) SLS which is referred to as Deutsche Telekom System Level Simulator (DT SLS) is used. It applies the following basic principles, which will be explained in more detail in Section 3.4:

1. The BSs of the network are placed according to a defined network layout. Although any kind of network layout is possible, often standardized layouts as described in Section 3.2 are used.
2. The MSs are dropped within the simulation area. Also in this case often standardized distributions are used. To model the variety of different locations of the users in real networks, the dropping of the MSs often contains a random component.
3. The MSs are attached to the BSs. This normally happens based on the downlink received signal strength of each MS.
4. It is by default assumed that all MSs request as much data as possible from the BSs. This is called full buffer simulation as the BSs always have a filled buffer

for transmission. As this happens in all BSs in the simulation, the network is fully loaded. This also causes that all MSs experience a high level of interference.

5. The scheduler in the BSs assigns the Physical Resource Blocks (PRBs) to the MSs and selects an Modulation and Coding Scheme (MCS) for each MS.
6. The radio transmission from the BSs to the MSs is simulated for a certain duration (normally in the range of hundreds of milliseconds). A detailed modelling of the radio channel by calculating the channel transfer function from the BSs to the MSs is used here. This is important as the characteristics of the radio channel strongly influence the performance of transmission-related technologies as MIMO techniques including beamforming and also CBF.
7. By calculating the Signal to Interference plus Noise Ratio (SINR), the probability that a transmission to an MS was successful can be calculated. If a transmission was not successfully decoded, a retransmission has to be initiated.
8. This process finally results in a number of bits that have been successfully received by each MS which is the one of the Key Performance Indicators (KPIs) of the simulation results (see Section 3.5).
9. To average the effects of different MS locations the same simulation is often repeated several times with a new drop of the MSs locations.

3.2 Network layout

Figure 3.1 shows an example for a network layout that is often used in LTE-A SLSs, and therefore also in the DT SLS. The network consists of seven Macro Base Station (MBS) sites with an Inter Site Distance (ISD) of 500m which is typical for urban networks. Each site hosts three BS sectors which can all use the complete frequency band and perform independent scheduling. Thus, each sector is modelled as a separate MBS in the DT SLS. Without additional means MSs near the edge or the simulation area (e.g. an MS located at $x = 0.5$ km and $y = 0.4$ km in Figure 3.1) experience lower interference than other MSs (as less BSs are in the vicinity of these MSs) which is not realistic as real networks would continue beyond this point. There are two options to avoid this effect. The first option is to analyse only the performance of MSs within an inner area of the simulated network. For these MSs a realistic interference situation is assumed. However,

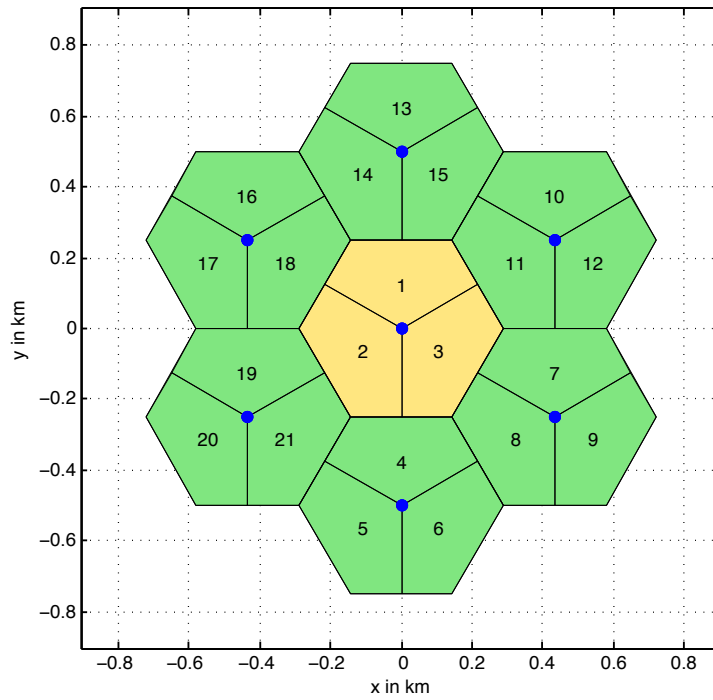


Figure 3.1: Deutsche Telekom System Level Simulator: Example for Network Layout

this approach has the effect that many MSs are simulated while only a (often rather small) proportion is analysed and is therefore not favourable from the computational complexity point of view.

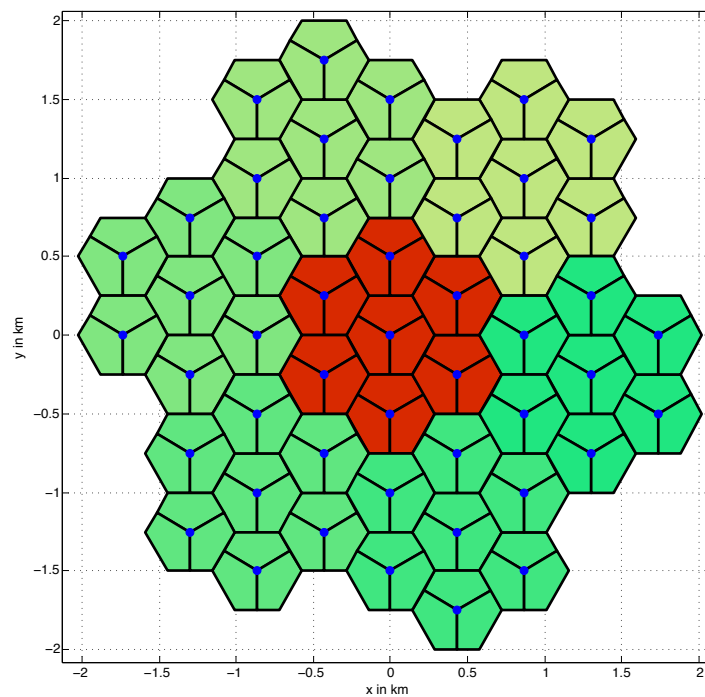


Figure 3.2: Deutsche Telekom System Level Simulator: Wrap Around Technique

The second approach is the so-called wrap around technique which is depicted in

Figure 3.2. Here the network including the MSs is set up as usual (red area in Figure 3.2). Afterwards the complete network is copied six times and arranged around the original network. The six copied parts are not simulated separately, instead they are an exact copy of the original network including the propagation and the scheduling. Therefore, they cause only very limited additional computational complexity. As a result, the interference situation within the original network is now realistic also in the outer area and all MSs within this part can be used for analysis.

3.3 Channel model

The DT SLS applies the Spatial Channel Model which is used in Third Generation Partnership Project (3GPP) [81] and which is also the basis for the International Telecommunication Union Radiocommunication Sector (ITU-R) Urban Macro and Urban Micro channel model [14]. It is based on the fact that radio signals propagate along either a direct path or a reflection at a scatterer. The model assumes a certain number of paths (e.g. six in an urban scenario) between an MS and a BS, each one of them enabled by one scatterer. Each path consists of a number of subpaths (20 in an urban scenario). Figure 3.3 shows this principle which aims at modelling the channel between the BS on the left side and the MS on the right side. In the figure the solid line between the BS and the MS represents one of the N (e.g. six) propagation paths and the two dashed lines represents two of the M (typically 20) subpaths. For each subpath there is an Angle of Departure (AoD) which describes the angle under which the path leaves the BS and a corresponding Angle of Arrival (AoA) at the MS. The subpaths belonging to the same path have only a slightly varying AoA and AoD, representing the fact that they belong to the same scatterer. The paths themselves have a higher variation in AoA and AoD. It is assumed that a signal leaving the BS antenna arrives at different times via the N paths at an MS antenna, whereas the signals of the M subpaths within one path arrive simultaneously. For this reason each path n is associated with a delay factor τ_n .

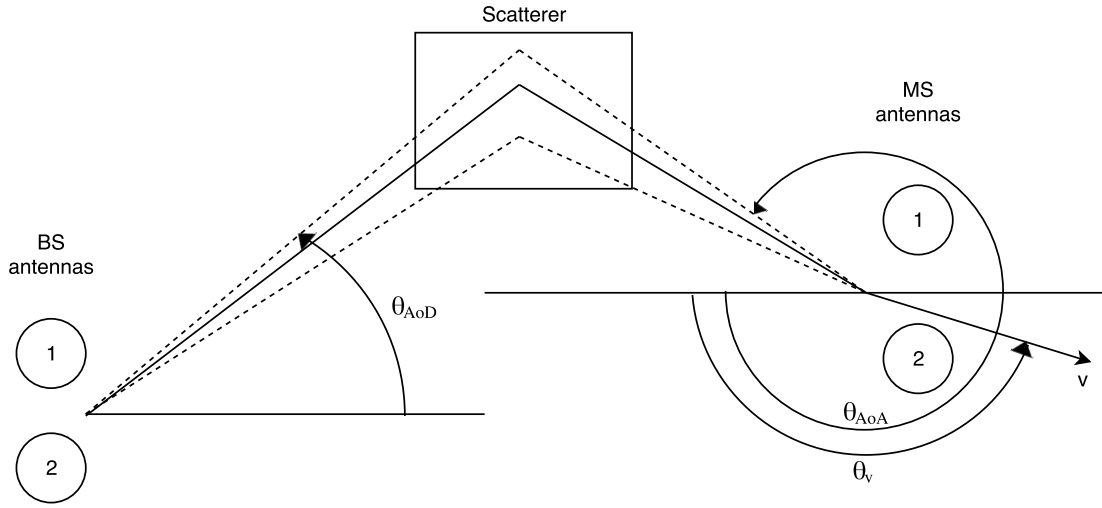


Figure 3.3: Spatial Channel Model: The radio propagation is modelled via paths and subpaths between the antennas of the transmitter and the receiver

Equation 3.1 describes how the channel coefficient for a path n between one receive antenna u and one transmit antenna s is calculated at time instance t . It is also dependent on the wavelength, represented by the wave number k ($2\pi/\lambda$ with λ being the wavelength).

$$\begin{aligned}
 h_{u,s,n,k}(t) = & \underbrace{\sqrt{\frac{P_n \sigma_{SF}}{M}} \sum_{m=1}^M}_{\text{Part 1}} \underbrace{\left(\sqrt{G_{BS}(\theta_{n,m,AoD})} e^{j(kd_s \sin(\theta_{n,m,AoD} + \phi_{n,m}))} \right)}_{\text{Part 2}} \\
 & \cdot \underbrace{\sqrt{G_{MS}(\theta_{n,m,AoA})} e^{j(kd_u \sin(\theta_{n,m,AoA}))}}_{\text{Part 3}} \cdot \underbrace{e^{jk\|v\| \cos(\theta_{n,m,AoA} - \theta_v)t}}_{\text{Part 4}}
 \end{aligned} \tag{3.1}$$

As the equation is complex, it is divided into parts:

- Part one allocates the power to the path. This happens by taking into account values that have been calculated beforehand, namely P_n (the power per path) and σ_{SF} for the shadow fading. The values are divided by M (the number of subpaths), as in the following the contributions from the individual subpaths will be summed up.
- Part two describes the effects at the BS side per subpath: G_{BS} is the antenna gain of the BS in the direction of the subpath $\theta_{n,m,AoD}$ and therefore influences the amplitude of the subpath. The second half of part two describes the effect of the AoD on the phase of this subpath. In it, k represents the wave number, d_s the distance from the antenna s to the reference antenna point at the BS and $\phi_{n,m}$ a random phase offset for this subpath.

- Part three describes the same effects on the MS side.
- Part four contains the effects which are caused by the movement of the MS over time, described by its speed $\|v\|$ and the angle θ_v , representing its direction.

For details on the calculation of the variables in Equation 3.1 the reader is referred to [81].

The output of the Spatial Channel Model is a representation of the channel impulse response in time domain (for each link between the two antennas) as depicted in Figure 3.4. Each path in the model results in a signal arriving after a delay τ_n . Over time, t the individual components of the channel can vary drastically due to the movement of the MS, represented by Part four of Equation 3.1. The channel depicted in Figure 3.4 can be converted into its equivalent in frequency domain (depicted in Figure 2.11) via the Fourier Transformation.

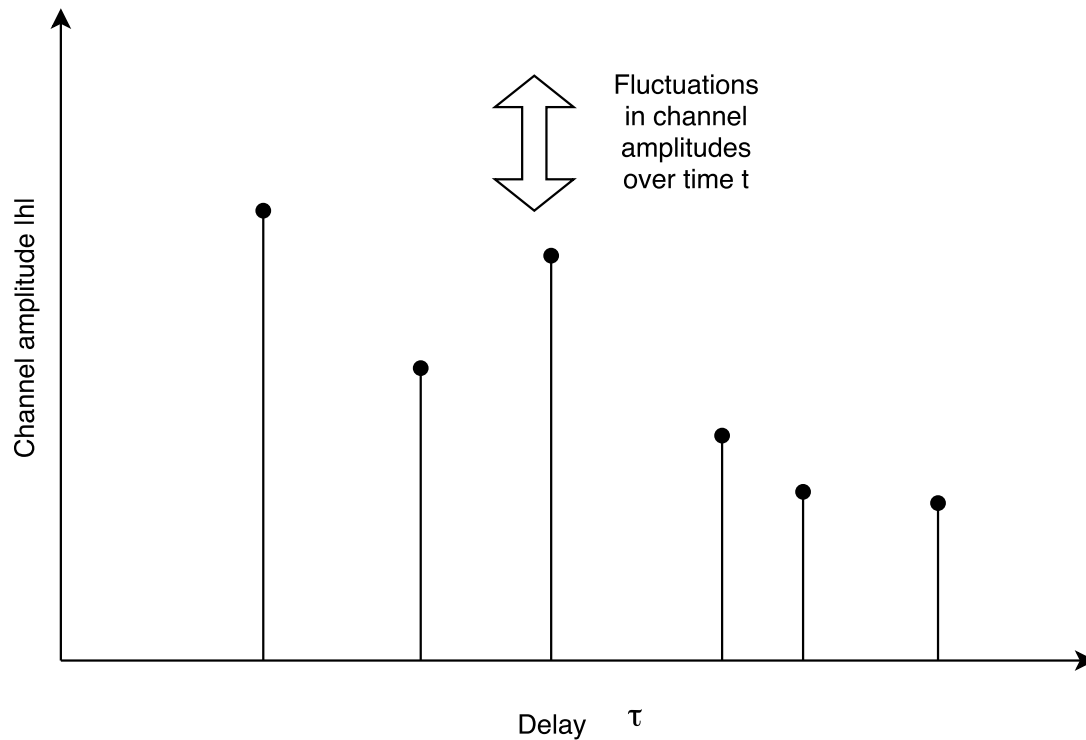


Figure 3.4: Output of the Spatial Channel Model in time domain

3.4 Simulation process

After Section 3.1 introduced the basic principle of the simulation process, Figure 3.5 shows the simulation process in more detail.

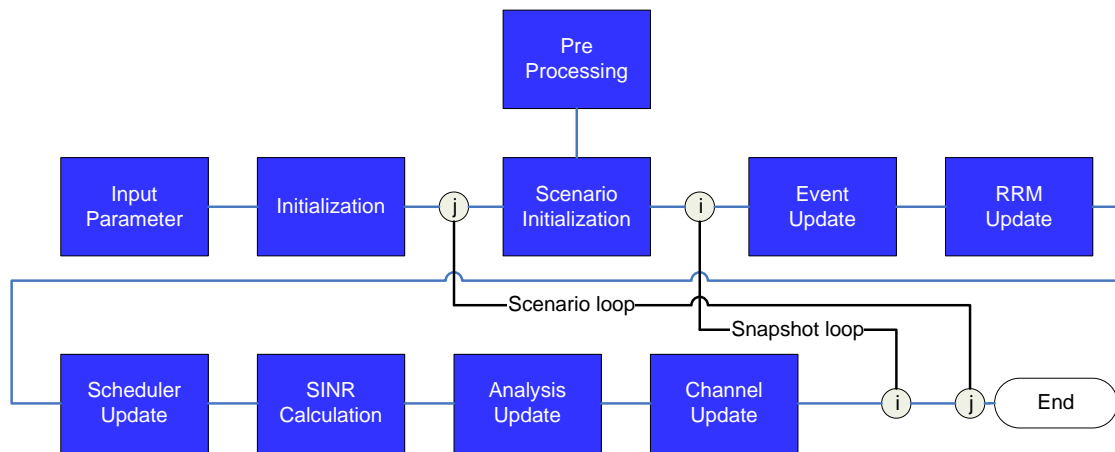


Figure 3.5: Deutsche Telekom System Level Simulator: Block diagram

The following steps are executed within a simulation:

1. **Input Parameter:** Provides the configuration of the simulation.
2. **Initialization:** Sets up all data structures that will be used within the simulation. This includes the set-up of the network layout (especially BS locations).
3. **Preprocessing:** The simulation area is divided into pixels. Before starting the simulation a set of parameters is calculated per pixel which can then be used during the simulation. These pre-calculated parameters contain per pixel and per BS:
 - The power received at the corresponding pixel from the corresponding BS. This value is calculated based on the propagation model.
 - Shadow fading: A value which defines an offset to the received power in order to model fading caused by shadowing effects (e.g. from buildings)
 - The angular spread: This parameter is used by the channel model (see Section 3.3) to generate the AoAs and AoDs.
 - The delay spread: A value related to the angular spread which defines how much the different reflections vary in terms of delayed arrival at the pixel.
4. **Scenario Initialization:** The MSs are now dropped into the network. This happens by default randomly, a second important way to place the MSs is the so-called hotspot distribution (for more details see Section 3.6). According to the values provided by the preprocessing, the power an MS receives from each BS can be calculated. Also the impulse response of the channel from each BS to the MSs can be calculated by the channel model using the angular and delay spread provided

by the preprocessing. By transforming the impulse response into the frequency domain via the Fast Fourier Transformation (FFT) the channel transfer functions are obtained.

5. Event Update: This part can contain functionalities that implement an event that should occur during a simulation (e.g. the outage of a BS).
6. Radio Resource Management (RRM) Update: Decides which MS connects to which BS. By default all MSs connect to the BS they are receiving with the strongest power. To implement Cell Range Expansion (CRE) for Pico Base Stations (PBSs) (see Section 2.3), a CRE offset can be used here. An MS will then connect to a PBS even if the received power is up to the CRE offset lower than the power received from the strongest MBS.
7. Scheduler update: Here the scheduler assigns the PRBs to the MSs. Scheduling often relies on feedback from the MSs. Therefore, the scheduling in the DT SLS consists of the following steps:
 - Analysing feedback from the MSs which was generated earlier (generation of MS feedback will be described in block "SINR calculation", where it takes place). Out of the feedback the scheduler can calculate the so-called supportable rate which indicates the expected throughput per MS and PRB.
 - Scheduling of re-transmissions: If a previous transmission failed, PRBs need to be reserved for retransmission which is a part of Hybrid Automatic Repeat Request (HARQ). The MSs acknowledge successfully received data and request a retransmission in case of an erroneous reception. If a retransmission takes place, an MS can combine the signals from the initial transmission and the retransmission (soft combining with chase combining or incremental redundancy).
 - The resource assignment itself. Based on different strategies (e.g. proportional fair, round robin), the PRBs are assigned to the MSs.
 - After the scheduler has decided which PRBs should be used for which MS the transmission parameters have to be defined. This consists of two parts:
 - Link adaptation: The scheduler chooses an MCS which fits best to the SINR at the scheduled PRBs. It should be noted that according to the

Long Term Evolution (LTE) standard it is only possible to select one MCS per MS. If an MS has been assigned multiple PRBs with varying SINR (or if the SINR varies within one PRB) it is not possible to choose different MCSs for the different PRBs. Instead, a compromise for the MCS must be found. There are two options for link adaptation in the used DT SLS:

- * Ideal link adaptation: The scheduler chooses the best MCS directly before the transmission using perfect channel knowledge. This option does not reflect a realistic implementation. However, it can be used to find the upper bound of the performance.
 - * Conventional link adaptation: In this mode the scheduler analyses the feedback from the MS. Out of the feedback it estimates the SINR that the MSs is experiencing and selects an MCS. This behaviour models the situation in real networks. Due to several reasons (e.g. delay in the MS feedback, quantization, feedback granularity in frequency domain) the MCS selected is not necessarily the best one.
- Precoding: The scheduler defines the precoder which can be designed to achieve different goals as described in Section 2.5.
- Allocation of a HARQ-process which will monitor the correct or incorrect reception, report a corresponding Acknowledgement (ACK) / Negative Acknowledgement (NACK) and take care of possible retransmissions.

8. SINR calculation: For each MS the following calculations are executed:

- The PRBs which were assigned to the corresponding MS by the scheduler are being identified.
- Calculation of the useful signal: For the sub-band which is used by these PRBs a detailed calculation of the SINR is performed: As already mentioned in the description of the preprocessing, the channel and the propagation model are independent functionalities. The propagation model provides the power the MS receives from the BS while channel model describes the characteristics of the frequency selective channel. To maintain this separation the channel transfer functions are normalized so that the average amplitude of a sample of the channel transfer function equals one. To calculate the SINR, the output of both models has to be combined which is implemented as follows: The

channel transfer function from the serving BS to the MS is obtained for the sub-band. It is then multiplied by the precoder the BS uses for this MS. The result is the so-called effective channel transfer function. The effective channel transfer function is then multiplied by the power the MS receives from the serving BS in this sub-band (which was calculated by the propagation model). If the MS uses more than one antenna also the receive combining vector needs to be multiplied with the result. The calculation finally ends in a not normalized effective channel transfer function from the BS to the MS for this sub-band.

- Calculation of the interfering signals: A corresponding calculation is done for the interfering channels. It is determined which other BSs also transmit on the same PRBs simultaneously. For each BS the transfer function of the interfering channel to the MS is calculated, multiplied with the received power and the precoding vectors. To reduce the computational effort this calculation is normally only executed for a set of the strongest interferers. For all other interfering BSs a simplified calculation is used where the channel transfer function is not taken into account, resulting in a flat channel for these BSs.
- Calculation of the noise power: The noise power depends on the characteristics of the receiver at the MS side. Based on the configured assumptions about the receiver noise figure, the noise power in the receiver is calculated.
- After executing these three calculations the not normalized effective channel transfer function of the serving as well as the interfering links and the noise power is available. The channel transfer functions exist in a sampled format (the spacing between the samples is by default 40kHz). For each of these samples an SINR value is now calculated by dividing the useful power by the interfering power and the noise power. These values are counted in the SINR distribution (see Section 3.5).
- Using the Mutual Information Effective SINR Mapping (MIESM) interface [82] the calculated SINR values are mapped to one single effective SINR value. With the help of look-up tables derived from link level simulations and the MCS which was set by the scheduler, the probability of a successful reception can then be determined.
- A random number between 0 and 1 is generated. If it is higher than the prob-

ability of a successful reception an erroneous reception is counted. The according feedback (NACK) is generated. Otherwise the data was successfully received. In this case an ACK is generated and successfully transmitted bits are counted as MS throughput.

Besides, this block also contains the generation of MS feedback. According to the SINR it experiences, an MS creates a feedback report which is stored and after a configurable delay processes by the BS scheduler (see first step at scheduler update).

9. Analysis Update: Collects the information that will form the output of the simulation. Especially the values to calculate the KPIs (see Section 3.5) are stored here.
10. Channel Update: The channel transfer functions are updated here. This is necessary to model the effects caused by the movement of the MSs. By default, the MSs have a speed of 3 km/h in a random direction, which represents a so-called nomadic user [?].
11. The steps 5 to 10 are now repeated within the so-called snapshot loop. The goal is to simulate the created network with all its functionalities for a certain time in order to get statistically reliable results. The number of snapshots that are necessary depends on the dynamics in the network and is normally in the range of 200 to 600. As one snapshot simulates a duration of one millisecond this means that the behaviour in the network is simulated for 200 to 600 milliseconds.
12. The steps 3 to 11 are repeated within the so-called scenario loop. This is necessary as the positioning of the MSs, the propagation and the channel model contain random components. To get statistically reliable results normally 3 to 6 iterations are necessary.

3.5 Key performance indicators

This section gives an overview about typical KPIs used in the DT SLS. It should be noted that the DT SLS is not limited to these outputs. Any kind of analysis functionality can be added to the DT SLS so that all kind of information that exists during a simulation can be logged and later on be analysed.

The most common KPI is the Cumulative Distribution Function (CDF) of the MS throughput as depicted in Figure 3.6. Often the following values are obtained from the graphs:

- 50 percentile: This is the median value of the MS throughput. 50% of all MSs achieve a throughput higher than this value and 50% a lower throughput. When comparing two different simulation results it is often reasonable to compare the median and not the mean throughput. The mean throughput can be biased by a small number of MSs which obtain a very low or very high throughput. This effect does not occur for the median. In Figure 3.6 the 50 percentile of the throughput distribution corresponds to approximately 600 kbit/s.
- 5 percentile: This is the throughput of MSs with the lowest performance. It is often a target to improve the 5 percentile of the throughput distribution as a low value here indicates that there are MSs with an (maybe unacceptable) low throughput. As MSs with a low throughput are often located at the cell edges, the 5 percentile of the MS throughput distribution is often also called the cell edge throughput. In Figure 3.6 this value corresponds to approximately 100 kbit/s.
- 95 percentile: This is the throughput of the MSs experiencing the best performance. This value is out of the x-axis range in Figure 3.6 as it corresponds to approximately 6 Mbit/s.

All throughput values that are recorded within a simulation are based on the number of successfully received bits (the so-called "goodput").

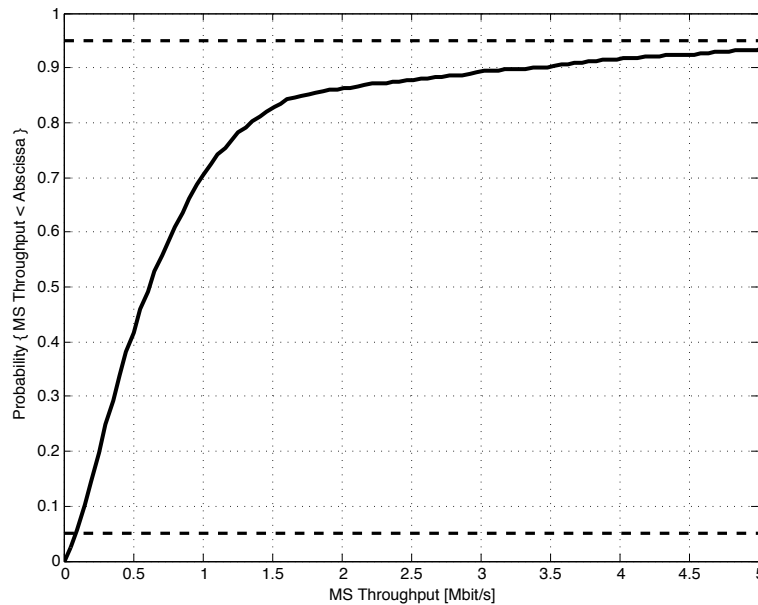


Figure 3.6: Key Performance Indicators of the Deutsche Telekom System Level Simulator: Example for Cumulative Distribution Function of Mobile Station Throughput

Besides the percentiles also the mean MS throughput is an important metric. For the simulation results which are the basis for Figure 3.6 the mean MS throughput is 1.4 Mbit/s which also shows the mentioned difference between mean and median.

The fairness of the scheduling process is analysed by calculating the normalized throughput distribution which is depicted in Figure 3.7. The blue line indicates a commonly used fairness criterion which has been defined in [83]. The normalized throughput distribution should be continuously below this line to comply with the fairness criterion. As this is not the case in Figure 3.7 the distribution cannot be called fair. In addition the MS throughput distributions the following other KPIs can be obtained:

- Distribution of BS throughput. A BS can show a high throughput if it serves mainly MSs with good radio conditions, a low throughput if MSs with poor radio conditions dominate. In the worst case there are no MSs in the coverage area of the BS so the BS throughput is zero.
- Radio propagation related KPIs:
 - User Geometry: After the MSs have been dropped into the simulation area, the power each MS receives from each BS is calculated. For each MS the received power from its serving BS is then divided by the sum of powers received from other BSs and the noise. The value obtained is called the wide band SINR. The

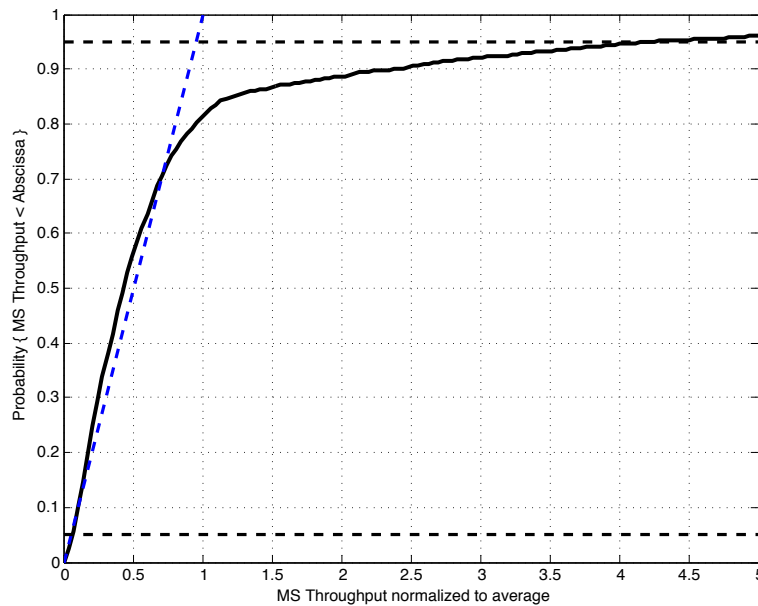


Figure 3.7: Key Performance Indicators of the Deutsche Telekom System Level Simulator: Example for the Cumulative Distribution Function of the normalized Mobile Station Throughput

so-called user geometry is defined as the distribution of all wide band SINR values of all MSs in the network at the beginning of the simulation. It is not influenced by the scheduling (as this has not been executed at that time) and the frequency-selectivity of the radio channel, but e.g. by the transmit power of the BSs, the antenna models, the radio propagation model and the locations of the MSs. Therefore, the user geometry can for example be used to analyse the coverage situation in the network.

- Geometry: The geometry also contains wide band SINR values of the MSs but includes scheduling decisions. After the scheduling has taken place in the BS, all wide band SINR values of the MSs that have been scheduled are counted for calculation of the geometry. As a result the geometry contains the distribution of wide band SINR of MSs that have been scheduled. By comparing the user geometry and the geometry of all MSs the behaviour of the scheduler can be analysed. If the scheduler assigns resources to all MSs equally, independent of their radio conditions, the user geometry equals the geometry. If a scheduler e.g. prefers MSs with good radio conditions to increase the BS throughput, the geometry shows higher values compared to the user geometry.
- SINR: As mentioned, geometry and user geometry only take into account the wide band SINR. The wide band SINR only reflects the total amount of power

an MS receives by from a BS (which is calculated by the propagation model). As described in Section 3.4 the channel model defines the frequency selectivity of the channel or in other words how the wide band received power is distributed within the frequency band. The SINR distribution also reflects the channel model as it contains the SINR per MS only for PRBs which the MS has been scheduled for. When comparing user geometry and SINR distribution the frequency selective behaviour of a scheduler can be analysed. In case a scheduler is able to exploit the frequency selectivity of the channel (see Section 2.6), it selects for each MS the PRBs where it experiences the best SINR. As a result a frequency selective scheduling gain is obtained in terms of higher values for SINR compared to geometry.

3.6 Study of the propagation conditions in a simulation of a heterogeneous network

In this section the propagation conditions in a heterogeneous network, modelled according to the above mentioned description, is studied. This mainly aims at providing a better understanding of the assignment of the Pico Mobile Stations (PMSs) and the load situation in the network (number of MSs at the PBS and the MBS).

The assignment of the MSs to the BSs in LTE-A networks is based on the Reference Signal Received Power (RSRP). The BSs of the network transmit reference symbols which are received and analysed by the MSs. The MSs then connect to the BS that provides the highest received power at their locations. The transmit power imbalance between MBSs and PBSs leads to an unbalanced assignment with few users assigning to the PBSs. To limit this effect a biasing of the assignment as described in Section 2.3 was introduced: An MS is then supposed to connect to a PBS even if the power received from it is up to the value of the CRE bias lower than the received power from a MBS. Table 3.1 provides the BS parameters (transmit power and antenna gain) which were used for the results presented in the following. A strong imbalance of 23 dB in terms of Equivalent Isotropically Radiated Power (EIRP) can be observed. A CRE of 6 dB (which is a common value [84]) would limit the imbalance to 17 dB. However, SLSs results using the ITU-R Urban macro and urban micro propagation model show a relatively high number of users assigned to the PBSs (details follow below). A main reason for it are the Line of

Sight (LoS) conditions as they will be explained in the following.

Parameter	MBS	PBS
Transmit power	46 dBm	37 dBm
Max. antenna gain	17 dBi	3 dBi
Equivalent Isotropically Radiated Power (EIRP)	63 dBm	40 dBm

Table 3.1: Base Station parameters used for the study of the propagation conditions

The LoS probabilities in the Urban Macro (UMa) and the Urban Micro (UMi) propagation model are depicted in Figure 3.8. The probability that an MS within the simulation area is in LoS to a BS degrades over the distance between MS and BS.

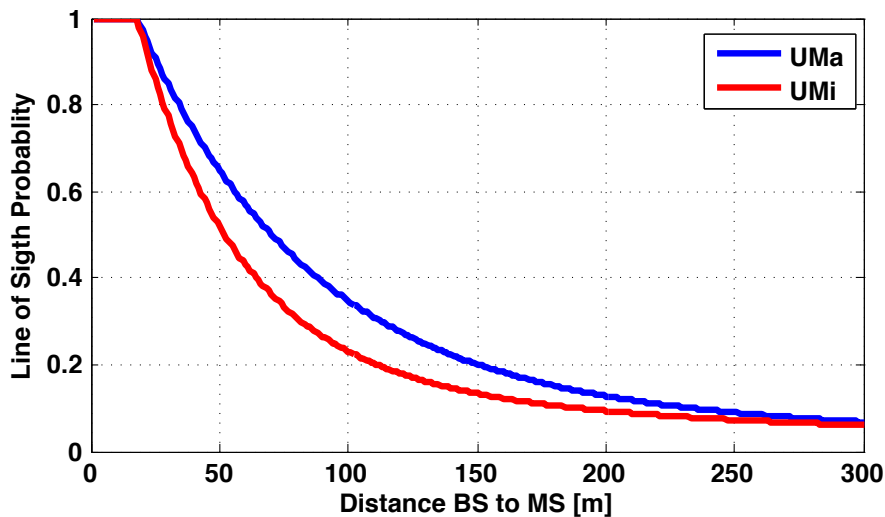


Figure 3.8: Line-of-Sight Probabilities in Urban Macro (UMa) and Urban Micro (UMi) Propagation Model

Figure 3.9 shows the influence of the LoS conditions on the pathloss between MS and BS. The difference between LoS (solid lines) and non Line of Sight (nLoS) is in the order of 20 dB. When comparing this value with the transmit power imbalance, it can be seen that LoS conditions can compensate the imbalance.

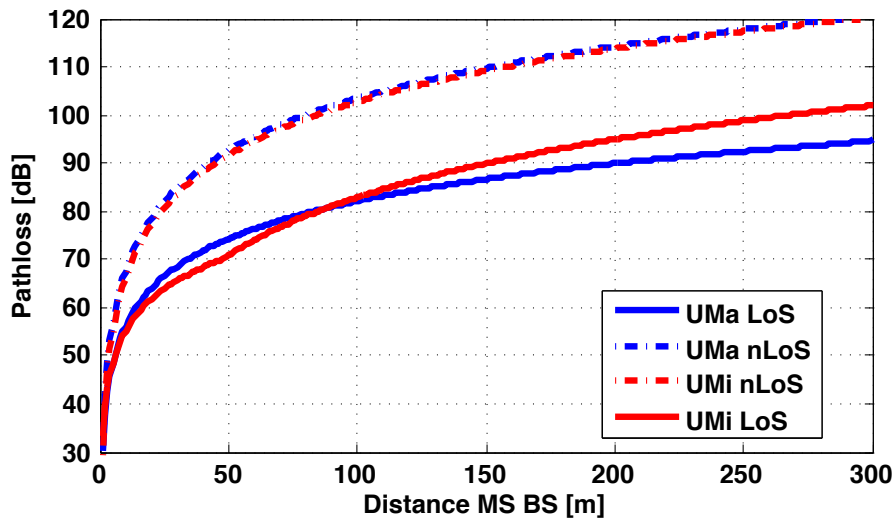


Figure 3.9: Pathloss for Line of Sight (LoS) and non Line of Sight (nLoS)

For a heterogeneous LTE-Advanced network the different pathlosses imply:

- MSs in LoS to an MBS *and* a PBS will likely assign to the MBS (due to the transmit power imbalance).
- The same holds true for MSs in nLoS to an MBS and a PBS.
- MSs in LoS to an MBS and nLoS to a PBS will most likely assign to the MBS (due to the higher pathloss of the nLoS link and the transmit power imbalance).
- For MSs in LoS to a PBS and nLoS to an MBS the situation is balanced. It depends on the detailed propagation conditions at the location of the MS whether it is assigned to the macro or the PBS.

In the following the situation will be analysed in more detail for two different deployments: In option 1 a PBS is placed 125 metres away from the MBS while in option 2 the distance is 250 metres. For a standard macro cell network with an inter-site-distance between the MBSs of 500 metres this leads to the situations depicted in Figure 3.10 and Figure 3.11. In the case of option 1 the PBSs (red points) are located at the centre of the MBS's sector while in option 2 they are located at the edge of the sector. Option 1 is therefore also referred to as PBS located at (macro) cell centre and option 2 as PBS located at (macro) cell edge. These two deployment options are selected as they represent, from an interference point of view, a good and a bad situation: In Figure 3.10, the PBSs are placed at a location with very strong signal from an MBS (causing heavy interference if not mitigated). In Figure 3.11 the PBSs are located at the cell edges, where the received

power from the MBSs is lower. In real networks, PBSs might have to be deployed at any location with a high number of users, such that both deployments are realistic.

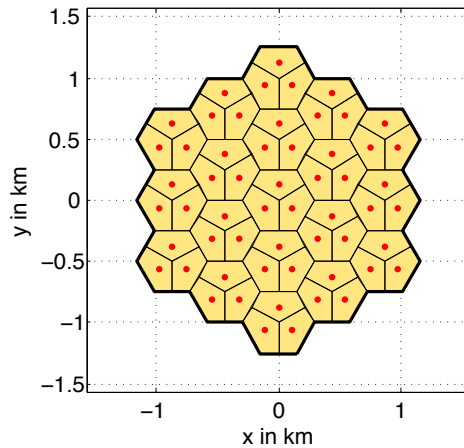


Figure 3.10: Deployment option 1: Pico base stations deployed 125 metres away from the macro base stations

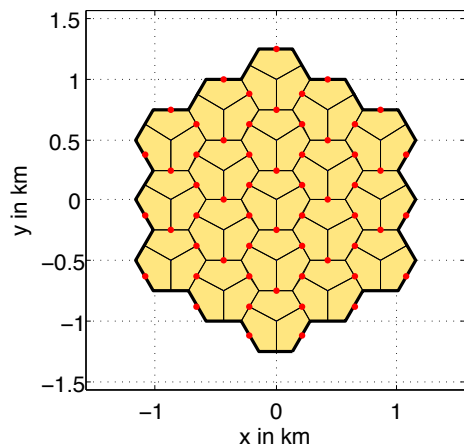


Figure 3.11: Deployment option 2: Pico base stations deployed 250 metres away from the macro base stations

The received power levels for LoS and nLoS under the assumptions from Table 3.1 are depicted in Figure 3.12 (option 1) and Figure 3.13 (option 2). Two main observations can be made:

1. Assuming LoS conditions to the MBS (solid blue line) the coverage area of the PBS is very limited, even under LoS to the PBS (approximately 20 metres for option 1 and 50 metres for option 2). The fact that the coverage area in option 1 is smaller than in option 2 fits to the common understanding that a pico cell shrinks the closer it is located to the MBS (due to the increasing signal strength of the MBS).

2. Assuming nLoS conditions to the MBS (dashed blue line) the size of the pico cell increases. A special situation occurs when LoS to the PBS is assumed: Here the region that can be covered by the PBS is larger for option 2. In option 2 only the locations with less than 75 metres distance to the PBS cannot be covered by it, while in option 1 the corresponding distance is 150 metres.

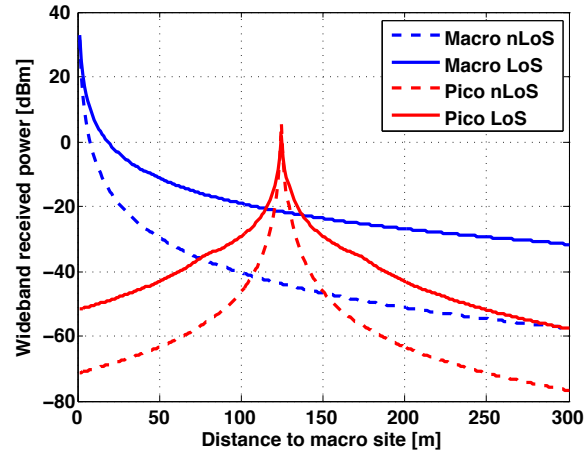


Figure 3.12: Received power levels for deployment option 1: Pico base stations deployed 125 metres away from the macro base stations

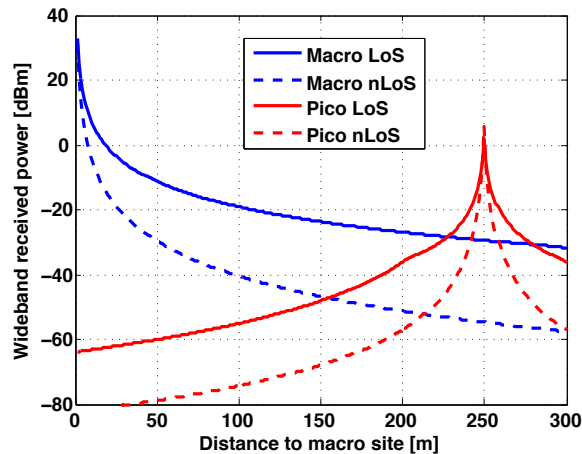


Figure 3.13: Received power levels for deployment option 2: Pico base stations deployed 250 metres away from the macro base stations

Summarizing the effects described in this section, two main factors can be seen:

- The assignment of an MS in a heterogeneous LTE-Advanced network heavily depends on the LoS conditions which the MS experiences.
- In case an MS is in nLoS to a PBS the chance that it can be served by this PBS is rather low (except it is located very close to the PBS).

In addition to the study above, also full SLSs were executed using DT SLS to investigate the assignment of MSs to the BSs in a heterogeneous LTE-Advanced network. This is especially required as some assumptions above were simplified in order to describe the effects. The antenna gain of the MBS for example depends on the azimuth and the elevation and is for many locations not at its maximum value of 17 dBi which was assumed before. In the DT SLS two different distributions of the MSs are used: A uniform user distribution where all MSs are randomly located inside the simulation area is the default case. To model the situation where an operator deploys a PBS at a location with a high density of users a second distribution was created. In this so-called hotspot distribution two third of the MSs are located in the vicinity (50 metre distance or less) of the PBSs while the remaining MSs are uniformly distributed over the simulation area (configuration 4b in [85]).

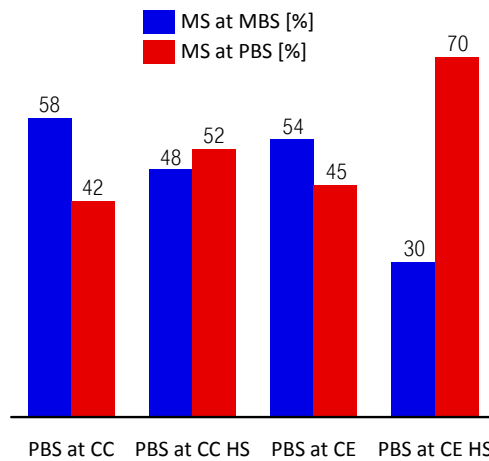


Figure 3.14: Assignment for the MSs

Figure 3.14 shows the resulting assignment in the simulation for different placements of the MSs and the PBSs:

- PBSs can be placed at the at the Cell Centre (CC) (as depicted in Figure 3.10) or at the Cell Edge (CE) (as depicted in Figure 3.11)
- The MSs can be distributed uniformly (this is default case) or with an HotSpot (HS) distribution

When comparing PBS at CC with PBS at CE (both with uniform MS distribution), only minor differences are observed. This can be explained with a balance of the observations one and two described for the received power levels above: PBS at the CE has advantages for locations where the MBS is in LoS. In parallel, PBS at the CC is advantageous if LoS

to the PBS and nLoS to the MBS occurs.

For the HS distribution differences can be observed: In the case of PBS at CC HS the PBS is only able to serve a part the MSs (two third) placed its vicinity. A main reason is the very low coverage area of the PBS when LoS to the MBS occurs (see Figure 3.10): It is often not possible to serve MSs from the PBS even if they are at a distance of less than 50 metres. For PBS at CE HS this problem does not occur (see Figure 3.11).

Figure 3.15 depicts the LoS conditions that occur in the simulation. It can be obtained that in case a MS is assigned to a PBS, it is very likely that it is in LoS to it. The trend holds true for both deployment options and for both MS distributions with minor differences.

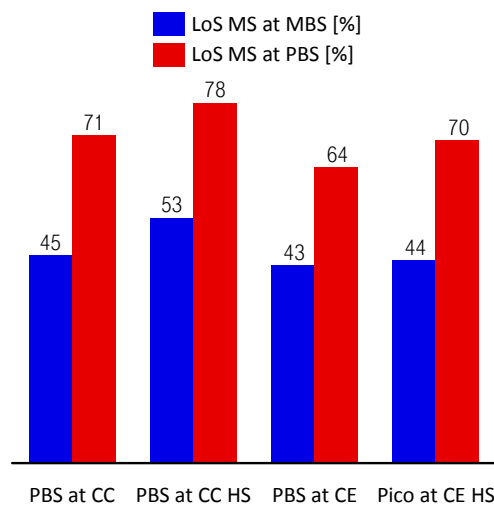


Figure 3.15: Line of Sight Conditions

Figures 3.16 to 3.22 show examples for the assignments of the four scenarios described above and the CDFs of the distances between the MSs and their serving BSs. MSs attached to a PBS are depicted in red, while MSs attached to an MBS are in blue colour. It can be seen (especially for the uniform MS distribution in Figure 3.16) that for the deployment option 1 (PBS at the cell centre of the MBS) the MSs are more widespread than for deployment option 2. This is again in line with the previous finding that in this deployment a wider area can be covered by the PBS.

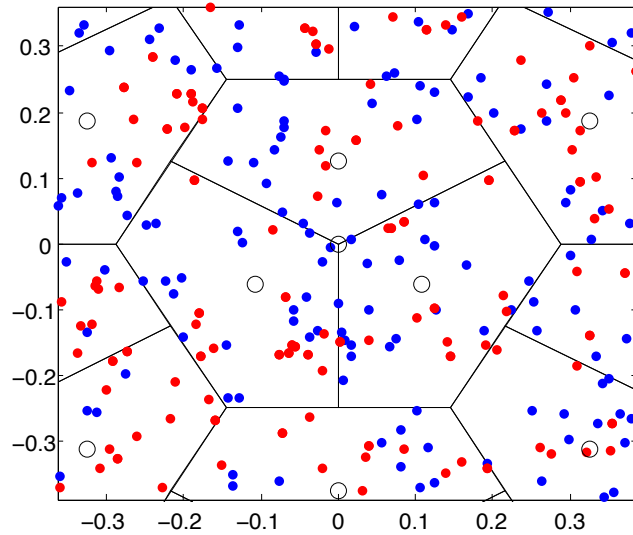


Figure 3.16: Example for an assignment of MSs for pico base stations deployed at cell centre of the macro base stations

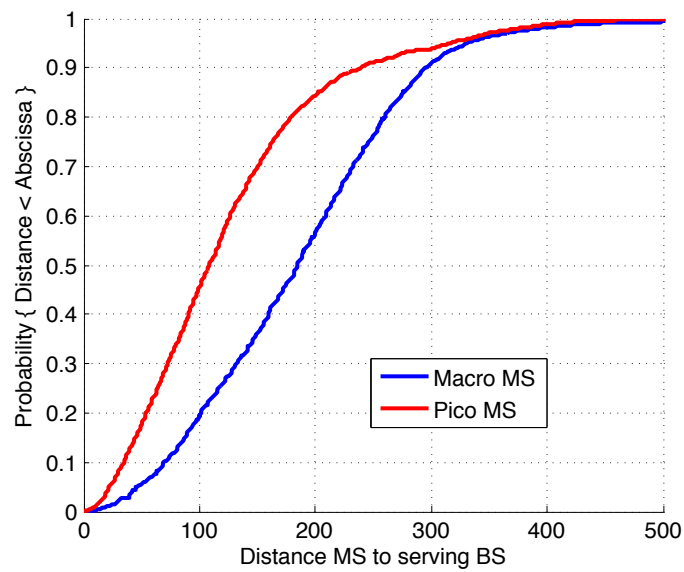


Figure 3.17: CDF of the distance between MSs and serving BSs for pico base stations deployed at cell centre of the macro base stations

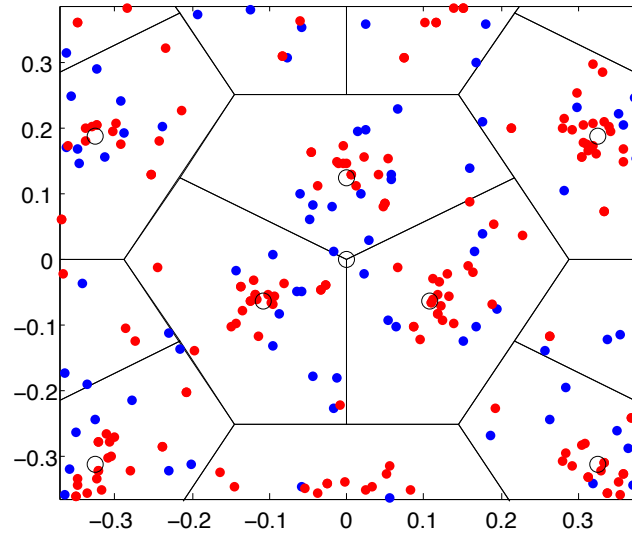


Figure 3.18: Example for the assignment of MSs for pico base stations deployed at cell centre of the macro base stations with hotspot distribution of MSs

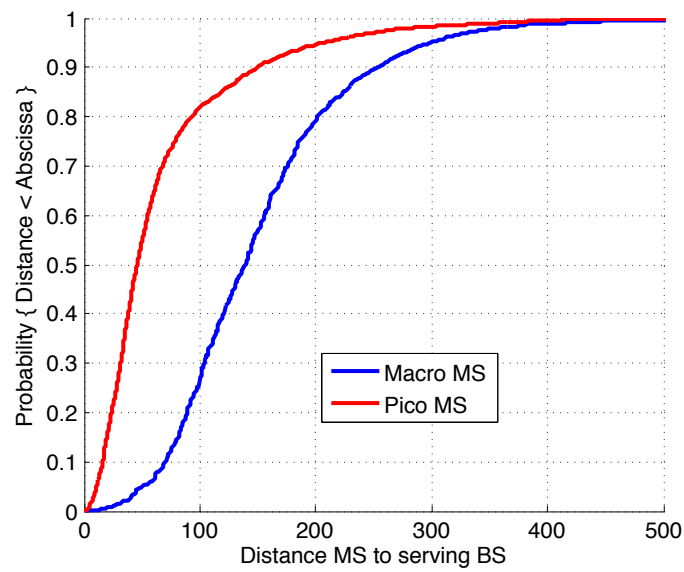


Figure 3.19: CDF of the distance between MSs and serving BSs for pico base stations deployed at cell centre of the macro base stations with hotspot distribution of MSs

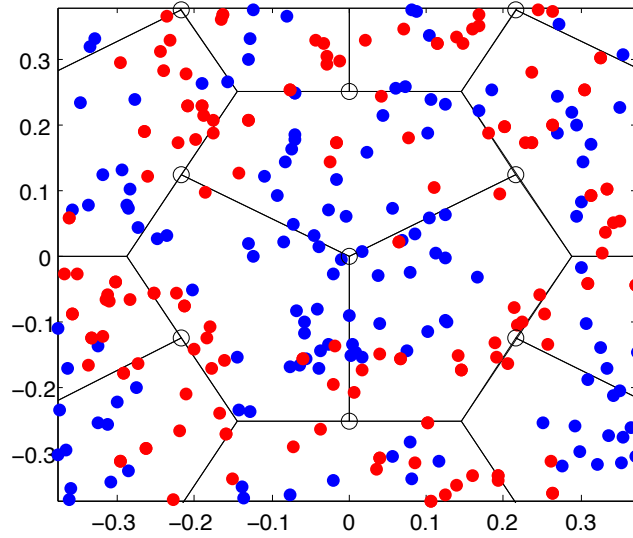


Figure 3.20: Example for an assignment of MSs for pico base stations deployed at cell edge of the macro base stations

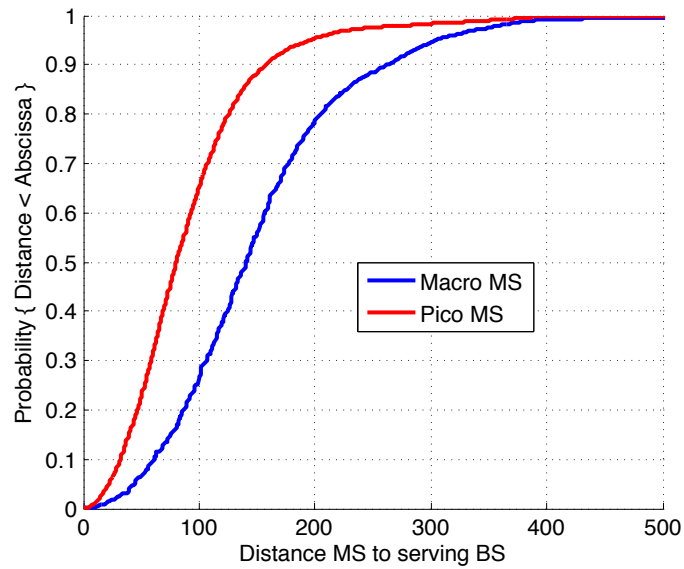


Figure 3.21: CDF of the distance between MSs and serving BSs for pico base stations deployed at Cell Edge of the macro base stations

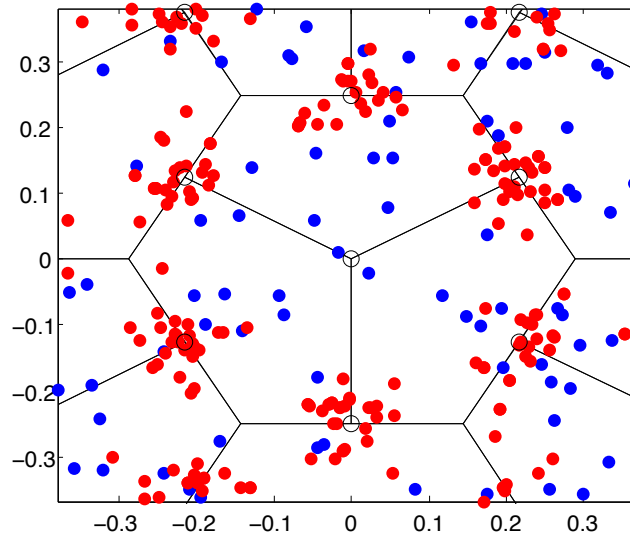


Figure 3.22: Example for an assignment of MSs for pico base stations deployed at Cell Edge of MBS with hotspot distribution of MSs

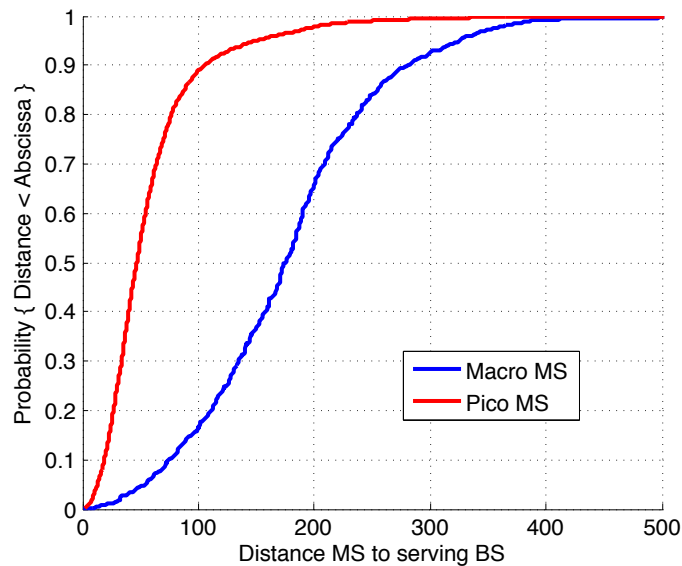


Figure 3.23: CDF of the distance between MSs and serving BSs for pico base stations deployed at Cell Edge of MBS with hotspot distribution of MSs

3.7 Calibration

SLSs are important tools used to investigate the performance of various technologies during the process of standardization. In this case, in order to have reliable and comparable results, the simulation tools used in 3GPP LTE standardization were calibrated. The calibration is based on the following process:

- In a first step, a detailed description of commonly used assumptions and settings is defined. This includes the propagation and channel model, the network layout, basic scheduling strategies and settings for required parameters such as transmit powers, carrier frequencies, channel bandwidths and Orthogonal Frequency Division Multiplexing (OFDM) parameters. The main assumptions and settings are defined in [85].
- The members of 3GPP and any other party that wants to calibrate a corresponding simulator implements a simulation on the basis of these assumptions and settings.
- Simulations are then executed and the results are compared in terms of different KPIs. As the commonly agreed assumptions and settings do not cover all aspects of a simulation in full detail, it is not expected that different simulation tools achieve exactly the same performance.

The results of the calibration in 3GPP are described in [86]. The DT SLS was not part of this 3GPP calibration activity itself. However, the simulations that were part of the calibration in 3GPP were also executed in the DT SLS. Figures 3.24 to 3.26 compare the results from other simulation tools (provided in [86]) with the results from the DT SLS.

Figure 3.24 shows the result for the User Geometry, wherein the results of the DT SLS are labelled "DTAG". As described in Section 3.5, the User Geometry is a basic measure which mainly reflects output of the propagation model. It is generated in the beginning of the simulation, such that at this point there is less potential for deviations between diverging implementations. As a result, all implementations, including the DT SLS, show very similar results.

Figure 3.25 shows the CDF of the SINR, which is additionally influenced by e.g. the channel model and especially the scheduling. It can be seen that more deviations between the individual implementations occur. The results for the DT SLS lies within the corridor of other implementations.

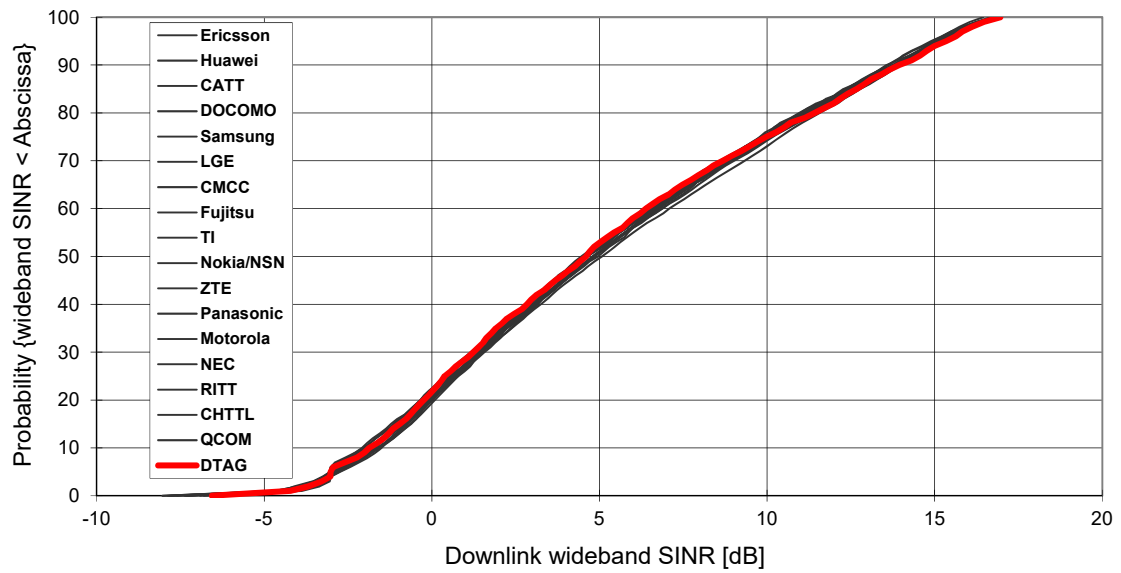


Figure 3.24: Simulator Calibration: User Geometry

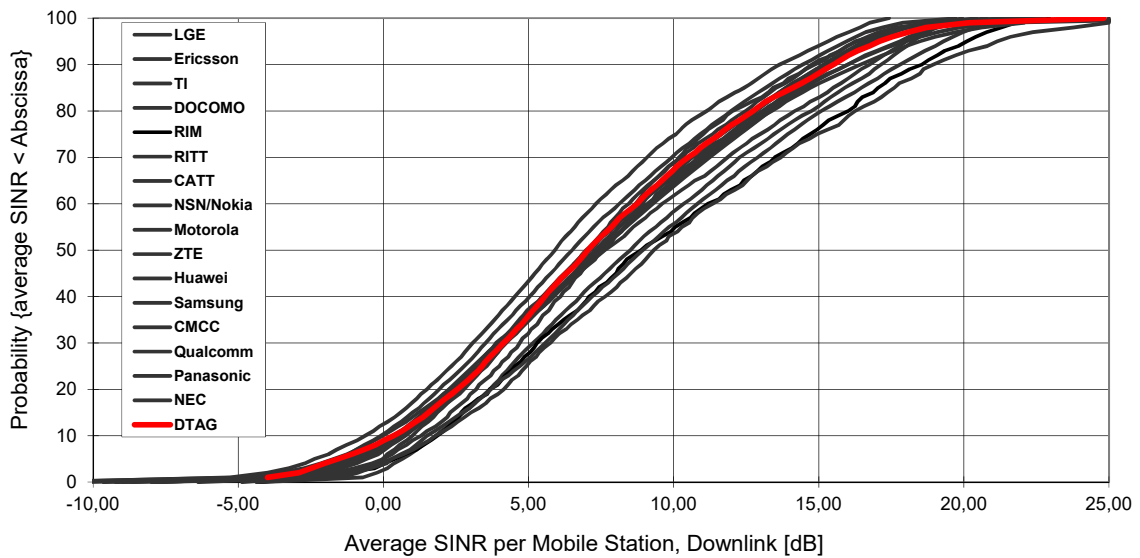


Figure 3.25: Simulator Calibration: Distribution of Signal to Interference and Noise Ratio at the Mobile Stations

Figure 3.26 shows the calibration results for the Spectral Efficiency (SE) as defined in Equation 3.2, expressed in bits per second per Hertz. The cell average SE refers to the mean throughput of one cell (i.e. one BS) in relation to the system bandwidth. The cell-edge SE refers to the five percentile of the MS throughput also in relation to the system bandwidth. Again the DT SLS lies within the range of other implementations.

$$\text{Spectral Efficiency} = \frac{\text{Throughput}}{\text{System Bandwidth}} \quad (3.2)$$

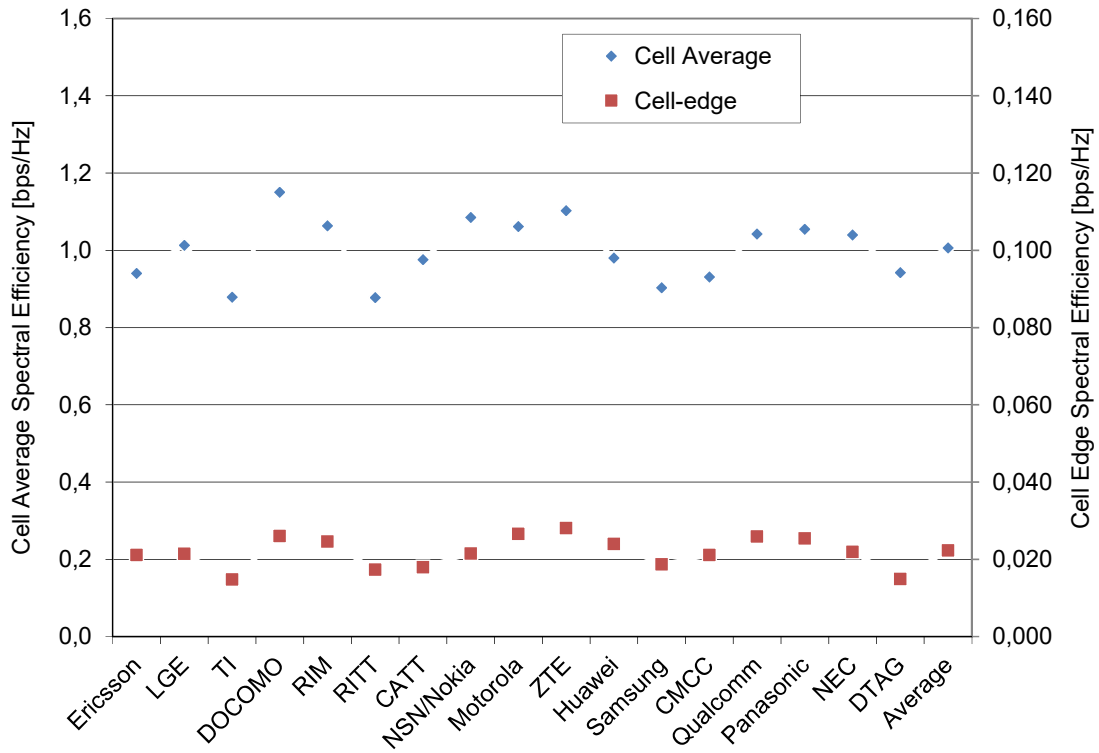


Figure 3.26: Simulator Calibration: Spectral Efficiency

Figure 3.27 shows a distribution of the MS throughput divided by system bandwidth. Within the terminology of the 3GPP calibration this is referred to as "Downlink Normalized User Throughput", as the throughput it divided ("normalized to") the system bandwidth. This terminology should not be confused with the normalized MS throughput described in Section 3.5. The values in Figure 3.27 can be interpreted as follows:

- 50% of the MSs achieve a normalized user throughput of e.g. more than $0.08 \frac{bps}{Hz}$. (As it can be seen from Figure 3.27, also other values are possible, depending on the implementation.)
- By multiplying this number with the system bandwidth, it can be converted into a throughput value.
- Equation 3.3 shows that for 10 Megahertz (MHz) system bandwidth, $0.08 \frac{bps}{Hz}$ converts into 0.8 Mbps.

Also for this metric the DT SLS lies within the range of other implementations.

$$0.08 \frac{bps}{Hz} \cdot 10MHz = 0.8Mbps \quad (3.3)$$

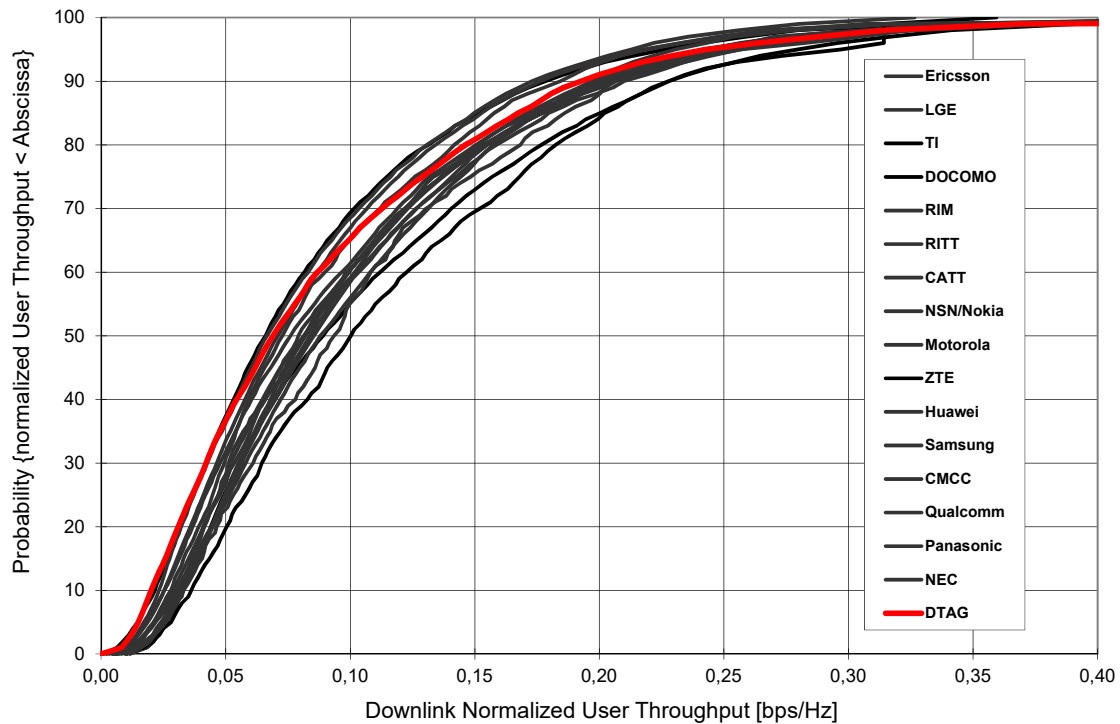


Figure 3.27: Simulator Calibration: Distribution of mobile station throughput divided by the system bandwidth (“Normalized MS throughput” in 3GPP terminology) [bps/Hz]

In summary, the DT SLS achieves results within the range of other simulator implementations used in 3GPP and is therefore regarded as calibrated.

3.8 Summary

This chapter listed the potential methodologies for addressing the research problem and then motivated why SLSs are a suitable tool in this direction. Therefore, the software to be used in the following, the Deutsche Telekom System Level Simulator (DT SLS), was described in detail.

As part of the definition research problem in Section 2.7, a set of requirements to be realized for the following analysis was established. Table 3.2 reviews these requirements and describes how they are addressed. It can be seen that most of the requirements are fulfilled by means of the DT SLS, with the exception of a suitable precoding and scheduling algorithm. The definition of a new scheduling and precoding algorithm is a contribution of this Thesis and is described in Chapter 4.

Table 3.2: Requirements for investigations of large-scale network performance

Requirement	Addressed by
A frequency selective radio channel	Part of the DT SLS as described in Section 3.3
An Orthogonal Frequency Division Multiple Access (OFDMA) multi-carrier system	Inherent part of the DT SLS
A multitude of MS served by time and frequency multiplexing of radio resources by means of scheduling	Inherent part of the DT SLS
A frequency selective scheduling algorithm	The DT SLS supports frequency selective scheduling. However, the corresponding scheduling process in the case of CBF has to be defined. The required algorithm is a contribution of this Thesis and is described in Chapter 4.
A large number of BSs	Inherent part of the DT SLS
Cell Range Expansion	Is supported by the DT SLS
A linear and non-iterative precoding technique that is capable of covering the full range of interference suppression from Zero Forcing (ZF) (full suppression) to Maximum Ratio Transmission (MRT) (no suppression)	The required algorithm is a contribution of this Thesis and is described in Chapter 4.

Chapter 4

Design of a Precoding and Scheduling Algorithm for Coordinated Beamforming in Heterogeneous Networks

This chapter describes the second of the three contributions of this Thesis, which is a new precoding and a scheduling algorithm for Coordinated Beamforming, based on the specifics of a heterogeneous networks. It will be used in the following chapters to identify performance limiting factors (Chapter 5) and is the basis for the HetNet RZF Scheduling Heuristic (HRSH) algorithm proposed in Chapter 6. In addition, it is also used within the Deutsche Telekom System Level Simulator (DT SLS), as shown in Section 3.8, to perform the performance analysis in Chapter 7. The following sections describe the implementations that were developed including their motivation. In more detail, Section 4.1 covers the precoding algorithm and Section 4.2 the corresponding scheduling implementation.

4.1 Relaxed zero forcing precoding algorithm for heterogeneous networks

This section introduces a new precoding algorithm which was designed to apply Coordinated Beamforming (CBF) in a heterogeneous network. The algorithm takes into account the specifics of such a network, especially caused by Cell Range Expansion (CRE), as described in Section 2.3. Section 4.1.1 introduces the new algorithm, before Sections 4.1.2

to 4.1.4 describe the individual steps in more detail. Section 4.1.5 gives an example and visualizes the output of the algorithm.

4.1.1 Overview and Introduction

The variety of existing precoding algorithms was described in Section 2.5. A basis for the selection of a suitable precoding approach was described in Section 2.7 where motivation for the usage of non-iterative linear precoding was motivated. Section 2.5 introduced two frameworks for non-iterative linear precoding that can generate precoders to trade off between Zero Forcing (ZF) and Maximum Ratio Transmission (MRT): Signal to Leakage and Noise Ratio (SLNR) precoding and Relaxed Zero Forcing (RZF). In this work RZF is applied with the motivation described in the following. Figure 4.1 shows the interaction between the precoding and the scheduling algorithm. In the case CBF is applied between an Macro Base Station (MBS) and a Pico Base Station (PBS), the precoding algorithm can design a precoder for each pair of one Macro Mobile Station (MMS) and one Pico Mobile Station (PMS) and each Physical Resource Block (PRB). The precoders can be designed in order to:

- maximize the received power at both Mobile Stations (MSs) (MRT precoding),
- minimize interference (ZF precoding),
- achieve a trade-off (SLNR and RZF precoding).

The scope of the precoding algorithm is limited to an individual PRB and the two MSs it is operating on. Its output (precoders per pair and PRB) is then forwarded to the scheduling algorithm, which jointly assigns the PRBs within the cooperation cluster consisting of the PBS and the MBS. Based on the input from the precoding algorithm, the scheduling algorithm can estimate the performance (e.g. in terms of throughput) per pair and PRB and then allocate the PRBs to the pairs. This allocation can happen based on a multitude of different targets:

- A maximization of fairness among the MSs
- The maximization of the system throughput
- The maximization of the throughput of individual MSs
- Adherence to quality of service guarantees

- Different trade-offs between the previously mentioned targets

In the scope of this work, the target of the scheduling algorithm is to maximize the system throughput (i.e. the system capacity) while maintaining a proportional fairness among the MSs.

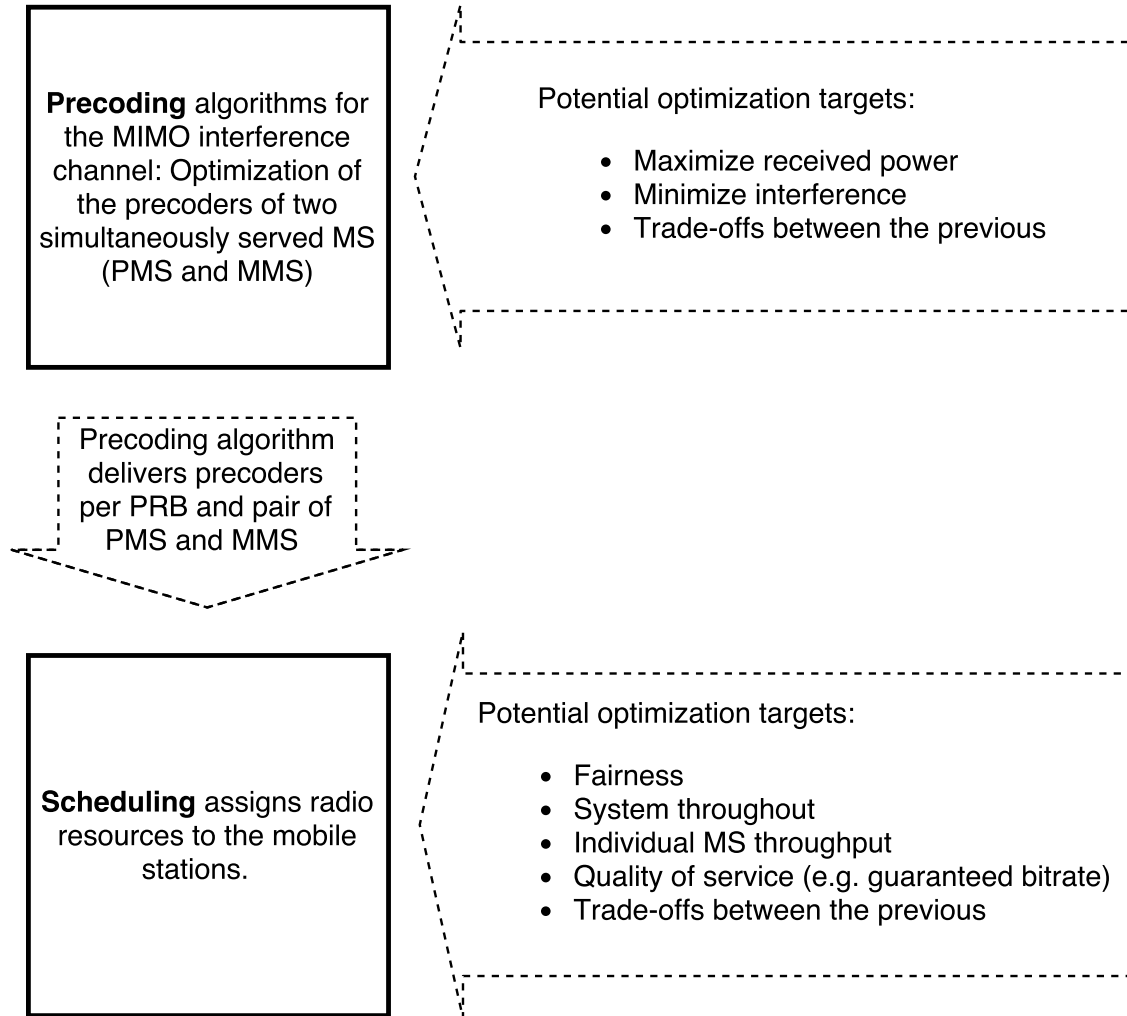


Figure 4.1: The interaction between scheduling and precoding including examples for the targets of scheduling and precoding algorithms

It can be seen that the targets of the scheduling algorithm do not necessarily comply with the targets of the precoding. In this regard, RZF offers a significant advantage compared to other precoding schemes: For each pair and PRB it delivers a set of precoders, out of which the scheduling algorithm can select and therefore adapt the precoding according to the current requirement from a system perspective. This is in contrast to SLNR precoding which independent of the scheduling algorithm finds one uncontrolled point in between ZF and MRT [61]. The following example illustrates the advance of RZF:

- A Base Station (BS) 1 serves an MS 1 and BS 2 serves an MS 2 on the same

time/frequency radio resource.

- Without coordination, MS 1 might for example be able to receive 1000 bits on this radio resource and MS 2 only 100 bits (due to strong interference).
- It is subject to a coordinated precoding algorithm (i.e. CBF is applied) to mitigate the resulting interference.
- In the case of SLNR precoding, a compromise between MRT and ZF is found at both BSs, which maximizes the SLNR. This results in a set of precoders 1 which in turn causes an Signal to Interference plus Noise Ratio (SINR) at both MSs and correspondingly a certain throughput, e.g. 800 bits at MS 1 and 200 bits at MS 2. However, also other precoders would be possible and can be generated by means of RZF, e.g. a set of precoders 2 where MS 1 receives 700 bits and MS 2 receives 300 bits.
- As the scheduler is not aware of potential other precoders in the case of SLNR precoding, it cannot take them into account when assigning radio resources and selecting precoders. For example, it might be the case that MS 2 uses a service with a guaranteed bitrate which is hard to fulfil due to its interference situation and MS 1 uses only a best effort service. Under these conditions, the set of precoders 2 might be beneficial, although it is not optimal from an SLNR point of view.

In addition, as described in Section 2.7, an objective of this work is also to determine and describe factors that influence the performance of CBF in a heterogeneous network. To this end, RZF provides the possibility to test different trade-offs between MRT and ZF for their effect.

However, in the literature non-iterative approaches to RZF only exist for the Multiple Input Single Output (MISO) interference channel, i.e. for MSs with one receive antenna. In the following a non-iterative RZF approach for the Multiple Input Multiple Output (MIMO) interference channel is presented. The new approach exploits the characteristics of the considered Heterogeneous Network (HetNet) scenario and is therefore called HetNet RZF. The goal of HetNet RZF is to reduce the interference from an MBS to a PMS. A mitigation of interference caused by a PBS to an MMS is not achieved by this algorithm. This is however of low impact in a heterogeneous network with CRE: CRE causes MSs attaching to a PBS, even if the received power level from an MBS is up to a factor of x (the CRE offset) higher than the receiver power from the PBS. Thus, an MMS must be at

a position where the power level from the MBS is significantly higher (e.g. at least four times higher at a CRE offset of 6 dB) than the power level of any PBS. The interference from a PBS to an MMS is therefore in general low and especially when other MBSs create significant interference to the MMS.

As for the description of HetNet RZF it is necessary to distinguish between different types of MSs (PMSs and MMSs) and BSs (PBSs and MBSs), an adapted description of the MIMO system is required (Equation 4.1).

$$\begin{aligned}
 y_p = & \underbrace{\sqrt{P_p \alpha_{pp}} u_p H_{pp} v_p s_p}_{\text{Wanted Signal at PMS}} + \underbrace{\sqrt{P_m \alpha_{pm}} u_p H_{pm} v_m s_m}_{\text{Interference MBS} \rightarrow \text{PMS}} \\
 & + \underbrace{\sum_{\substack{1 \leq j \leq k \\ j \neq m, j \neq n}} \sqrt{P_j \alpha_{pj}} u_p H_{pj} v_j s_j}_{\text{Interference from other BSs}} + \underbrace{n_p}_{\text{Noise}}
 \end{aligned} \tag{4.1}$$

In it, y_p indicates the signal received at the PMS. It consists of the wanted signal coming from the PBS, with P_p being the transmit power of the PBS, α_{pp} the pathloss between PMS and PBS, u_p the receive combining vector of the PMS, H_{pp} the radio channel between PMS and PBS, v_p the precoder at the PBS and s_p the data being sent by the PBS. The corresponding setup is depicted in Figure 4.2.

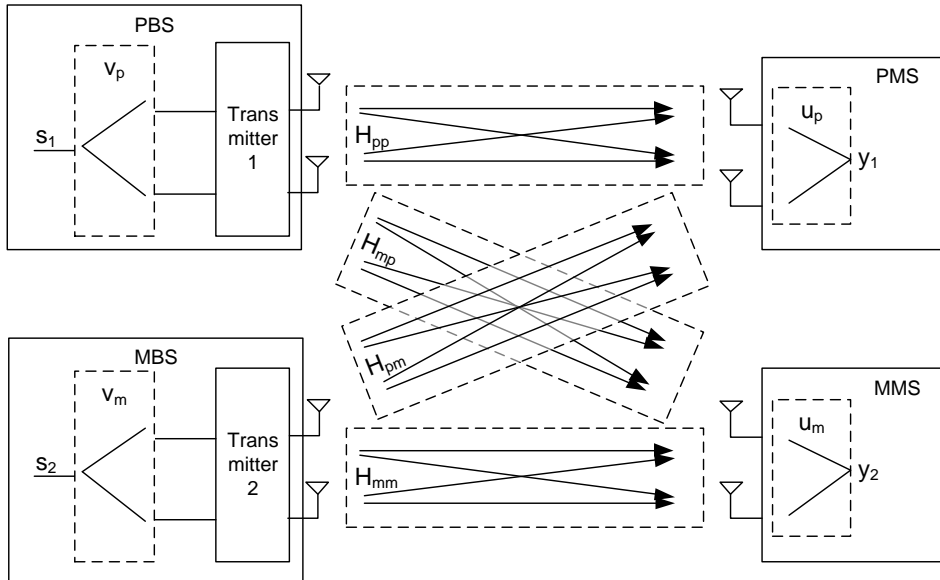


Figure 4.2: Setup for HetNet Relaxed Zero Forcing

A critical problem in the design of a non-iterative precoding algorithm in this setup is caused by the following combination:

- The receive combining vectors of the PMS and the MMS are means for the receivers

to adapt to the current channel conditions. The channel conditions also include the precoder selected at the serving BS. For example, this can be seen in Equation 4.2 for the Maximum Ratio Combining (MRC) receiver [55].

$$u = \frac{(Hv)^*}{\|Hv\|} \quad (4.2)$$

- A ZF precoder in the case of an MS with two antennas has to ensure that the interfering signals within the receiver sum up to zero as expressed by Equation 4.3, wherein H_{int} stands for the interfering channel (e.g. H_{pm} for the PMS in Figure 4.2) and v_{int} for the precoder of the interfering BS (e.g. v_m for the PMS).

$$uH_{int}v_{int} = 0 \quad (4.3)$$

- As a result, all variables in the setup in Figure 4.2 (v_m, v_p, u_p, u_m) are dependent on each other:
 1. v_p depends on u_m ,
 2. u_m depends on v_m ,
 3. v_m depends on u_p ,
 4. u_p depends on v_p which again depends on u_m .

HetNet RZF solves this problem by exploiting the above mentioned fact of low interference from the PBS to the PMS. If no interference suppression from the PBS to the MMS is required, the PBS can use MRT precoding such that v_p no longer depends on u_m .

As a result, HetNet RZF aims to define a set of precoders for the MBS which cause different levels of interference at the PMS. It is then a task of the scheduling algorithm to select one element out of this set. It is assumed here that the coordinated scheduler has the knowledge (e.g. about the radio channels) for both BSs.

The principle of HetNet RZF is depicted in Figure 4.3. The steps that are required to generate the precoders are located in the middle of the figure and the solid lines indicate the execution of the individual steps. The parallelograms on the right and left side of the figure indicate information that is required to generate the precoders. A flow of information (in- or output) is represented by a dashed line. The algorithm starts with generating the MRT precoder for the PBS v_p , which requires Channel State Information (CSI) in terms of an information about H_{pp} . v_p and H_{pp} are then used to calculate the receive

combining vector at the PMS (u_p). Using this and the knowledge of H_{pm} , a ZF precoder for the MBS (v_{mZF}) can be calculated. The generation of the MRT precoder at the MBS (v_{mMRT}) requires knowledge of H_{mm} . Both precoders v_{mZF} and v_{mMRT} can then be combined to generate the RZF precoders. In the following all steps mentioned in Figure 4.3 are described in more detail.

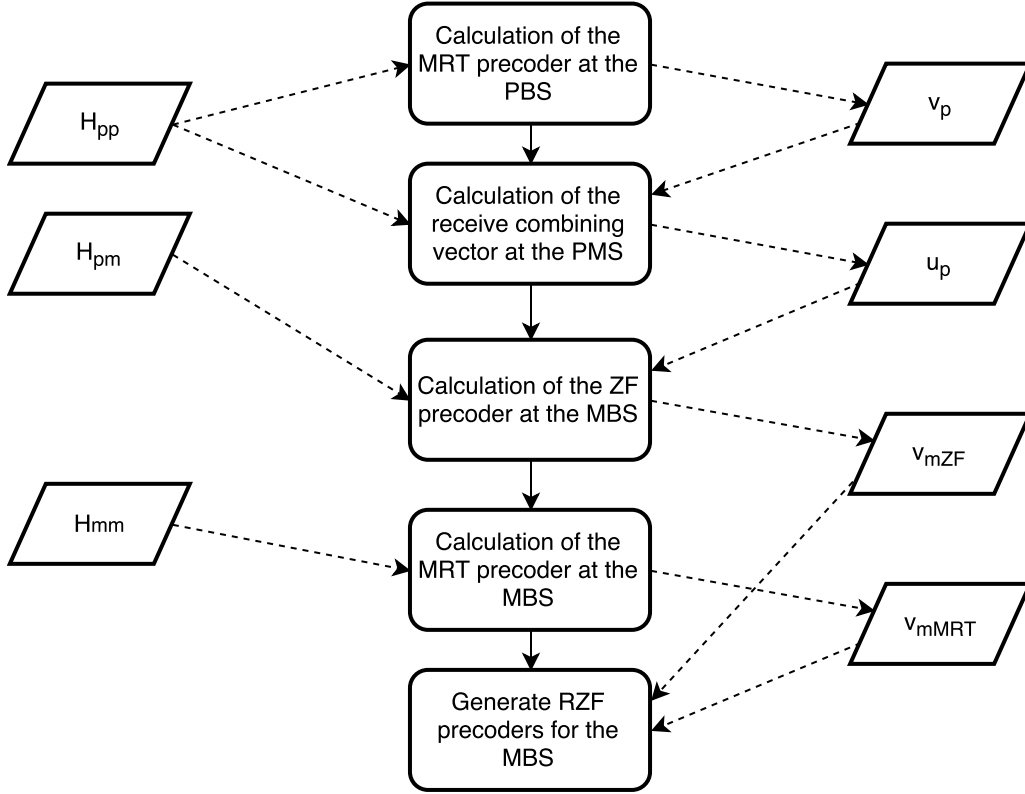


Figure 4.3: Flowchart of Relaxed Zero Forcing for Heterogeneous Networks

4.1.2 Precoder for the Pico Base Station and Receive Combining Vector for the Pico Mobile Station

As discussed above, a principle of HetNet RZF is that the PBS applies MRT precoding. The MRT precoder can be obtained with the help of the Singular Value Decomposition (SVD) (Equation 4.4).

$$\begin{aligned}
 H_{pp} &= USV^* \\
 v_p &= \begin{pmatrix} V_{11} \\ V_{21} \end{pmatrix}
 \end{aligned} \tag{4.4}$$

A detailed example for the calculation of the MRT precoder with the help of the SVD can be found in Appendix A.1.

With respect to the calculation of the receive combining vectors at the PMS, it can be seen from Figure 4.3 that HetNet RZF relies on knowledge of the receive combining vector u_p at the MBS to calculate the ZF precoder at the MBS. In case the PMS uses an MRC receiver (which is assumed here), the receive combining vector can directly be calculated from the channel matrix H_{pp} and the precoder v_p (Equation 4.5). This can be obtained by means of signalling from the PMS to the coordinated scheduler.

$$u_p = \frac{(H_{pp}v_p)^*}{\|H_{pp}v_p\|} \quad (4.5)$$

4.1.3 Zero Forcing and Maximum Ratio Transmission Precoder for the Macro Base Station

In contrast to the PBS, a set of different precoders is calculated for the MBS. Using the information on v_p and u_p , at first an ZF precoder v_{mZF} for the MBS can be calculated as explained in the following. In Figure 4.4 the flow of signals from the MBS to the PMS is depicted. From the first antenna of the MBS, signals propagate through the blue paths towards the PMS. The contribution of the signals from the first antenna of the MBS is described by Equation 4.6. Similarly, the signals from the second antenna propagate through the red paths. Their contribution is described by Equation 4.7.

$$[H]p_1 = H_{pm_{1,1}}u_{p_1} + H_{pm_{2,1}}u_{p_2} \quad (4.6)$$

$$[H]p_2 = H_{pm_{1,2}}u_{p_1} + H_{pm_{2,2}}u_{p_2} \quad (4.7)$$

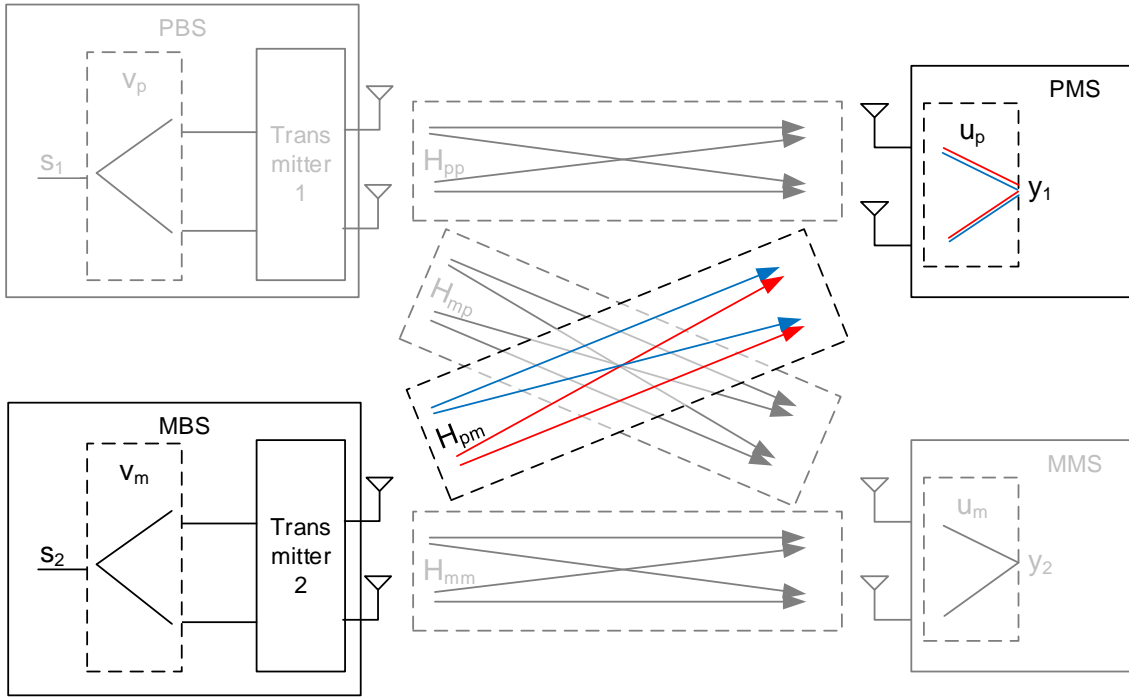


Figure 4.4: Relaxed Zero Forcing for Heterogeneous Networks: Starting situation for the calculation of the Zero Forcing precoder

The target of ZF precoding is to shape the outgoing signals of the MBS by means of the precoder v_{mZF} such that they sum up to zero within the PMS (Equation 4.8).

$$u_p H_{pm} v_{mZF} = 0 \quad (4.8)$$

This is achieved by the principle depicted in Figure 4.5. It shows (as an example) two randomly chosen realizations of p_1 and p_2 . As a first step, p_2 is modified such that its phase equals the phase of p_1 plus π (p_{2a} in Figure 4.5, represented by the dashed blue arrow). As a second step, p_{2a} is modified such that its amplitude equals the amplitude of p_1 (p_{2b} in Figure 4.5, represented by the dotted blue arrow in Figure 4.5). As a result, the sum of p_1 and p_{2b} equals zero. Equations 4.9 to 4.10 describe this in more detail: The first element of the precoder V_{mZF} equals one (Equations 4.9), as this path is supposed to be unchanged. The second element is constructed such that it modifies p_2 in accordance to what has been described before: Its phase is shifted by a factor of $\pi + \arg p_1 - \arg p_2$ (with $\arg p_1$ being the phase of p_1) to achieve the phase difference of π between p_1 and p_{2a} . In addition, the amplitude is modified by the factor of $\frac{|p_1|}{|p_2|}$ to achieve p_{2b} having the

same amplitude as p_1 .

$$v_{mZF_1} = 1 \quad (4.9)$$

$$v_{mZF_2} = e^{j(\pi + \arg p_1 - \arg p_2)} \quad (4.10)$$

Equation 4.11 covers an aspect which has not been described before: The newly generated precoder (consisting of the two elements calculated before) has to be normalized in order to not increase or decrease the transmit power of the MBS.

$$v_{mZF} = \frac{\begin{pmatrix} v_{mZF_1} \\ v_{mZF_2} \end{pmatrix}}{\| \begin{pmatrix} v_{mZF_1} \\ v_{mZF_2} \end{pmatrix} \|} \quad (4.11)$$

With respect to Figure 4.5, this results in both vectors p_1 and p_{2a} being multiplied by the same factor, which does not change the fact that they sum up to zero. This methodology of calculating v_{mZF} can also be described with finding the kernel of $u_p H_{pm}$ (Equation 4.12).

$$v_{mZF} = \ker \begin{pmatrix} p_1 \\ p_2 \end{pmatrix} = \ker(u_p H_{pm}) \quad (4.12)$$

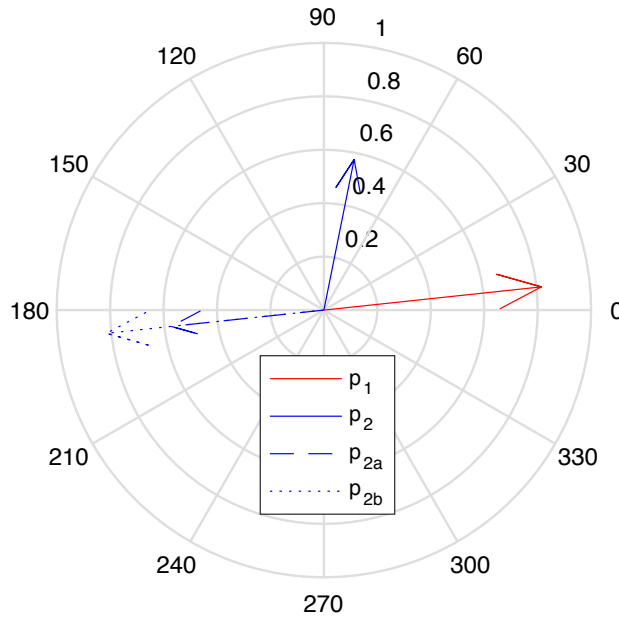


Figure 4.5: Calculation of the Zero Forcing Precoder: Modification of the signals such that they sum up to zero

The MRT precoder for the MBS v_{mMRT} can be calculated following the same principle as for the PBS (Equation 4.13).

$$\begin{aligned}
H_{mm} &= USV^* \\
v_{mMRT} &= \begin{pmatrix} V_{11} \\ V_{21} \end{pmatrix}
\end{aligned} \tag{4.13}$$

4.1.4 Combination of Maximum Ratio Transmission and Zero Forcing Precoding

The main functionality of RZF is to provide precoders that achieve a trade-off between ZF and MRT. This is achieved by creating linear combinations of the two precoders as described by Equation 4.14.

$$v_m = \lambda_1 v_{mMRT} + \lambda_2 v_{mZF} \tag{4.14}$$

In it, λ_1 which can take a value from zero to one defines the level of interference suppression (Equation 4.15) at the PMS.

$$\lambda_1 = [0, 1] \tag{4.15}$$

A selection of zero results in no interference from the MBS to the PMS (MRT is fully suppressed), whereas one means full interference. In case $\lambda_1 < 1$, only a part of the transmit power (indicated by λ_1) is allocated to the MRT transmission. The remaining transmit power at the MBS can be allocated to a ZF transmission, such that the norm of v_m equals one (Equation 4.16).

$$\|v_m\| = 1 \tag{4.16}$$

Equations 4.17 to 4.30 describe how this is achieved:

- Equation 4.17 describes the target, which is to find a setting of λ_2 , such that Equation 4.16 is fulfilled. All other variables ($\lambda_1, v_{mMRT}, v_{mZF}$) have been fixed at this point. To simplify the description, in the following $\lambda_1 v_{mMRT}$ is denoted as v_a and v_{mZF} as v_b .

$$\| \underbrace{\lambda_1 v_{mMRT}}_{v_a} + \underbrace{\lambda_2 v_{mZF}}_{v_b} \| = 1 \tag{4.17}$$

- Equation 4.18 follows the definition of the Euclidean norm.

$$\sqrt{|v_{a,1} + \lambda_2 v_{b,1}|^2 + |v_{a,2} + \lambda_2 v_{b,2}|^2} = 1 \tag{4.18}$$

- Equation 4.19 removes the square root and again introduces two abbreviations (v_c and v_d).

$$\underbrace{|v_{a,1} + \lambda_2 v_{b,1}|^2}_{v_c} + \underbrace{|v_{a,2} + \lambda_2 v_{b,2}|^2}_{v_d} = 1 \quad (4.19)$$

- In Equation 4.20 the calculation of the amplitude of v_c and v_d is applied, wherein $Re^2(x)$ stands for the real part of x to the power of two and $Im^2(x)$ for the imaginary part of x to the power of two.

$$\left[\sqrt{Re^2(v_c) + Im^2(v_c)} \right]^2 + \left[\sqrt{Re^2(v_d) + Im^2(v_d)} \right]^2 = 1 \quad (4.20)$$

- Equation 4.21 is a simplified version of Equation 4.20.

$$Re^2(v_c) + Im^2(v_c) + Re^2(v_d) + Im^2(v_d) = 1 \quad (4.21)$$

- Equation 4.22 changes back the abbreviations introduced in Equation 4.19, such that λ_2 appears again.

$$\begin{aligned} & Re^2(v_{a,1} + \lambda_2 v_{b,1}) + Im^2(v_{a,1} + \lambda_2 v_{b,1}) \\ & + Re^2(v_{a,2} + \lambda_2 v_{b,2}) + Im^2(v_{a,2} + \lambda_2 v_{b,2}) = 1 \end{aligned} \quad (4.22)$$

- In Equation 4.23 it is made use of the fact that

$$Re^2(a + b) = [Re(a + b)]^2 = [Re(a) + Re(b)]^2.$$

The same is applied to $Im^2(a + b)$.

$$\begin{aligned} & [Re(v_{a,1}) + Re(\lambda_2 v_{b,1})]^2 + [Im(v_{a,1}) + Im(\lambda_2 v_{b,1})]^2 \\ & + [Re(v_{a,2}) + Re(\lambda_2 v_{b,2})]^2 + [Im(v_{a,2}) + Im(\lambda_2 v_{b,2})]^2 = 1 \end{aligned} \quad (4.23)$$

- In Equation 4.24 the quadratic terms have been removed.

$$\begin{aligned} & Re^2(v_{a,1}) + 2\lambda_2 Re(v_{a,1})Re(v_{b,1}) + \lambda_2^2 Re^2(v_{b,1}) \\ & + Im^2(v_{a,1}) + 2\lambda_2 Im(v_{a,1})Im(v_{b,1}) + \lambda_2^2 Im^2(v_{b,1}) \\ & + Re^2(v_{a,2}) + 2\lambda_2 Re(v_{a,2})Re(v_{b,2}) + \lambda_2^2 Re^2(v_{b,2}) \\ & + Im^2(v_{a,2}) + 2\lambda_2 Im(v_{a,2})Im(v_{b,2}) + \lambda_2^2 Im^2(v_{b,2}) = 1 \end{aligned} \quad (4.24)$$

- In Equation 4.25 the elements of Equation 4.24 have been reordered such that the

three simplifications can be applied. $v_a \cdot v_b$ represents the dot product of v_a and v_b .

$$\begin{aligned}
& \underbrace{Re^2(v_{a,1}) + Im^2(v_{a,1}) + Re^2(v_{a,2}) + Im^2(v_{a,2})}_{\|v_a\|^2} \\
& + 2\lambda_2 \left[\begin{array}{c} Re(v_{a,1})Re(v_{b,1}) + Im(v_{a,1})Im(v_{b,1}) + \\ \underbrace{Re(v_{a,2})Re(v_{b,2}) + Im(v_{a,2})Im(v_{b,2})}_{v_a \cdot v_b} \end{array} \right] \\
& + \lambda_2^2 \left[\underbrace{Re^2(v_{b,1}) + Im^2(v_{b,1}) + Re^2(v_{b,2}) + Im^2(v_{b,2})}_{\|v_b\|^2} \right] = 1
\end{aligned} \tag{4.25}$$

- Equation 4.26 shows the simplified equation which is reordered in Equation 4.27.

$$\lambda_2^2 \|v_b\|^2 + 2\lambda_2 v_a \cdot v_b + \|v_a\|^2 = 1 \tag{4.26}$$

$$\lambda_2^2 \|v_b\|^2 + 2\lambda_2 v_a \cdot v_b + \|v_a\|^2 - 1 = 0 \tag{4.27}$$

- The two solutions for the quadratic Equation 4.27 are described by Equation 4.28.

$$\lambda_{2_{1/2}} = \frac{1}{2\|v_b\|^2} \left[-2v_a \cdot v_b \pm \sqrt{4(v_a \cdot v_b)^2 - 4\|v_b\|^2(\|v_a\|^2 - 1)} \right] \tag{4.28}$$

- Finally, Equation 4.29 changes back the abbreviations introduced in Equation 4.17.

$$\begin{aligned}
\lambda_{2_{1/2}} = & \frac{1}{2\|v_{mZF}\|^2} \cdot \left[-2\lambda_1 v_{mMRT} \cdot v_{mZF} \right. \\
& \left. \pm \sqrt{4(\lambda_1 v_{mMRT} \cdot v_{mZF})^2 - 4\|v_{mZF}\|^2(\|\lambda_1 v_{mMRT}\|^2 - 1)} \right]
\end{aligned} \tag{4.29}$$

- Out of the two solutions for λ_2 , Equation 4.30 selects the one with the lower amplitude. This is due to the fact that a precoder with a lower amplitude of λ_2 results in a characteristic of v_m that is closer to v_{mMRT} (which increases the received power at the MMS) whereas a larger amplitude of λ_2 would modify v_m more than necessary.

$$\lambda_2 = \begin{cases} \lambda_{2_1} & |\lambda_{2_1}| \leq |\lambda_{2_2}| \\ \lambda_{2_2} & |\lambda_{2_1}| > |\lambda_{2_2}| \end{cases} \tag{4.30}$$

4.1.5 Example and Visualization

In the following an example visualizes the operation of the HetNet RZF algorithm. The randomly generated channel matrices as described by Equations 4.31 to 4.34 are used.

$$H_{pp} = \begin{bmatrix} 0.7748 + 0.1400i & 0.6936 + 0.4288i \\ 0.8774 + 0.5411i & -0.3638 - 0.8745i \end{bmatrix} \quad (4.31)$$

$$H_{pm} = \begin{bmatrix} 0.6763 + 0.3337i & -0.7071 - 0.0034i \\ -0.4338 + 0.4185i & -0.1533 - 0.8115i \end{bmatrix} \quad (4.32)$$

$$H_{mp} = \begin{bmatrix} -0.5131 + 0.0467i & -0.1591 - 0.2977i \\ 0.0126 + 0.6772i & 0.5676 - 0.7715i \end{bmatrix} \quad (4.33)$$

$$H_{mm} = \begin{bmatrix} 0.0303 + 0.3785i & -0.5435 + 0.8957i \\ -0.9066 + 0.7993i & 0.0878 - 0.5000i \end{bmatrix} \quad (4.34)$$

In addition, examples for the values of the received power levels (for one Orthogonal Frequency Division Multiplexing (OFDM) subcarrier, at the MSs) and the noise power were extracted from a sample of a simulation in the DT SLS described in Chapter 3 (Equations 4.35 to 4.39).

$$P_p \alpha_{pp} = 14.4009 \cdot 10^{-12} W \quad (4.35)$$

$$P_p \alpha_{pm} = 66.0539 \cdot 10^{-12} W \quad (4.36)$$

$$P_m \alpha_{mp} = 3.6188 \cdot 10^{-15} W \quad (4.37)$$

$$P_m \alpha_{mm} = 5.5002 \cdot 10^{-12} W \quad (4.38)$$

$$n_p = 0.4743 \cdot 10^{-15} W \quad (4.39)$$

It should be noted that these values can (as described in Section 3.4) be influenced (amplified or attenuated) by the instantaneous channel realization H .

In a first step, MRT precoders for the PBS as well as the MBS can be calculated following Equations 4.4 and 4.13, which results in the vectors of Equations 4.40 and 4.41.

$$v_p = \begin{pmatrix} -0.7594 \\ 0.3271 - 0.5623i \end{pmatrix} \quad (4.40)$$

$$v_{mMRT} = \begin{pmatrix} -0.5621 \\ 0.3026 + 0.7696i \end{pmatrix} \quad (4.41)$$

The MRC receive combining vector for the PMS can be calculated using Equation 4.5, with the result shown in Equation 4.42.

$$u_p = \frac{(H_{pp}v_p)^*}{\|H_{pp}v_p\|} = [(-0.8477 + 0.2508i)(-0.8997 + 0.3468i)] \quad (4.42)$$

On the basis of u_p and H_{pm} a precoder can be found that nulls out interference at the PMS. In the case of this example this precoder is described by Equation 4.43.

$$v_{mZF} = \ker(u_p H_{pm}) = \begin{pmatrix} -0.326 - 0.7121i \\ 0.621 - 0.2914i \end{pmatrix} \quad (4.43)$$

Figure 4.6 visualizes the two precoders. The two elements (for the two antennas) of the precoder v_{mMRT} are shown in blue (the first element is depicted as a solid line, the second as a dashed line) and the precoder v_{mZF} is depicted in red. It can be seen that there is a difference between the precoders, especially in terms of the phase.

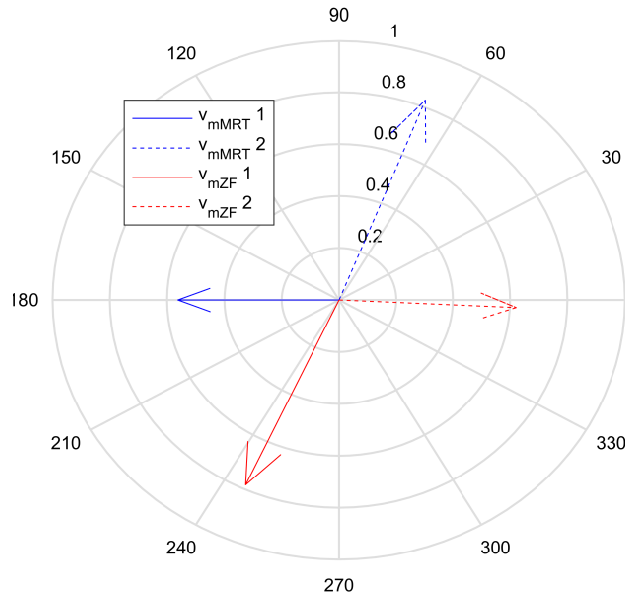


Figure 4.6: HetNet Relaxed Zero Forcing Example: Visualization of the Zero Forcing and Maximum Ratio Transmission precoders

Using the approach described in Equations 4.14 to 4.16, the two precoders can be combined as a function of the parameter λ_1 . Figure 4.7 shows the result of this process. The first precoder in Figure 4.7 ($\lambda_1 = 0$) is the ZF precoder and the last precoder ($\lambda_1 = 1$) is the MRT case. The settings in between show the combinations of both precoders. It can be seen that precoders with a low setting of λ_1 (e.g. 0.1 and 0.2) are similar to the ZF precoder and with high settings of λ_1 (e.g. 0.8 and 0.9) precoders similar to the MRT one

are generated.

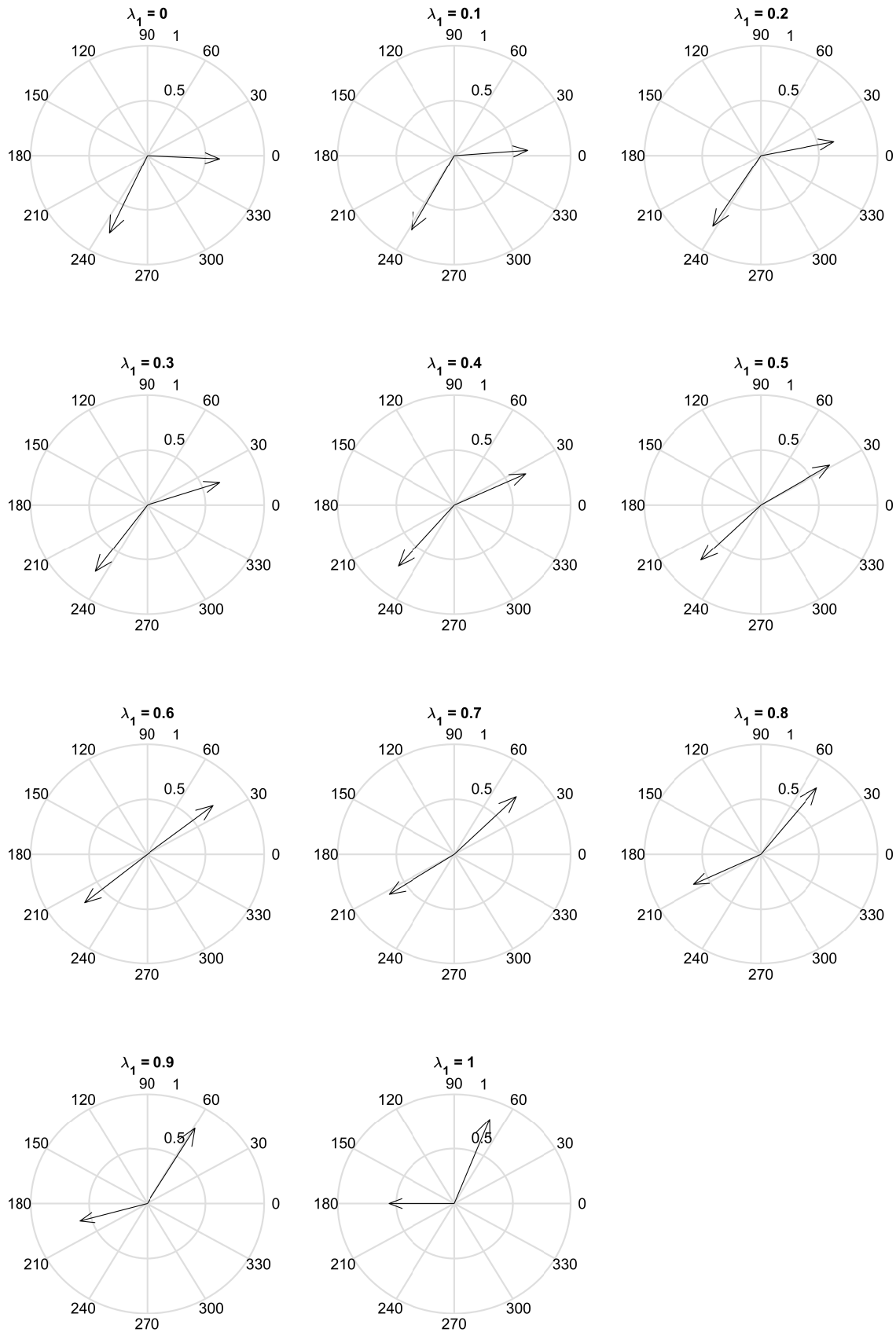


Figure 4.7: HetNet Relaxed Zero Forcing Example: Visualization of the full set of pre-coders

To see the effect when using the different precoders, Figure 4.8 shows how each individual precoder affects the power levels at the receivers of the PMS and the MMS. The following observations can be made:

- The intended power level at the PMS is not affected by the choice of λ_1 . This is due to the fact that the PBS always transmits using MRT precoding
- The interfering power at the PMS is, as expected, heavily influenced by the selection of λ_1 . For $\lambda_1 = 0$, i.e. the ZF case, the interference is zero, while for $\lambda_1 = 1$ (the MRT case) there is heavy interference. Here the interference power is higher than the intended signal. In general, this can occur due to the effects of CRE (see Section 2.3) and this example is a result of the powers assumed in Equations 4.35 and 4.35, where the PMS receives (without the consideration of precoding) more power from the MBS than from the PBS.
- The intended power level at the MMS is also strongly affected by the selection of λ_1 . As expected, it is lowest when using ZF and highest for MRT precoding. The selection of λ_1 can increase the received power from $5.5 \cdot 10^{-12}$ W at $\lambda_1 = 0$ to $11.7 \cdot 10^{-12}$ W at $\lambda_1 = 1$, i.e. by more than 100%.
- The interference level at the MMS is very low (at approximately 10^{-15} W). It is slightly (not visible in the Figure) affected by the choice of λ_1 , due to a side effect: The choice of the precoder at the MBS (i.e. the choice of λ_1) affects the choice of the receive combining vector and therefore also the interference. This effect can be positive as well as negative (reducing / amplifying interference).

The result of the four changing power levels in Figure 4.8 is shown in Figure 4.9 where the SINR (in dB) at the PMS and the MMS is depicted. Again the heavy influence of the selection of λ_1 onto the performance of the PMS is visible: For $\lambda_1 = 0$, the SINR at the PMS is effectively the Signal to Noise Ratio (SNR), as no interference is present. Here the PMS can be served under very good conditions (i.e. an SINR higher than 40 dB) whereas for $\lambda_1 = 1$ the SINR drops below 0 dB, i.e. data transmission would only be possible at a very low rate. With respect to the MMS, a less drastic impact is obtained: Here the SINR increases from 34 dB at $\lambda_1 = 0$ to 39.4 dB at $\lambda_1 = 1$.

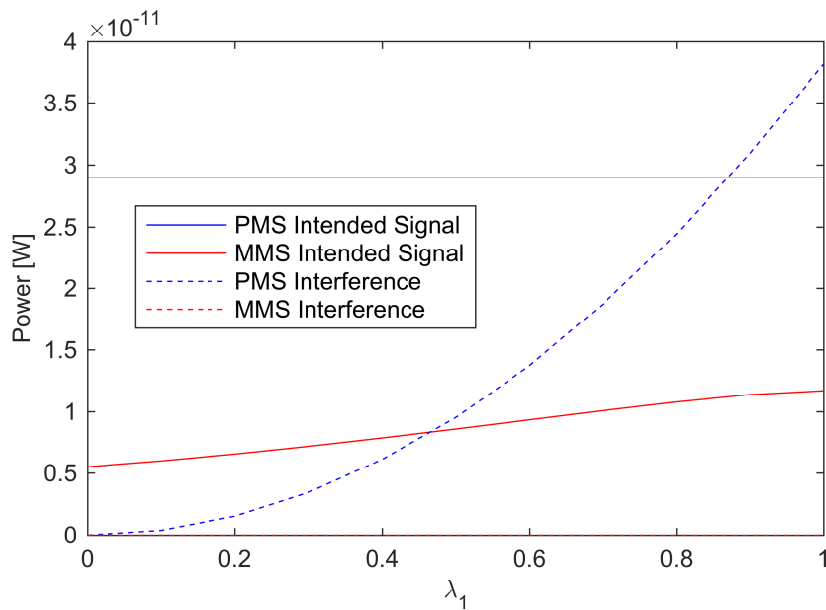


Figure 4.8: HetNet Relaxed Zero Forcing Example: Power Levels (interfering and intended) at the PMS and the MMS

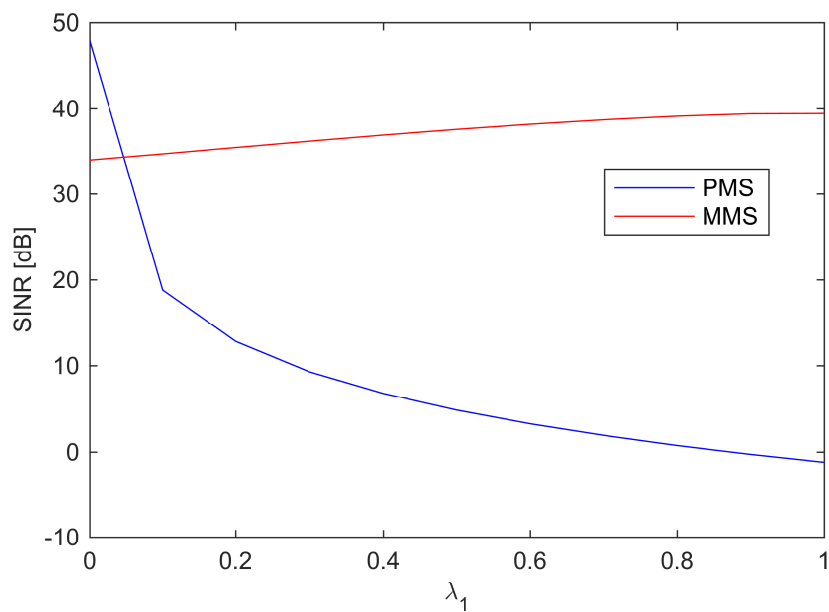


Figure 4.9: HetNet Relaxed Zero Forcing Example: Resulting SINR at the PMS and the MMS

This example showed the principles of HetNet RZF. Its main ability is that by means of the parameter λ_1 , the performance of the PMS and the MMS in terms of SINR can be controlled. The result is a trade-off between the performance of the MMS and the PMS which can be balanced using the scheduling. From Figure 4.9 it might be observed that a setting of $\lambda_1 = 0$ is most beneficial, due to the high SINR of the PMS and the relatively low difference in terms of SINR for the MMS when comparing $\lambda_1 = 0$ and $\lambda_1 = 1$. This

is however, caused by the absence of Out of Cluster Interference (OOCI) in this example (there are no other BSs than the MMS and the PMS). As it will be shown in Chapter 5, OOCI has a strong influence on the achievable performance of the PMS, i.e. the steepness of the blue curve in Figure 4.9. This is also a subject of the detailed simulation results in Chapter 7.

4.2 Scheduling

As introduced in Section 2.6, the process of scheduling assigns the Orthogonal Frequency Division Multiple Access (OFDMA) radio resources to the MSs. The usage of a radio resource is coupled with a set of parameters on physical layer that are also set by the scheduler, such as the Modulation and Coding Scheme (MCS) and the precoder.

The proportional fair scheduling principle is a widely used strategy to assign radio resources [87] [72] [75] [76]. It achieves a trade-off between performance (which would be maximized by serving the MS with the highest SINR only) and fairness (which would be maximized when achieving the same throughput for all MSs). This is achieved by serving the MS j which maximizes the proportional fair metric as expressed by Equation 4.44 [72].

$$j = \arg \max_{1 \leq i \leq N} M_{PFS}(n, i) = \arg \max_{1 \leq i \leq N} \frac{r_i(n)}{R_i(n-1)} \quad (4.44)$$

In Equation 4.44, j indicates the MS to be served, out of the total N MSs. $M_{PFS}(n, i)$ represents the instantaneous proportional fair metric value of MS i , calculated as ratio of the instantaneous (at the current time instance n) achievable rate of an MS i $r_i(n)$ and its historic rate $R_i(n-1)$ (Equation 4.45).

$$R_i(n-1) = \beta \cdot R_i(n-2) + (1-\beta) \cdot r_i(n-1) \quad (4.45)$$

$R_i(n-1)$ is updated after each resource assignment (also in case the MS was not granted access, then $r_i(n-1)$ in Equation 4.45 equals zero). β (a value between zero and one) is the so-called forgetting factor, which enables MSs that once gained access to the channel (and therefore have a high value of R_i) to re-gain it.

In other words, the objective of proportional fair scheduling is, at each time instance, to perform the resource allocation with the highest proportional fair metric, i.e. to serve the MS with the best trade-off between its current achievable rate and its importance in terms of fairness. This should, however, not be confused with maximizing the pro-

portional fair metric of the MSs, which is not a suitable objective: For example, serving no MSs at all would in the long term lead to $R_i(n-1) = 0$, which would result in $M_{PFS}(n, i) = \infty$.

Proportional fair scheduling was adapted to be frequency selective in an OFDMA system [75] [76]. Here the scheduling assigns access to subbands (e.g. one radio resource) instead of granting access to the full channel bandwidth. The proportional metric therefore is calculated based on achievable rate per subband (r^{SB}) in Equation 4.46.

$$M_{PFS}(n) = \frac{r_i^{SB}(n)}{R_i(n-1)} \quad (4.46)$$

In the following, the principle of proportional fair scheduling is applied for a coordinated scheduling algorithm at an MBS and a PBS including the calculation of HetNet RZF precoders. Here, each resource block is assigned to one pair, consisting of one PMS and one MMS. Additionally, for each pair the control parameter λ_1 can be configured, which results in different instantaneous achievable data rates at both MSs. Whereas in a proportional fair scheduling for a single BS the target was to assign resources to the MSs with the highest proportional fair metric, the target is therefore now to assign resources to the pair and configuration λ_1 with the highest proportional fair metric. Within a pair, the PMS contributes to the current proportional fair metric (according to its current trade-off between instantaneous data rate and importance in terms of fairness) and in the same way does the MMS. The proportional fair metric of a pair p , consisting of MMS l and PMS k is therefore defined as the sum of its individual metrics as expressed by Equation 4.47.

$$M_{PFS}^{HetNet}(p, n, \lambda_1) = \frac{r_{PMSk}^{SB}(n, \lambda_1)}{R_{PMSk}(n-1)} + \frac{r_{MMSl}^{SB}(n, \lambda_1)}{R_{MMSl}(n-1)} \quad (4.47)$$

The target of a corresponding scheduling algorithm is therefore for each radio resource to find a pair p , consisting of the two MSs PMS k and MMS l , in combination a setting of λ_1 , that maximizes the instantaneous sum proportional fair metric M_{PFS}^{HetNet} . This is expressed by Equation 4.48, wherein M stands for the total number of pairs.

$$p, \lambda_1 = \underset{\substack{1 \leq m \leq M \\ 0 \leq \lambda \leq 1}}{\arg \max} M_{PFS}^{HetNet}(m, n, \lambda) \quad (4.48)$$

This is achieved in the form of the algorithm that is depicted in Figure 4.10. It executes the following steps:

1. The scheduling is jointly executed for one PBS and one MBS. The input is defined by the group of PMSs attached to this PBS and the corresponding group of MMSs attached to the MBS.
2. All possible combinations of a potential resource assignment to the MSs are created, i.e. all possible pairs containing one MMS and one PMS.
3. The scheduling algorithm is designed to apply HetNet RZF. However, it is also capable of creating coordinated resource assignments without using HetNet RZF. This is important in order to generate a reference of the performance without HetNet RZF. In the following, the resource assignment procedure for the HetNet RZF case will be described. The case without HetNet RZF is described afterwards.
4. For each PRB there are two degrees of freedom: In terms of the pair that can be allocated to use it and in terms of the precoders to apply, i.e. the setting of λ_1 . To find the resource assignment that maximizes the proportional fair metric, all achievable throughput values have to be calculated. This step is explicitly calculated knowing the level of interference a realization of λ_1 causes at both MSs. As a result, for each PRB the achievable throughput per pair and for different realizations of λ_1 is available.
5. Using this information, the proportional fair metric M_{PFS}^{HetNet} as described by Equation 4.47 can be calculated per PRB, pair and realization of λ_1 .
6. Each PRB is then assigned to the pair and realization of λ_1 that maximizes M_{PFS}^{HetNet} .
7. The result of this process is the resource assignment itself, i.e. as description of how the PRBs of the MBS should be distributed among the MMSs and accordingly for the PMSs at the PBSs. In addition the precoders have been set (through the selection of λ_1).
8. The corresponding transmissions can be executed based on the output of the scheduling algorithm.

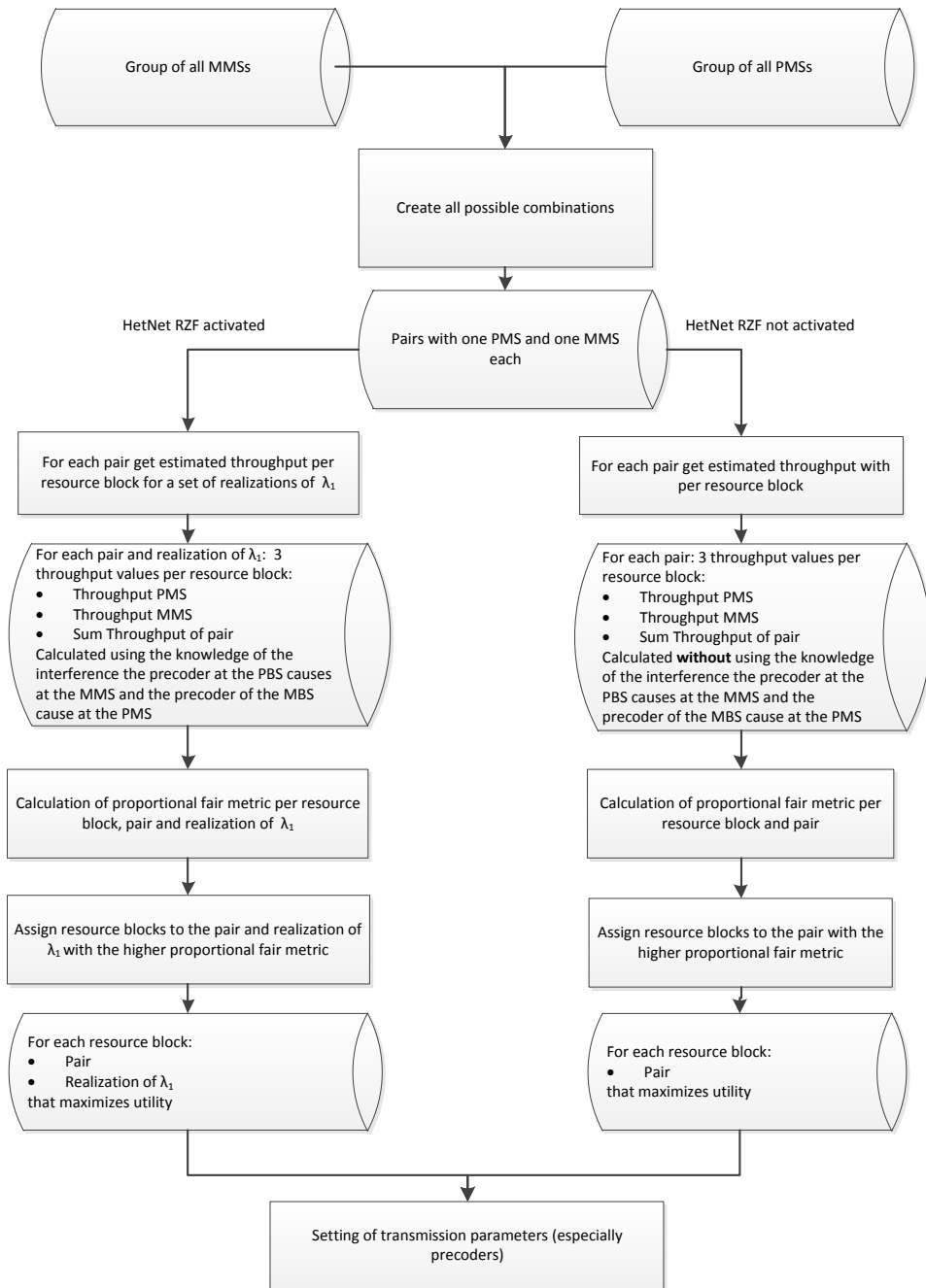


Figure 4.10: Flowchart for Proportional Fair Scheduling that applies HetNet Relaxed Zero Forcing

Step 4 of this algorithm can be seen as the core of the scheduling process for CBF: At this point, the scheduling algorithm tests different precoders (i.e. "beams") for the consequences the cause. This is executed jointly for the PBS and the MBS and therefore results in a coordinated assignment of the precoders. It may for example happen in this process that a certain precoder for an MMS (represented by a realization of λ_1) is not used as it causes high interference at an PMS. As mentioned at step 3, the scheduling algorithm is also capable of creating resource assignments not using HetNet RZF for generating a

reference without CBF. In this case, the procedure is alike, with the following differences:

1. There is no calculation of RZF precoders and thus not selection of λ_1 required. Instead for each MS MRT precoding is used.
2. An important difference occurs at step 4. Here the achievable throughput is calculated without of the knowledge of which precoder the cooperating BS selects.

This second difference can have significant impact on the throughput of the MSs. Even if HetNet RZF is restricted to apply MRT precoding only ($\lambda_1 = 1$), e.g. for complexity reasons as it will be described in Chapter 6, it has the ability to project the impact of a scheduling decision in terms of the interference the precoders will cause. As an example, for a PRB 1 an MMS 1 might be associated with an MRT precoder 1 that causes heavy interference at PMS 1. If HetNet RZF is activated, the scheduling algorithm is able to detect this and take potential other allocations into account, such as serving PMS 1 on PRB 1 jointly with an MMS 2 and MMS 1 on a different PRB.

4.3 Summary

This section proposed a new precoding algorithm for the MIMO Interference Channel (IC), named HetNet RZF, which makes uses of the specific interference conditions in a heterogeneous network. It therefore fulfils the second objective of this work described in Section 2.7. One of the fundamental aspects of HetNet RZF is its ability to calculate the full range of precoders (from full to no interference suppression at the PMS). This property will be used in the following Chapter 5 to find fundamental performance limiting factors when using CBF in a heterogeneous network.

In addition, a corresponding scheduling algorithm was described, which extends the proportional fair scheduling principle to a cluster of two BSs. It is designed to decide how and for which MSs HetNet RZF should be applied.

As part of the first objective in Section 2.7, a set of requirements for investigating the performance of CBF in a heterogeneous network was created. Section 3.8 showed that most of these requirements can be fulfilled by using the DT SLS, with the exception of a suitable precoding and scheduling algorithm. HetNet RZF in combination with its corresponding scheduling algorithm therefore complement the DT SLS and gives the ability to assess the performance of CBF in detail, which will be the content of Chapter 7.

Chapter 5

Performance limiting factors in HetNet Coordinated Beamforming

As the first contribution of this Thesis, this chapter describes fundamental factors that limit the performance of Coordinated Beamforming (CBF) in a large-scale heterogeneous network which were found by extensive simulations. Unlike the previous and the following chapters, this chapter does deliberately not make use of detailed System Level Simulations (SLSs) but uses a simplified modelling for the following reason: SLSs give detailed insights on the performance in large-scale multi-carrier networks. However, the results of an SLS are influenced by a huge combination of different algorithms and models that operate simultaneously. In terms of CBF, the performance of the precoding scheme can for example be influenced by the scheduling (which might decide not to select a certain precoder), the interference conditions in the network or in more general the propagation and channel modelling. When analysing the results of an SLS, it can be difficult to find out how the result was influenced by which factor.

This chapter therefore uses a dedicated modelling to evaluate what impact different factors have on the performance of CBF in a heterogeneous network. For this purpose it makes use of the features of HetNet Relaxed Zero Forcing (RZF) precoding which was introduced in Chapter 4.

The result of these evaluations are used in Chapter 6 to design a scheduling heuristic named HetNet RZF Scheduling Heuristic (HRSH) with reduced computational complexity. In addition, they provide important insights to understand the outcome of the SLSs in Chapter 7.

This chapter is structured as follows: Section 5.1 describes the impact of the so-called

Out of Cluster Interference (OOCI), which is analysed by means of a dedicated simulation. A new metric, named Out of Cluster Interference Ratio (OOCIR), is introduced to quantify the current level of OOCI. Section 5.2 describes a second performance limiting factor which is the number of Mobile Stations (MSs). Again, a dedicated simulation is used to evaluate its effect. Section 5.3 then provides a summary.

5.1 Out of cluster interference

Out of Cluster Interference (OOCI) is an important impairment for any kind of interference-mitigating coordination [6]. The aim of this section is to determine how and under which conditions it affects the performance of CBF in a heterogeneous network and in more detail the performance of HetNet RZF.

Equation 5.1 shows the total interference at a Pico Mobile Station (PMS) i , with the following definitions:

- P_j indicates the transmit power of BS j ,
- α_{ij} the pathloss between PMS i and BS j ,
- u_i the receive combining vector of PMS i ,
- H_{ij} the channel transfer function between PMS i and BS j ,
- v_j the precoder at the BS j and
- s_j the data being sent by BS j .

$$\begin{aligned}
 I_i &= \sum_{\substack{1 \leq j \leq k \\ i \neq j}} \sqrt{P_j \alpha_{ij}} u_i H_{ij} v_j s_j \\
 &= \underbrace{\sqrt{P_l \alpha_{il}} u_i H_{il} v_l s_l}_{\text{Interference from cooperating MBS } l} + \underbrace{\sum_{\substack{1 \leq j \leq k \\ i \neq \{j, l\}}} \sqrt{P_j \alpha_{ij}} u_i H_{ij} v_j s_j}_{\text{Interference from all BSs except } l} \quad (5.1)
 \end{aligned}$$

As shown, this interference can be decomposed into two parts: The interference coming from the cooperating Macro Base Station (MBS) l and the interference from all other Base Stations (BSs). This second part is called Out of Cluster Interference (OOCI) as it represents the uncoordinated interference from outside the cooperation cluster.

In the following a new metric, named Out of Cluster Interference Ratio (OOCIR) is proposed. As it will be shown, this metric can be used to measure the effect of OOCI and is a main input to HRSH as it will be presented in Chapter 6.

Equation 5.2 shows the OOCIR for a PMS i . It expresses the ratio of uncoordinated versus coordinated interference and is defined as the sum of interference from not cooperating BSs versus the interference coming of the cooperating MBS l .

$$\text{OOCIR}_{i,l} = \frac{\sum_{\substack{1 \leq j \leq k \\ i \neq \{j,l\}}} |\sqrt{P_j} \alpha_{ij} u_i H_{ij} v_j s_j|^2}{|\sqrt{P_l} \alpha_{il} u_i H_{il} v_l (MRT) s_l|^2} \quad (5.2)$$

In Equation 5.2 it is assumed that the BSs do not select a precoder which is particularly suitable to reduce the interference, i.e. Maximum Ratio Transmission (MRT) precoding is used.

Knowledge about the OOCI and the OOCIR of an MS can be obtained by feeding back a Channel Quality Indication (e.g. an SINR estimate) from the MS to the BS. By using the CSI (see Section 2.5), especially the pathloss component it includes, the OOCI and OOCIR can be extracted. In addition, measurements for handover between cells (mobility management) which contain the reference signal received power at the MS for different BSs [88] can be used to estimate OOCI and OOCIR.

The key finding with respect to the OOCIR is as follows: If for a PMS i , served by Pico Base Station (PBS) i , OOCI dominates such that $\text{OOCIR}_{i,l} \gg 1$, there is only a low influence of the precoder v_l onto the performance of PMS i . In contrast, $\text{OOCIR}_{i,l} \ll 1$ indicates a strong influence of v_l onto the performance of PMS i .

Figure 5.1 details this by depicting the maximum achievable spectral efficiency gain factor at different levels of OOCIR. A factor of $10^0 = 1$ stands for no achievable performance gain and a factor of 10 stands for a tenfold spectral efficiency when using Zero Forcing (ZF) precoding. The results were calculated under the assumption of an Signal to Noise Ratio (SNR) of 30 dB. For different levels of interference (expressed by the Signal to Interference Ratios (SIRs)) the achievable spectral efficiency gain can be estimated based on the Shannon capacity (Equation 2.1). The gain is based on the assumption that a part of the interference (the one which is originating from the coordinating BS) can be removed completely through ZF precoding at the coordinating BS. The highest gains are achievable for very strong levels of interference (SIR = -15 dB). Here, without interference mitigation nearly no communication is possible. If it is assumed that a vast majority of this interference comes from inside the interference cluster (OOCIR = -20 dB) and thus can be removed, the spectral efficiency can be improved by a factor of 65. For lower levels of interference (e.g. SIR = 10 dB), lower gains are achievable due to an improved performance without coordination. With a growing fraction of interference from outside

the cooperation cluster, the gains are reduced. At high levels of OOCIR no significant gains are possible. The fact that at low SIRs high gains are achievable also underlines the suitability of CBF in heterogeneous networks with cell range expansion as described in Section 2.3.

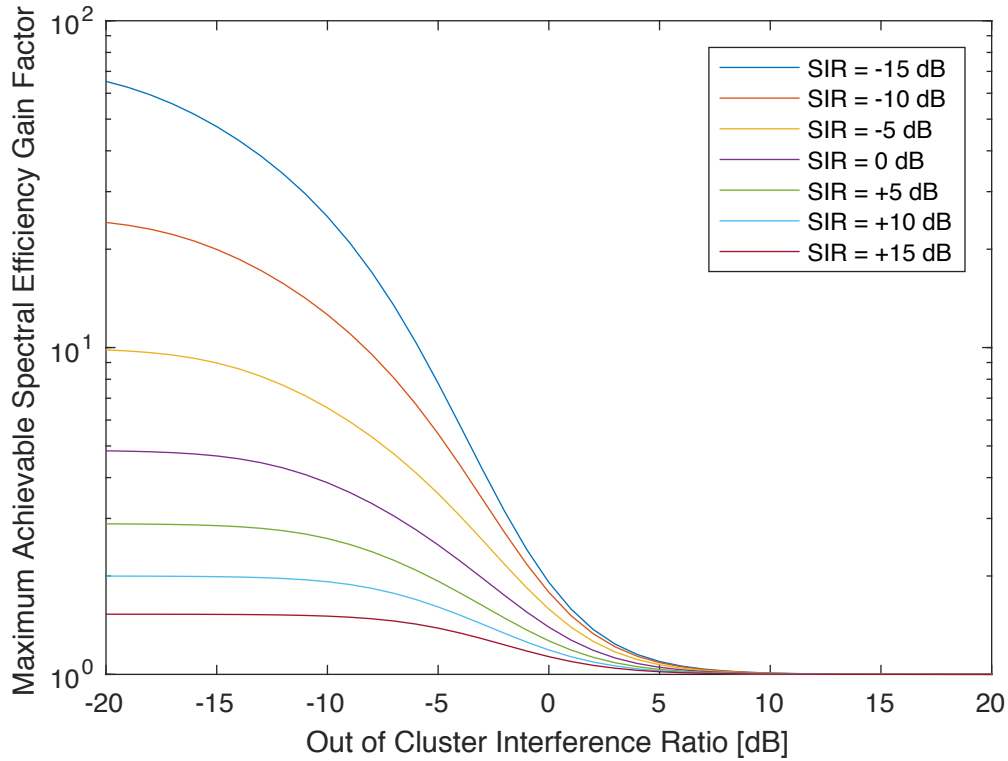


Figure 5.1: Maximum achievable spectral efficiency gain factor for different levels of Out of Cluster Interference

In the following the results of a simulation that studies the effect of OOCI in more detail are described. Figure 5.2 shows the network layout which is used for this. It consists of three BSs: One PBS which cooperates with an MBS and one MBS which is not part of the cooperation. Each BS serves one corresponding MS, indicated by the lines. The MSs are named as follows:

- Cooperating Pico Mobile Station (cPMS): MS attached to the cooperating PBS
- Cooperating Macro Mobile Station (cMMS): MS attached to the cooperating MBS
- Not Cooperating Macro Mobile Station (ncMMS): MS attached to the not cooperating MBS

The pathloss is assumed to be the free space propagation loss and the channel transfer function created based on the assumption of Rayleigh fading. The system is assumed to

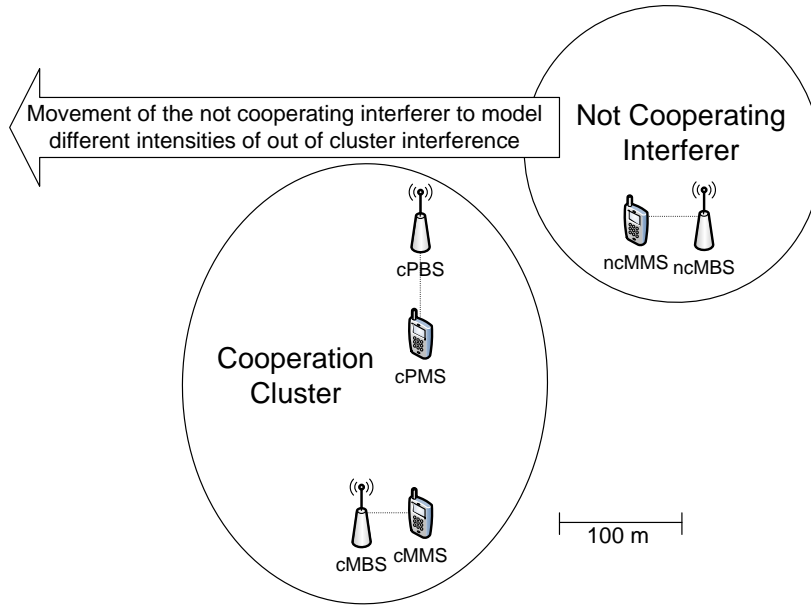


Figure 5.2: Network Layout with three Base Stations

be single-carrier system and as there is only one MS per BS, no scheduling is required. The cooperating BSs coordinate their beams (precoders) using HetNet RZF. The ncMBS does not take into account the cooperation and uses MRT to maximize the power the ncMMS receives.

The intention of this simulation is to expose the cooperation cluster to different levels of OOCI and to evaluate the effect which OOCI causes. In this simulation, modifying the level of OOCI is achieved by changing the location of the ncMBS and the ncMMS. By doing so, the pathloss between the ncMBS and the cPMS/cMMS ($\alpha_{ncMBS,cPMS}$ and $\alpha_{ncMBS,cMMS}$) and thus the level of OOCI can be varied. It should be noted that this approach is not a means for modifying OOCI in practical systems, as BSs are installed at fixed locations there.

As the investigation focuses on the performance of the cPMS under different levels of OOCI, in the following several performance indicators will be studied with respect to the distance between the source of the OOCI (the ncMBS) and the cPMS. The ncMBS is moved from the location where it is located in Figure 5.2 to the left (as indicated by the arrow), thus creating more and more OOCI. In the worst case, the distance between ncMBS and cPMS gets as low as 100 metres (when the ncMBS is located at the same position as the cPBS). After this point the situation improves again and less OOCI occurs.

Figure 5.3 shows two basic measures of the situation at the cPMS. The red curve shows the so-called geometry (for more details see Section 3.5). It is defined as the ratio between the power the cPMS receives from the cPBS and the sum of the power it receives

from cMMS and ncMMS (Equation 5.3).

$$G_{cPMS} = \frac{P_{cPBS} \alpha_{cPBS,cPMS}}{\sum_{i=cMBS,ncMBS} P_i \alpha_{i,cPMS}} \quad (5.3)$$

This value is purely based on the power level at the receive antenna of the cPMS. It does not take into account any gains that can be obtained from signal processing (precoding at the BSs, receive processing at the MS). The blue curve shows the OOCIR as described by Equation 5.2.

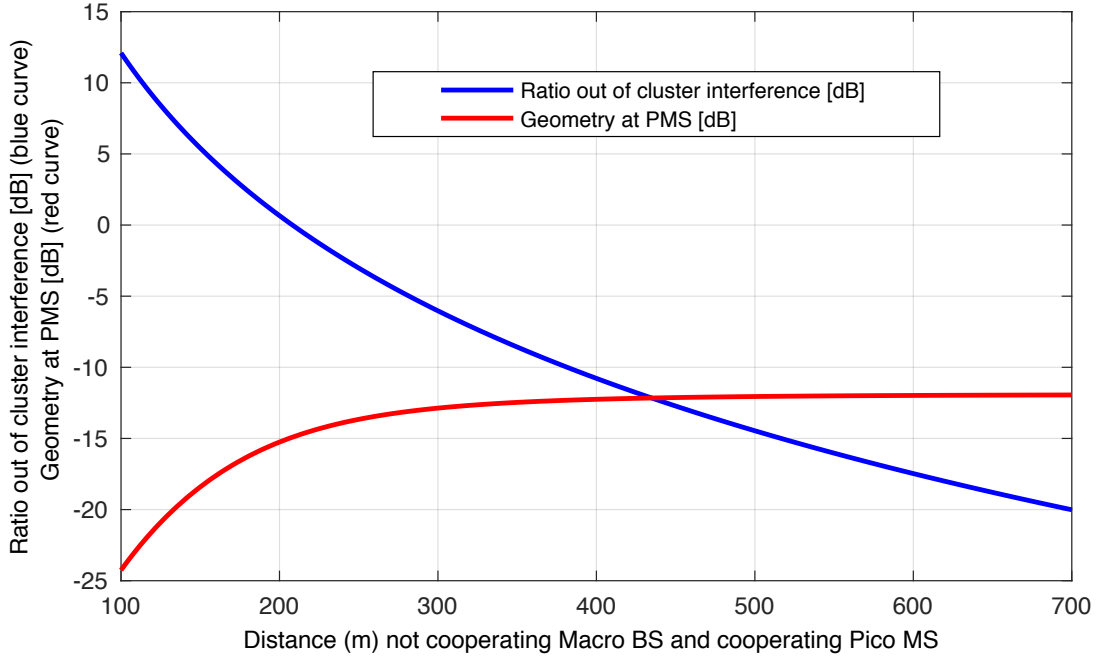


Figure 5.3: Geometry and Out of Cluster Interference Ratio of the Pico MS

Both measures are depicted with respect to the distance between the ncMBS and the cPMS. They can be seen as a representation of the network layout from the cPMS's point of view as they describe the powers which arrive there. As mentioned before, the worst situation occurs when the distance between ncMBS and cPMS equals 100 metres. At this point the geometry is approximately -24 dB, meaning that the cPMS receives interference (from ncMBS and cMBS) which is 24 dB stronger than the power it receives from the cPBS. The OOCIR is around 12 dB, meaning that the vast majority of the interference comes from outside of the cooperation cluster. As the distance between the ncMBS and the cPMS grows, the situation improves: The geometry increases and more and more of the interference originates from inside the cooperation cluster (decreasing OOCIR).

Figure 5.4 shows the amount of interference which is present in the receiver of the cPMS when taking into account signal processing at the BSs (precoding) and receive

combining at the MS. The simulation is executed with different settings of λ_1 , ranging from 1 (MRT) to 0 (ZF). At a distance of 100 metres between ncMBS and cPMS the interfering power is nearly equal for all settings. The reason is the high OOCI: The cooperation can only reduce interference from inside the cooperation cluster (from the cMBS) which is a small fraction at this point. The lower the OOCI gets, the higher is the gain from mitigating interference by means of selecting lower values of λ_1 . This reduction in interfering power is the benefit of the cooperation. Figure 5.5 shows the cost of the cooperation: A reduction of the useful signal at the cMMS (as also discussed in Section 4.1.5). As the distance between cPMS and cPBS is constant, it does not change with a varying distance between cPMS and ncMBS.

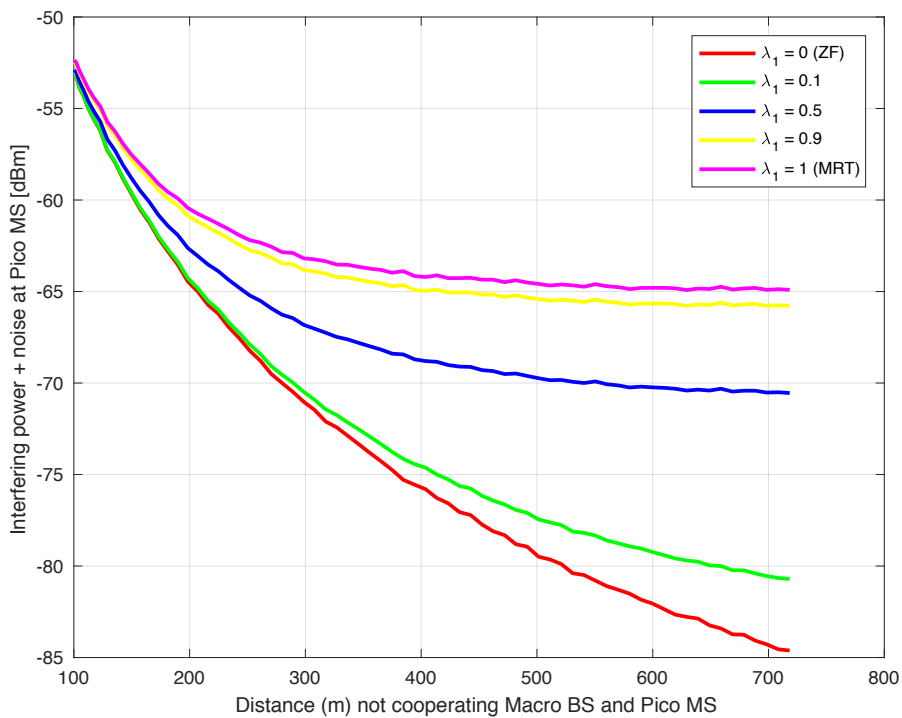


Figure 5.4: Interfering Power at the cooperating Pico MS

Figure 5.6 show the spectral efficiency the cPMS and the cMMS can achieve (estimated via the Shannon capacity definition as given in Equation 2.1). For distances of 100 to 150 metres between cPMS and ncMBS the spectral efficiency is very low. Additionally, there are nearly no gains from CBF in this region. For higher distances gains from CBF can be obtained. A comparison of Figure 5.3 and Figure 5.6 reveals two important points:

- With a low OOCI ratio (e.g. -15 dB at 500 metres) it is possible to achieve relatively high spectral efficiencies, despite the low geometry at the cPMS. This proves the potential of CBF, especially for cases with a low geometry, as it is caused by Cell

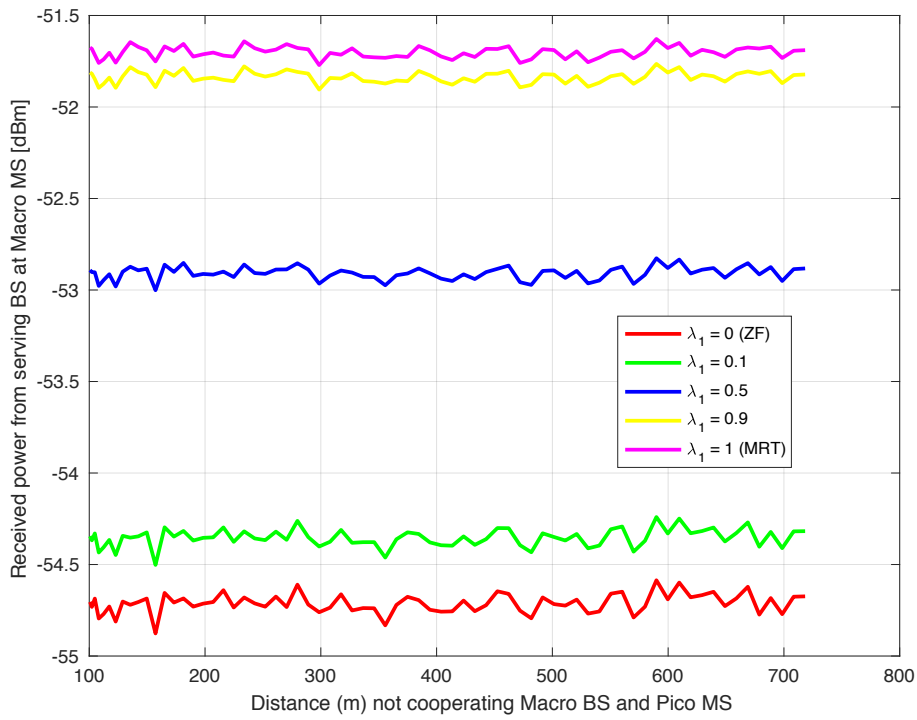


Figure 5.5: Useful Power at the cooperating Macro MS

Range Expansion (CRE).

- Gains from CBF can be obtained mainly in the regions where the OOCI ratio is negative (distance more than 200 metres).

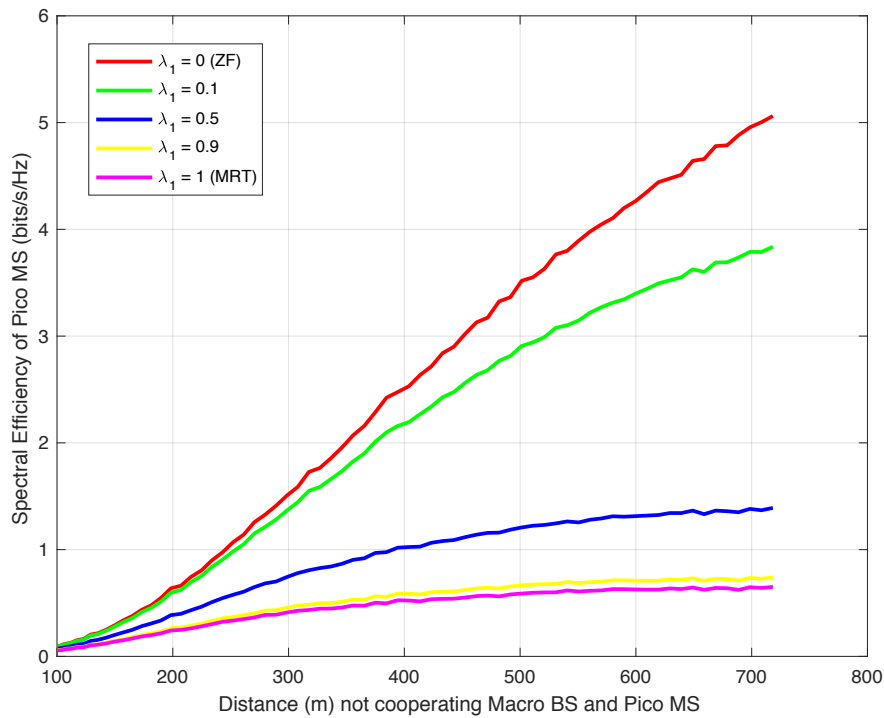


Figure 5.6: Spectral Efficiency at the cooperating Pico MS

Figure 5.7 shows the spectral efficiency of the cMMS. As the cMMS is also interfered by the ncMMS, its spectral efficiency increases with an increasing distance between the MBS and the cPMS due to lower interference. Again, the cost of the cooperation can be seen: The cMMS achieves the best performance when an MRT transmission is used, whereas a ZF transmission reduces its performance.

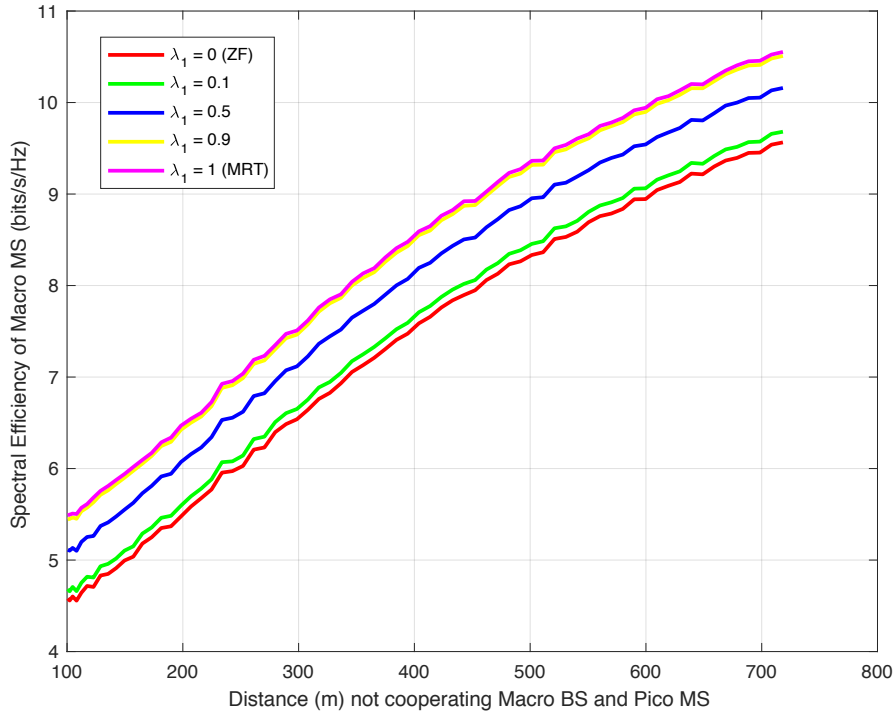


Figure 5.7: Spectral Efficiency at the cooperating Macro MS

Figure 5.8 shows the sum of the spectral efficiencies of the cMMS and the cPMS. It can be seen that there is a crossing point at approximately 290 metres. From a sum spectral efficiency point of view it is at lower distances beneficial to only apply MRT precoding. Beyond this point, ZF precoding becomes beneficial. However, it should be noted that for the PMS already at 200 metres distance substantial gains be realized (see Figure 5.6). In a large scale system with multiple MSs this can be important, e.g. in case a certain PMS has a higher demand than other MSs or achieves an unacceptable low performance without CBF. To summarize, this section described the effect of OOCI, which can significantly limit the performance of CBF. A new metric, named OOCIR was introduced. It provides an insight on the situation with respect to OOCI at the PMSs and therefore can be used to determine whether CBF can be beneficial under the current conditions.

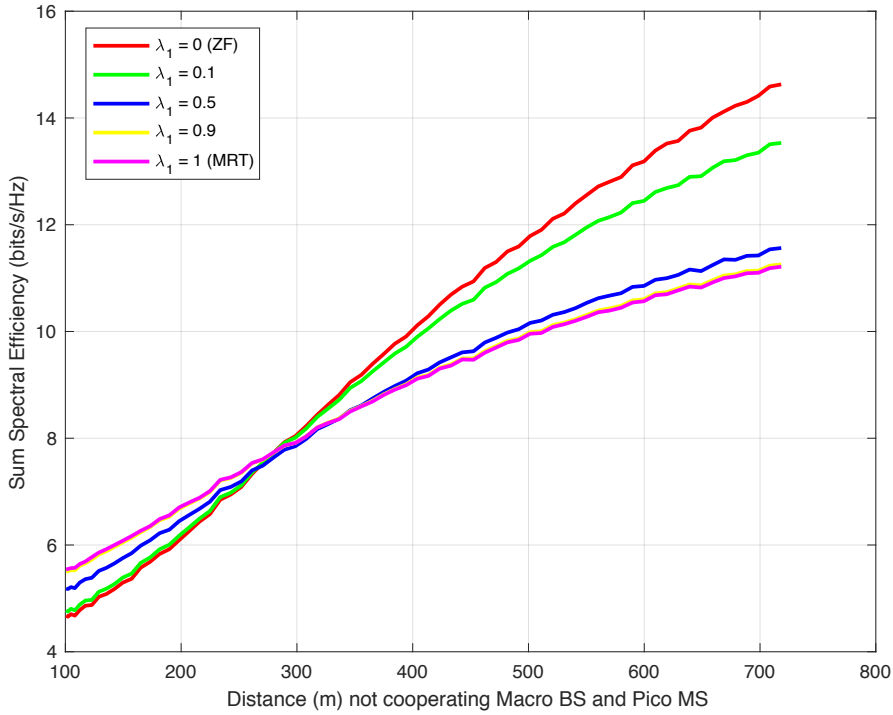


Figure 5.8: Sum Spectral Efficiency of Pico and Macro MS

5.2 Influence of the number of MSs per BS

A second factor that influences the performance of CBF is the number of MSs in the system. Its effect is based on the degrees of freedom throughout the scheduling process, as it will be described in the following. For an PMS i , served by PBS i , the coordinated scheduler selects a second MMS l to be served using the same radio resource at the cooperating MBS l . Even if the MBS uses MRT precoding only ($\lambda_1 = 1$) there is a potential for the coordinated scheduler to reduce interference at the PMS: Each MMS is associated with a corresponding precoder v_l that would be used to serve it. As each precoder v_l causes a different level of interference at the PMS i , the selection of an MMS l decides also on the level of interference at PMS i . The potential for an interference suppression at a PMS when using MRT only grows with the number of Macro Mobile Stations (MMSs): The higher it is, the higher is the variety of precoders out of which the coordinated scheduler can select. In the same way the corresponding likelihood increases that this includes a precoder with a significantly reduced interference at PMS i .

With respect to calculating additional precoders with interference suppression at the MBS ($\lambda_1 < 1$), the situation is vice versa. If for a PMS i there is an MMS l which significantly mitigates the interference while it is served with MRT precoding, there is only a low potential for improvement by calculating additional precoders. In contrast,

if there is only one MMS attached to MBS l , the degrees of freedom collapse to zero, meaning that this MMS has to be served in order make use of the corresponding Physical Resource Block (PRB). This happens without respect to how much interference occurs at PMS i . In such cases there can be a high benefit from calculating additional precoders that suppress interference.

To underline the considerations with respect the number of MSs a simplified simulation for a single-carrier with Rayleigh fading and without pathloss (i.e. $P = \alpha = 1$, the elements of H follow a Gaussian distribution in amplitude and phase) was carried out. OOCI was not considered in this simulation. Figure 5.9 shows an example for a result that was obtained with it: It assumes the presence of 50 MMSs and 50 PMS and depicts the level of interference at the PMS i when it is simultaneously served with an MMS l . The following effects can be seen:

- Certain PMSs experience a low level of interference in general (e.g. PMS 8), others a high level (e.g. PMS 14). This is caused by the amplitude of the interfering radio channel from the MMS to the PMSs. If this amplitude is low, the corresponding PMS in general shows a low level of interference, independent of which MMS is served in parallel. The opposite effect occurs for an radio channel with a high amplitude. These differences in amplitude do however not provide a means for interference suppression as in order to maintain fairness also MSs with a high level of interference have to be served.
- The interference at the PMSs is affected by the selection of the MMS to be served simultaneously. This can for example be observed at PMS 3, which shows a higher interference when served in combination with MMS 2 instead of MMS 1.

To generalize this example a simulation with multiple runs was executed. Its procedure is depicted in Figure 5.10 and executes the following steps:

1. The simulation starts with one PMS and one MMS. At a following step these numbers will be increased.
2. For the current number of MSs the interference at the PMS(s) is investigated, which heavily depends on the radio channels. To gain reliable results, this calculation must be repeated multiple time with different realizations of the radio channel. Therefore the following calculation is repeated in a loop.
 - (a) Generation of the radio channels

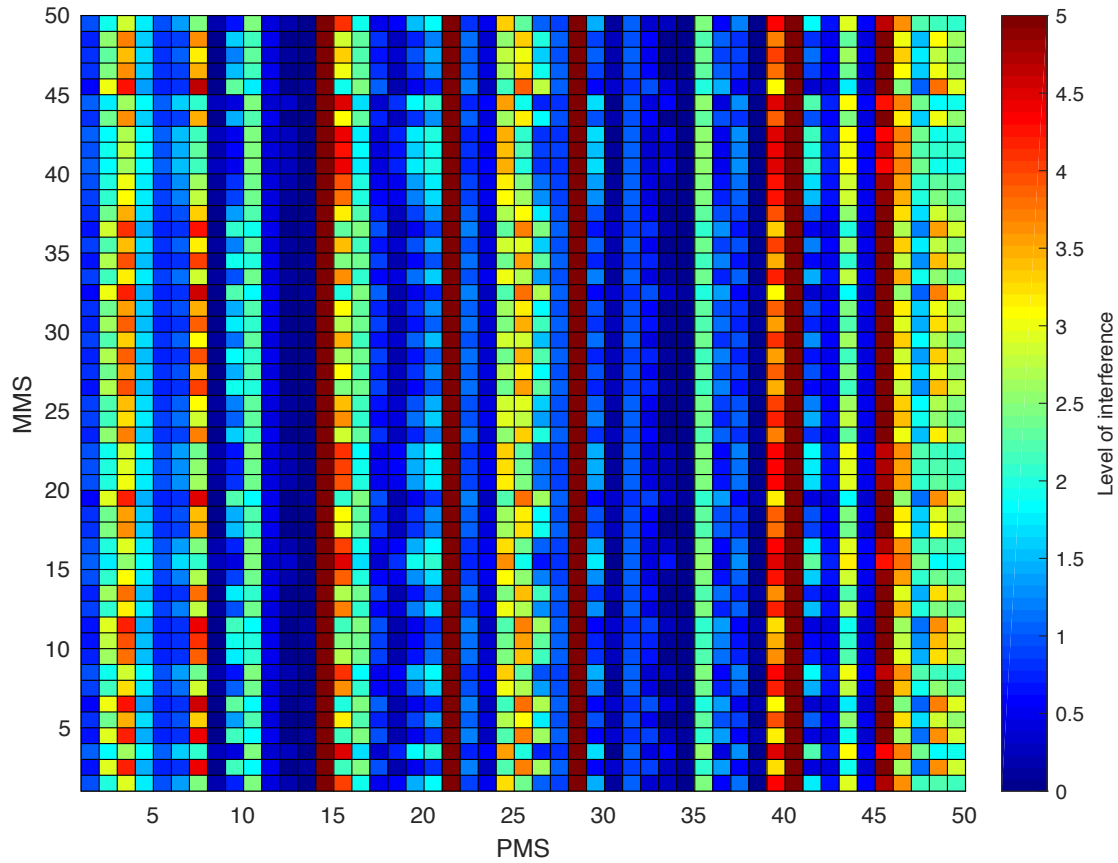


Figure 5.9: Example for the influence of the number of MSs in the system: Interference Level at the PMS when begin simultaneously served with an MMS

- (b) Calculation of the minimum interference I_{min} per PMS: Here the different MMSs (in case their number is greater than one) are tested for the interference they cause at the each PMS. The minimum interference per PMS is stored.
 - (c) In case there are multiple PMSs, the mean of I_{min} is saved as I_{run} .
3. After finalizing this loop, a number of results for I_{run} are available, containing the result of the individual runs within the loop. The mean of these values is stored as I_{mean} . It represents the final result for the current number of PMSs and MMSs.
 4. The number of MMSs is increased and the calculation described above is repeated for this new configuration.
 5. Similarly, also the number of PMSs is increased and the corresponding calculation is repeated (starting with one MMS again).

This simulation gives an insight on the minimum interference at the PMS(s) when using MRT only in a coordinated manner. It is based on the assumption that in a coordinated scheduling each PMS is combined with the MMS that minimizes the interference.

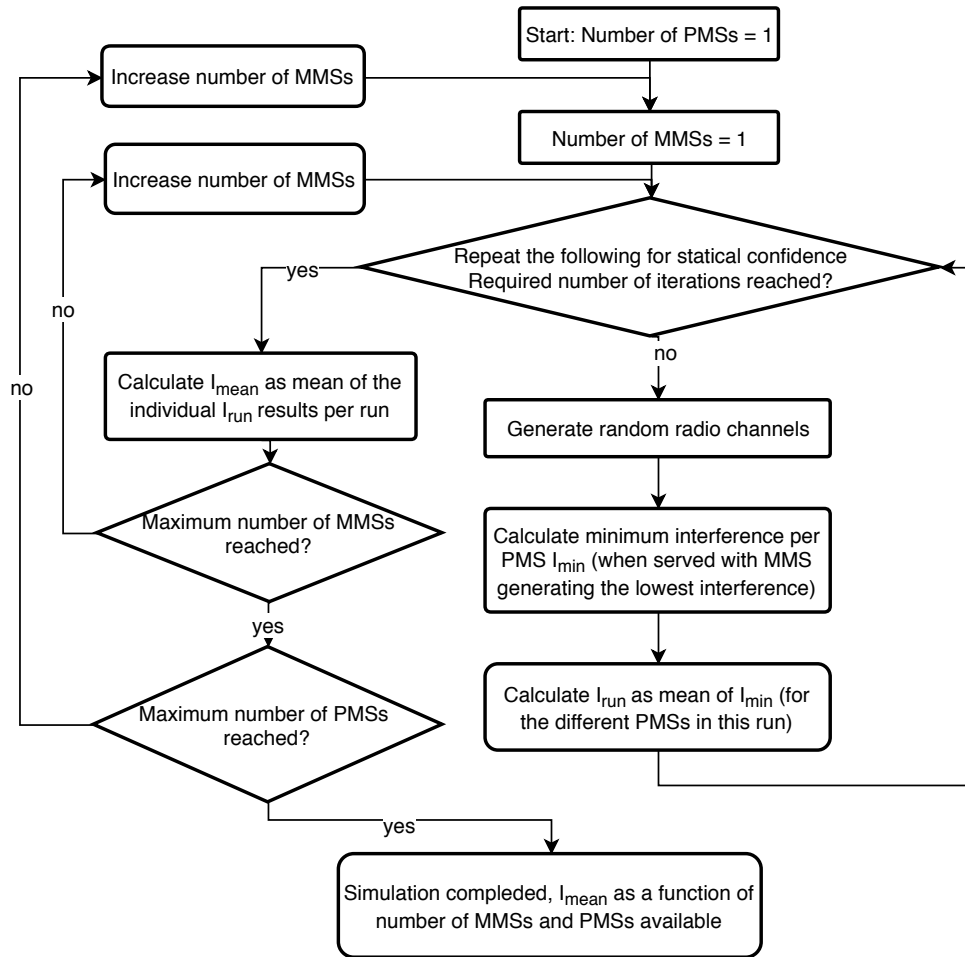


Figure 5.10: Flowchart of the simulation to evaluate the effect of the number of mobile stations in the system

Figure 5.11 shows results obtained from this simulation with 1000 runs per number of MSs. As expected, a significant impact of the number of MMSs is observed, whereas there is no impact of the number of PMSs. Under the ideal assumption in this simplified calculation this is expected, as each PMS is studied independently and statistically receives the same interference, independent of the number of other PMSs in the system.

In a complete system with multiple PRBs and a detailed scheduling algorithm it is not always possible to serve the MSs under the assumptions above due to fairness constraints. In a case with two MMSs and one PMSs it is for example not possible to only serve the MMS that minimizes interference at the PMS. Therefore the following changes to the results in Figure 5.11 are expected: The impact of the number of MMSs is foreseen to be lower due to constraints in the resource assignment that make certain allocations impossible. On the other hand, an increased number of PMSs increases the degrees of freedom in the resources allocation and can therefore cause reductions in interference which are not observed here.

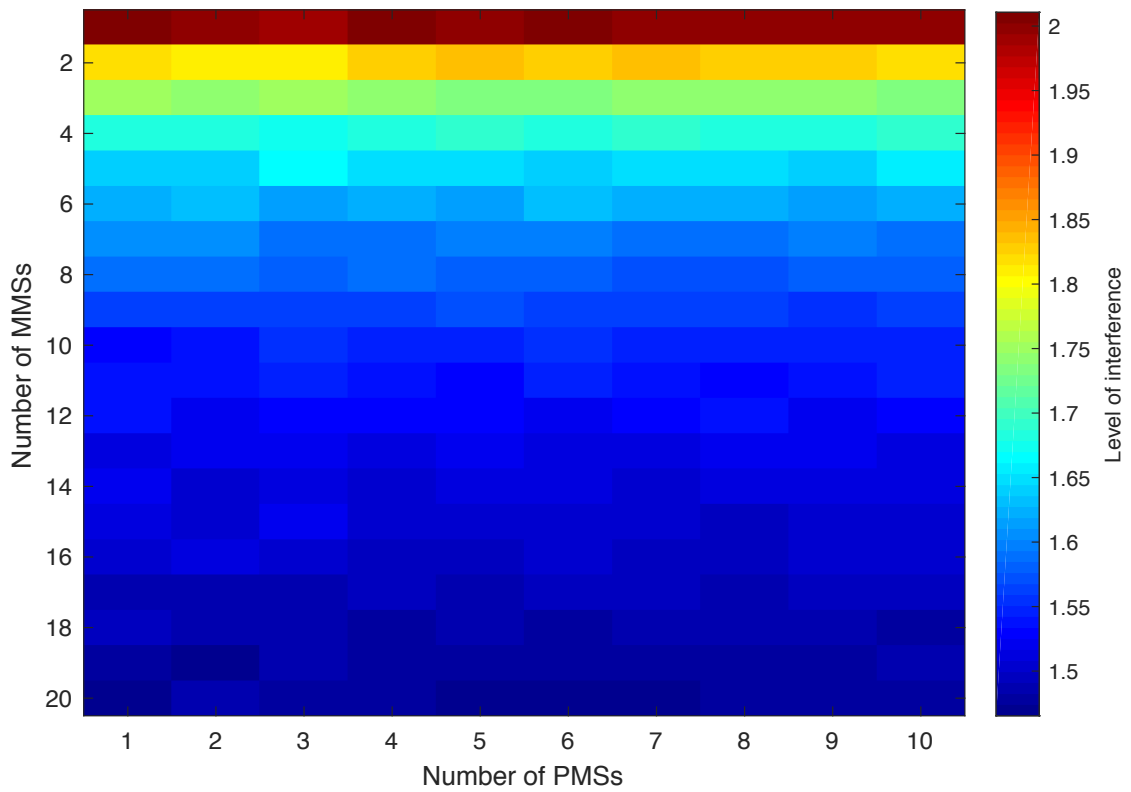


Figure 5.11: Simulation result for the effect of the number of MSs on the interference at the PMSs

Figure 5.12 shows a more detailed view on the result in Figure 5.11 by showing the interference for the case of a single PMS as a function of the number of MMSs. It can be seen that for an increase in the number of MMSs has a significant impact until the effect saturates at six MMSs.

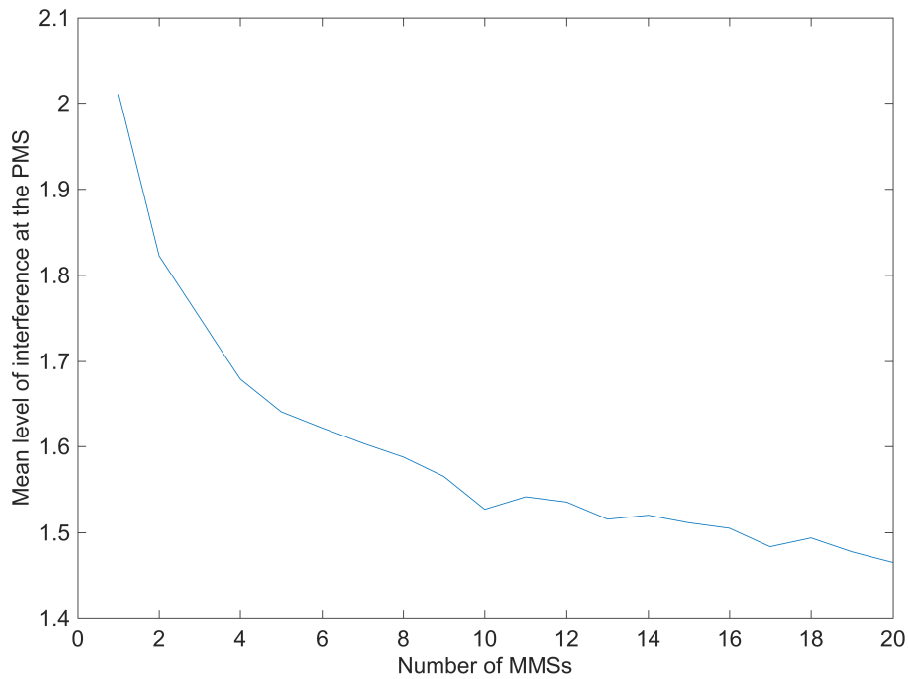


Figure 5.12: Simulation result for the effect of the number of MMSs on the interference at the PMS

5.3 Summary

This chapter described the two performance limiting factors which were identified by means of extensive simulations and under the usage of HetNet RZF:

- Out of Cluster Interference (OOCI) can significantly impact the achievable gain. Therefore a new metric, named Out of Cluster Interference Ratio (OOCIR), was defined. It can be used to measure the estimated benefit of reducing interference at a PMS by means of precoding at the MBS. It was shown that at low levels of OOCI, e.g. $\text{OOCIR} = -20$ dB, a 65-fold spectral efficiency can be possible, whereas at $\text{OOCIR} = 20$ dB no gains are achievable.
- The number of MSs in the system affects the performance of CBF in a different way: At a high number of MSs, a coordinated scheduler (as described in Section 4.2) can make use of the variety of available MRT precoders and therefore does not require the calculation of additional interference-suppressing precoders.

The findings on the performance limiting factors will be used in following Chapter 6 to reduce the computational complexity in the scheduling process. With the identification of two performance limiting factors, the first objective as part of the research problem

(Section 2.7) was addressed. However, as part of the definition of this first objective, also a list of important assumptions made for large-scale multi-carrier networks was established, which are only partly covered in this chapter due to the simplified simulations used here. To fully address the first objective, Chapter 7 therefore complements the simulation results provided here with detailed System Level Simulations (SLSs).

Chapter 6

Reduced Complexity Scheduling

Heuristic for Coordinated Beamforming

The scheduler is a core functionality of a Base Station (BS) [71]. Besides its main task of assigning Physical Resource Blocks (PRBs) to the Mobile Stations (MSs), it also controls a set of other related functions, such as the precoding and the modulation and coding. In total, the process of scheduling can be computationally complex, especially in the case of Coordinated Beamforming (CBF), as it will be shown in the following.

With respect to applying CBF, the description of the design of HetNet Relaxed Zero Forcing (RZF) in Chapter 4 showed an important advantage of RZF in general and therefore also of HetNet RZF: The HetNet RZF precoding algorithm reveals a set of different precoders to the scheduling algorithm. As a result, there is an additional degree of freedom in the scheduling: The control of HetNet RZF through the selection of the control parameter λ_1 . However, this additional degree of freedom also comes with the cost of an increased complexity of the scheduling process. Section 6.1 describes this fact in more detail. The findings from Chapter 5 are then used in Section 6.2 to propose a scheduling heuristic named HetNet RZF Scheduling Heuristic (HRSH) with limited computation complexity, which is the third contribution of this Thesis. HRSH is based in the scheduling algorithm described in Chapter 4. Section 6.3 discusses its expected performance and the determination of its configuration parameters before Section 6.4 provides a summary.

6.1 The complexity of scheduling in the case of coordination beamforming

Section 4.2 introduced a scheduling algorithm for a cooperation cluster of one Macro Base Station (MBS) and one Pico Base Station (PBS). It is designed to control the HetNet RZF precoding. This scheduling algorithm is also the basis for the HRS algorithm that will be proposed in Section 6.2. The aim of this section is to assess the computational complexity of the scheduling process defined in Section 4.2 and to provide a metric to quantify it.

The output of the coordinated scheduling algorithm described in Section 4.2 is the following decision, per PRB:

1. Assignment of the PRBs to the MSs, whereas one PRB is assigned to a pair of one Macro Mobile Station (MMS) and one Pico Mobile Station (PMS).
2. Selection of precoders, which is in the case of HetNet RZF especially the selection of λ_1 per PRB.

To find the best scheduling decision, the potential options must be evaluated and compared, which in the context of this work is to calculate their benefit in terms of the proportional fair metric. Each potential scheduling decision realizes, for each PRB, a different throughput at the MBS and at the PBS. Besides the proportional fair metric itself, therefore also network performance is heavily influenced by the quality of the scheduling. Finding the best scheduling decision is computationally complex due to the large number of potential assignments. Equation 6.1 describes the number of options in the scheduling process ($N_{choicesRR}$) for one PRB. It scales linearly with the number of PMSs, the number of MMSs and the number of realizations of λ_1 . Each option requires the calculation of two precoders (one per MS).

$$N_{choicesPRB} = N_{PMS} \cdot N_{MMS} \cdot N_{Steps\lambda_1} \quad (6.1)$$

As a scheduling decision is required for each PRB, the total number of options scales with the number of PRBs N_{PRB} (Equation 6.2).

$$N_{choicestotal} = N_{choicesPRB} \cdot N_{PRB} \quad (6.2)$$

Each potential decision leads to an expected data rate for the two transmissions. Along with the principle of proportional fair scheduling, these instantaneous data rates, in combination with the data rates the two MSs achieved in the past, can be used to calculate the proportional fair metric (Equation 4.47). The target is for each PRB to find the setting (in this case the pair and the configuration of λ_1) with the highest metric value. Figure 6.1 visualizes this with an example from a simulation where nine pairs of one PMS and one MMS exist. Each sub-figure depicts the metrics per pair (x-axis) and PRB (y-axis). The different settings of λ_1 cause significant difference in terms of the metric in this example. Pair one for example shows higher metric values at $\lambda_1 = 0$ whereas pair nine should be served at higher values of λ_1 . In addition, there are significant fluctuations from PRB to PRB for each pair. This example for nine pairs caused the calculation of 9900 precoders (9 pairs, 2 precoders per pair, 50 PRBs, 11 realizations of λ_1) and 4450 metric values that have to be analysed with the aim of finding the highest value per PRB.

There is a trade-off between the computational complexity of the scheduling process and the quality of the decision: Finding the PRB with the highest metric value causes that all $N_{choicestotal}$ precoders have to be calculated and evaluated in terms of their metric. This is especially challenging due to the real-time requirements: A scheduling decision has to be taken periodically per Time Transmission Interval (TTI) (e.g. per millisecond in the case of Long Term Evolution (LTE)), meaning that the calculations for a decision have to be finalized before generating the next one. Reducing the complexity is possible by not evaluating every single scheduling decision. However, this implies the risk that also the potential decision with the highest metric is not found and thus the performance of the network is degraded.

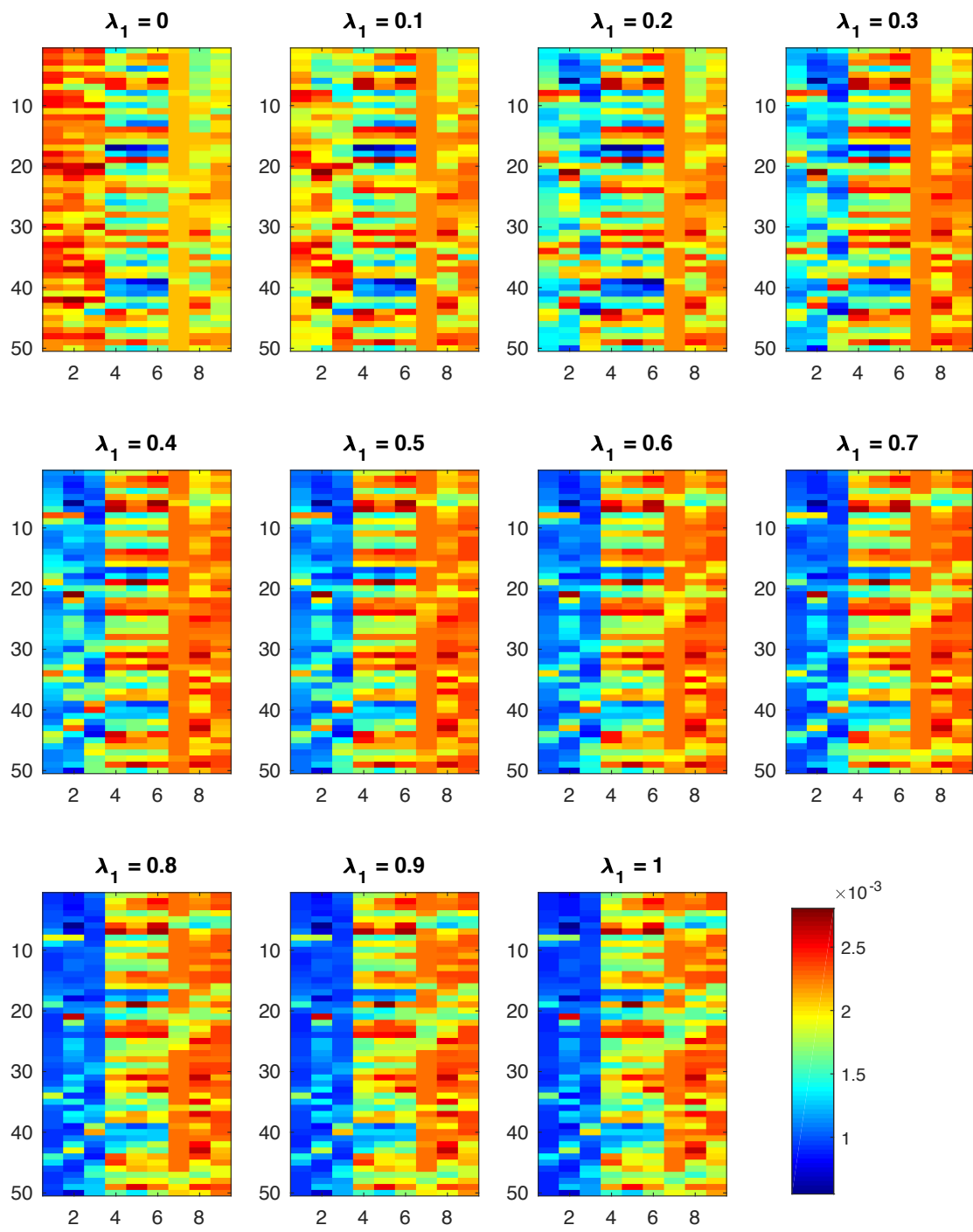


Figure 6.1: Example for proportional fair metric values in the case of HetNet RZF. Each figure depicts the proportional fair metrics for the pairs (x-axis) and the PRBs (y-axis)

6.2 HetNet RZF scheduling heuristic

In the following, a heuristic approach for reducing the computational complexity of the scheduling process is presented, named HetNet RZF Scheduling Heuristic (HRSH). HRSH is designed to effectively apply HetNet RZF in a coordinated scheduler. It relies on the fact that certain requirements have to be fulfilled for advantageous effects of suppressing interference at the PMS which were identified in Chapter 5. If these requirements are currently not fulfilled, selected transmission parameters can be excluded from the considerations in the scheduling process. As these transmission parameters would show lower or equal performance compared to others, their exclusion can theoretically happen without affecting the performance.

Section 6.1 showed the number of potential scheduling decisions when HetNet RZF is applied. Investigating every potential decision is computationally complex but guarantees that the element with the highest metric is found. Restricting the search space implies the risk of leaving out the best element and thus generating a sub-optimal decision. However, for an implementation in real systems where computational resources are limited, lower complexity is important, even if it does not achieve optimal performance. This is especially relevant as the number of potential decisions scales linearly with the number of MMSs and at the same time with the number of PMSs (Equation 6.1). For a large number of MSs the problem therefore becomes highly complex. As it will be shown in Section 7.4, this can for example require for a network with 315 MSs and 42 BSs the calculation of 27.9 million transmission parameters within a time frame of 6 seconds.

HRSH makes use of the performance influencing factors described in Chapter 5 to restrict the computational complexity of the scheduling process. The target is for each PRB to find the two MSs PMS i and MMS l , in combination with the corresponding precoders, that maximize the proportional fair metric M_{PFS}^{HetNet} (Equation 4.47). At the same time, the number of assessed potential scheduling decisions N should be low compared to the total of options (Equation 6.3).

$$N \ll N_{choicestotal} \quad (6.3)$$

Chapter 5 showed that in a heterogeneous network with HetNet RZF the following trends apply:

1. The lower the OOCIR is, the higher the benefit of a reduced interference from

MBS l to a PMS i . In cases of low OOCIR, calculating the full range of HetNet RZF precoders ($\lambda_1 = [0, 1]$) should be considered.

2. The larger the number of MSs at MBS l is, the larger is the diversity of precoders available in case only Maximum Ratio Transmission (MRT) is used ($\lambda_1 = 1$). Therefore, lower gains can be achieved by calculating additional precoders with $\lambda_1 < 1$.

These trends can be converted into two thresholds: Calculating more than the MRT precoders is especially beneficial, in case

1. the OOCIR is below a threshold $T_{OO CIR}$ and
2. the number of MSs at MBS_l is below a threshold T_{nMS}

HRSR restricts the calculation of interference suppressing precoders ($\lambda_1 < 1$) to the cases where both thresholds are kept. In case one or both thresholds are reached or exceeded, only MRT precoders are calculated. Out of the reduced set of potential decisions the coordinated scheduler then selects the pair and a precoder with the highest proportional fair metric for each PRB. Figure 6.2 shows this process in more detail. As stated before, the heuristic is executed for a cooperation cluster of one MBS and one PBS. Its target is to assign each PRB to one PMS and one MMS. This decision has to happen inline with a calculation of the corresponding precoders. The process starts with generating all possible pairs of one PMS and one MMS in a cooperation cluster. It then continues with finding the assignment for the first PRB. To do so, it is checked pair by pair, whether the before-mentioned thresholds are kept for this PRB and this pair of two MSs. If yes (case 1), it is foreseen that the usage of interference suppressing precoders might be beneficial. Here a set of precoders is generated as described in Section 4.1. If one or both thresholds are exceeded (case 2), it is considered that generating a single MRT precoder per MS is sufficient. This separation of the pairs into two classes is the key element of HRSR. It enables that for a part of the pairs computations are avoided. Each pair has now been associated with corresponding precoders. This can either be a set of precoders (case 1) or a single MRT precoder per MS (case 2). The throughput that each pair can achieve is estimated in the next step. This can again be a multitude of values (case 1) or a single value per MS (case 2). The throughput values are then converted into proportional fair metric values (Equation 4.47). The PRB is finally assigned based on finding the highest metric value. This is also directly coupled to the selection of the precoder: If the pair

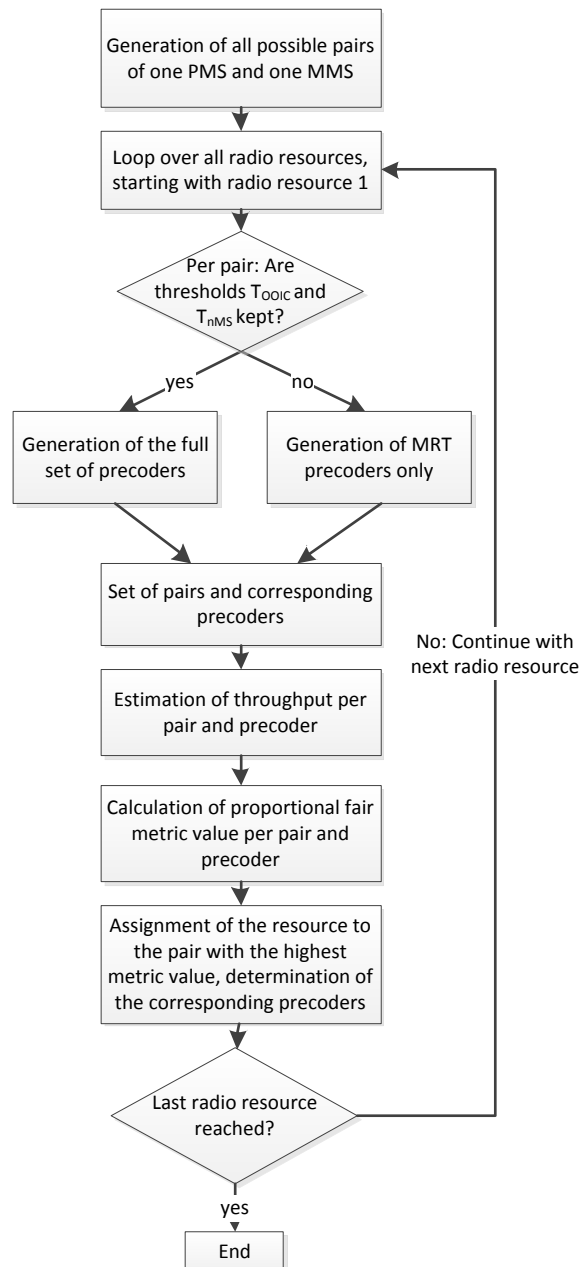


Figure 6.2: Flowchart of the HetNet RZF Scheduling Heuristic

is associated to a single MRT precoder per MS (case 2) the corresponding precoders are used. If there are multiple precoders for one pair (case 1), each precoder achieves a different performance and therefore is coupled with a different metric value. The highest metric value therefore in this case points not only to the pair to select but also to precoder to use. The process is then executed in the same manner for the remaining PRBs.

6.3 Configuration of the threshold parameters and expected performance

To find the configuration of the threshold parameters T_{OOCIR} and T_{nMS} , the results from Chapter 5 can be used. With respect to T_{OOCIR} , the general consideration in Figure 5.1 show that at with a growing Out of Cluster Interference Ratio (OOCIR) lower gains can be expected. At $OOCIR > 0$ dB the potential for a performance increase significantly reduces. It is therefore recommended to select T_{OOCIR} in this region. There is the possibility to relax the requirement e.g. by configuration $T_{OOCIR} = 3$ dB which might increase the performance on the cost of complexity. Also a more strict configuration e.g. $T_{OOCIR} = -3$ dB can be selected to reduce computational complexity on the cost of performance.

Looking at the configuration parameter T_{nMS} , the results in Figure 5.12 show that up to four MMSs there is a significant increase in performance possible after which the curve flattens out. It is therefore recommended to select T_{nMS} in the region of four. However, it should be noted that the results for the number of MSs in Chapter 5, in contrast to the results for Out of Cluster Interference (OOCI), depend on the conditions of the radio channel H : For a high number of MMSs a low potential for performance gains from calculating additional precoders is expected. This is due to the fact, that the diversity in the different realizations of H for the individual MMSs leads to different MRT precoders from which the scheduling algorithm can select. However, it might also be the case that MMSs have very similar realizations of H e.g. if they are located in close vicinity. For practical systems, it might therefore be required to calibrate this parameter based on different radio channel conditions.

In general the results in Chapter 5 describe the *potential* for performance gains which the scheduling algorithm might not be able to realize, due to other constraints such as fairness. It could for example be the case that an PMS is under excellent conditions for CBF such that all potential precoders are calculated. If, however, there is a second PMS which has to be served due to fairness reasons, the potential gains of the first PMS cannot be realized. This fact motivates the selection of more tight threshold parameters as only parts of the potential performance gains can be realized.

6.4 Summary

This chapter proposed a scheduling heuristic named HRSB with a reduced computational complexity, which is the third contribution of this Thesis and addressed the third objective described as part of the research problem (described in Section 2.7). The scheduling heuristic is designed to find a scheduling decision with a high proportional fair metric, without evaluation all potential options. To achieve this, it applies the knowledge of the performance limiting factors, gained in Chapter 5.

Section 6.3 showed how the findings from Chapter 5, namely the simulation results provided there, can also be used to set the configuration parameters of HRSB.

The following Chapter 7 will apply the detailed simulation methodology described in Chapter 3 to evaluate of the performance of HRSB. As it will be shown, HRSB can significantly reduce the computational complexity with only a small degradation in terms of the MS throughput.

Chapter 7

Performance Analysis

In this chapter simulation results that were obtained with the Deutsche Telekom System Level Simulator (DT SLS) are presented, with the following targets:

- Chapter 5 identified two performance limiting factors, addressing the first objective as part of the research problem in Section 2.7. However, as part of the definition of the first objective, also a list of important assumptions made for large-scale multi-carrier networks was established, which were not completely covered in Chapter 5 due to the simplified simulations used there. To fully address the first objective of this work, this chapter therefore complements the simulation results provided in Chapter 5 with detailed System Level Simulations (SLSs). As it was shown in Section 3.8, the DT SLS, in combination with the precoding and scheduling algorithm designed in Chapter 4 fully covers the assumptions for large-scale multi-carrier networks made in Section 2.7.
- The heuristic scheduling algorithm HetNet RZF Scheduling Heuristic (HRSB), proposed in Chapter 6.1 should be simulated to validate its performance, especially in terms of reducing the computational complexity.

This chapter is structured as follows: Section 7.1 describes the selected simulation parameters. Section 7.2 shows the results of simulations evaluating the effect of the number of Mobile Stations (MSs), as described in Section 5.2. Section 7.3 then gives performance results for two different large networks consisting of tens of Base Stations (BSs) such that especially the Out of Cluster Interference (OOI) is modelled realistically. Section 7.4 evaluates the HRSB algorithm proposed in Section 6.2 in terms of the computational complexity. In Section 7.5, it is discussed how far the results presented here are also

applicable to other precoding and scheduling algorithms as well as other traffic models. Section 7.6 then provides a summary of the simulation results.

7.1 Simulation parameters

The simulation parameters under which the following results were obtained are listed in Table 7.1. The majority of the parameters have been selected according to settings used in Third Generation Partnership Project (3GPP) simulations [89][90][91][85], which is also indicated in the table. In addition, the parameters were selected such that HetNet Relaxed Zero Forcing (RZF) can be applied, which is especially the of antennas at the MSs and BSs (2) and the MS receiver type (Maximum Ratio Combining).

Table 7.1: System level simulation parameters

Parameter	Value	Reference
Inter Site Distance	500 m (3GPP case 1)	[85][91]
System Bandwidth	10 MHz, DL (50 PRBs)	[90][85][91]
Carrier Frequency	2 GHz	[90][85]
Macro Base Station (MBS) transmit power	46 dBm	[90][85]
Antennas at BS and MS	2	[90][85][91]
MBS antenna pattern	3GPP 2D ant. model with 14 dBi max. gain	[90][85]
Pico Base Station (PBS) transmit power	37 dBm	[90][85]
PBS antenna pattern	Omni directional in azimuth with 3 dBi gain	
Cell Range Expansion Offset (Section 2.3)	9 dB	[25]
Channel and Propagation Model	ITU-R M.2135 Urban Micro (PBS) / Urban Macro (MBS)	[14]
MS receiver type	Maximum Ratio Combining	
MS Speed	3 km/h	[90][85][91]
Traffic Model	Full buffer	[90][85][91]
Link Adaptation	Ideal	Motivated in Section 2.7
Channel State Information	Ideal	Motivated in Section 2.7
Number of MSs and BSs	Varying, see different simulations below	
Network Layout	Varying, see different simulations below	[90]

7.2 Influence of the number of mobile stations in a network with two base stations

To complement the simplified simulations in Section 5.2, this section studies the effect of the number of MSs by means of SLS. To investigate the effect of the number of MSs without other influences, a special network configuration without OOCI is required, which is described in the following. It consists of a single MBS with one PBS inside its coverage area (with 225 metres distance between MBS and PBS). To avoid also OOCI between sectors (sector one of site one creates OOCI in sector two of site one), the MBS was configured with an omni-directional antenna without sectorization. The so-called hotspot MS distribution (configuration 4b in [85]) was used, such that two-thirds of the MSs are located in the vicinity of the PBS. This reflects the fact that operators will tend to install PBSs at locations with a high density of MSs in order to fulfil the corresponding traffic demand in such areas. In a series of simulations, an increasing number of MSs were placed in this network to investigate the effect as described in subsection 5.2.

Figure 7.1 shows the throughput the MSs attached to the PBSs achieved for three MSs in the network. The threshold $T_{OOCIR} = -\infty$ (red curve) is by default reached or exceeded by any amount of OOCI. Thus HRSR assumes for all transmissions that calculating additional precoders ($\lambda_1 < 1$) is not beneficial and only MRT precoding is used. For the blue curve, $T_{OOCIR} = \infty$ causes that T_{OOCIR} is never reached and thus a full set of precoders is calculated. In the case of three MSs in the network, two of them attach to one BS whereas the remaining MS attaches to the second BS (wherein one BS is a PBS and one BS is an MBS). This causes that only two pairs of one PMS and one MMS can be formed. For MRT precoding only, this low degree of freedom results in no performance gain in comparison to the uncoordinated case. Calculating the full set of precoders results in high gains. The mean throughput of the Pico Mobile Stations (PMSs) increases from 12.7 Mbit/s (no coordination) to 19.9 Mbit/s (RZF with $T_{OOCIR} = \infty$) resulting in a gain of 57%. For RZF with MRT precoding only it remains at 12.7 Mbit/s. The high gains for RZF with $T_{OOCIR} = \infty$ are expected in this scenario, because it includes ZF precoders that null out interference. As no OOCI is present, this can improve the SINR drastically.

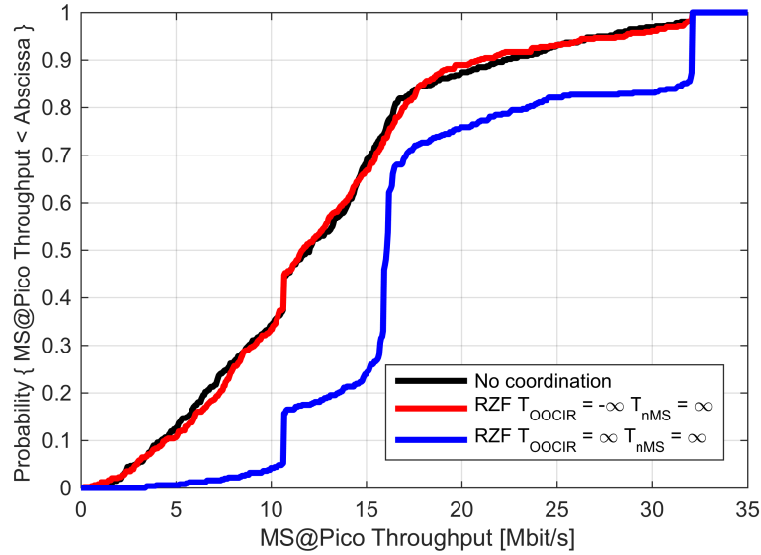


Figure 7.1: Throughput of MS associated to the PBS in a network with two BSs and 3 MSs

Figure 7.2 shows results for the same setup, with the difference that now six MSs are placed in the system. With a growing number of MSs, coordinated scheduling with MRT precoding only is able to achieve significant gains over the uncoordinated case. The mean throughput of the PMSs increases from 10.5 Mbit/s to 12.9 Mbit/s (23% gain). Due to the absence of OOCI, calculating the full set of precoders is still highly beneficial. The mean throughput grows to 16.4 Mbit/s, which results in a gain of 27% over MRT precoding only and of 56% over no coordination.

For twelve MSs in the system (Figure 7.3), the trend continues. Due to the increasing number of pairs, the performance for MRT precoding approaches the case where all precoders are calculated. The mean throughput grows from 8.4 Mbit/s (no coordination) to 11.4 Mbit/s ($T_{OOCIR} = -\infty$) and 13.4 Mbit/s ($T_{OOCIR} = \infty$). The resulting throughput gains now equal 36% (MRT precoding vs. no coordination), 18% (RZF with $T_{OOCIR} = \infty$ vs. RZF with $T_{OOCIR} = -\infty$) and 60% (RZF with $T_{OOCIR} = \infty$ vs. no coordination)

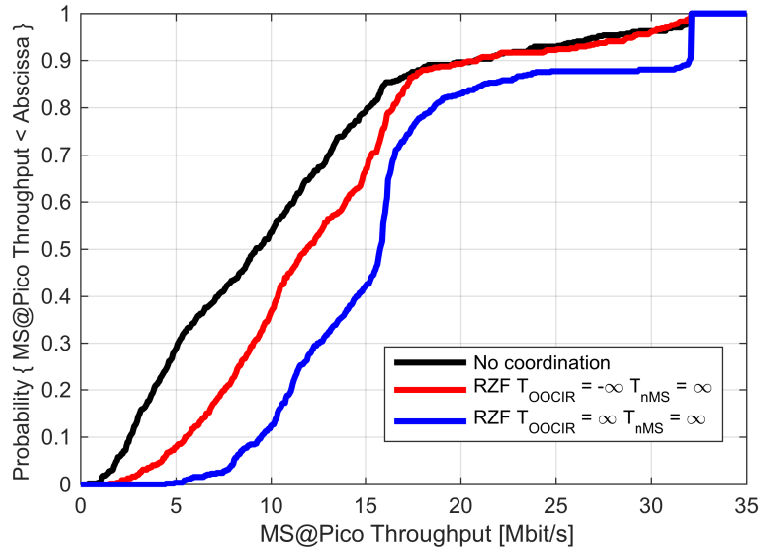


Figure 7.2: Throughput of MS associated to the PBS in a network with two BSs and 6 MSs

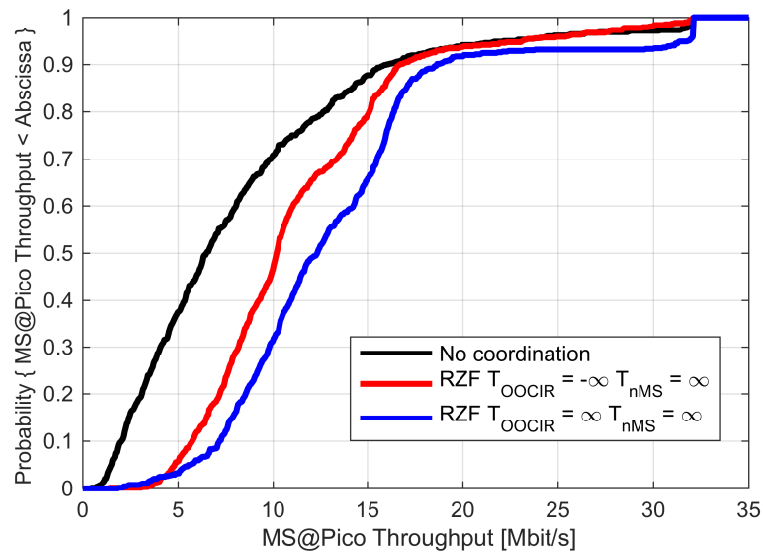


Figure 7.3: Throughput of MS associated to the PBS in a network with two BSs and 12 MSs

7.3 Performance analysis for large networks

In this section, the main results of full System Level Simulations (SLs) are presented, which enable a realistic modelling of OOCI in a large network. The results presented in this section show the performance of the PMSs, as improving their performance is the aim of HetNet RZF. Simulation results for the Macro Mobile Stations (MMSs) are show in Appendix B.

The first set of simulation results is provided for the network depicted in Figure 2.2. In it, each PBS and the overlaying MBS form a cooperation cluster. HRSH operates in each cooperation cluster. The PBSs in Figure 2.2 are located in the centre of the coverage areas of the cooperating MBSs. This causes a strong interference from the cooperating MBS, and thus a relatively low OOCIR. Afterwards also a second network with a higher OOCIR is analysed.

In the simulation area a varying number of MSs is dropped in a random process. Again the so-called hotspot MS distribution was used, such that two-thirds of the MSs are located in the vicinity of a PBS.

Figure 7.4 shows the simulation result in the case when 42 MSs (one per BS) are placed inside this network. Similar to the results from Figure 7.1, coordinated scheduling with MRT precoding only ($T_{OOCIR} = T_{nMS} = -\infty$) shows low gains compared to the case without coordination. The mean throughput of the PMSs in this case grows by 2%. Also similar to the results in Figure 7.1, calculating additional precoders shows performance gains. For the configuration of HRSH, two different threshold settings were used ($T_{OOCIR} = 0$ dB, $T_{nMS} = 6$ and $T_{OOCIR} = -3$ dB, $T_{nMS} = 4$). The more strict threshold settings ($T_{OOCIR} = -3$ dB, $T_{nMS} = 4$) exclude more potential scheduling decisions and therefore show a lower performance. Here the gain in terms of the mean throughput of the PMSs is 11%. In general, HRSH is close to the results for an exhaustive search ($T_{OOCIR} = T_{nMS} = \infty$), which achieves 13% mean throughput gain.

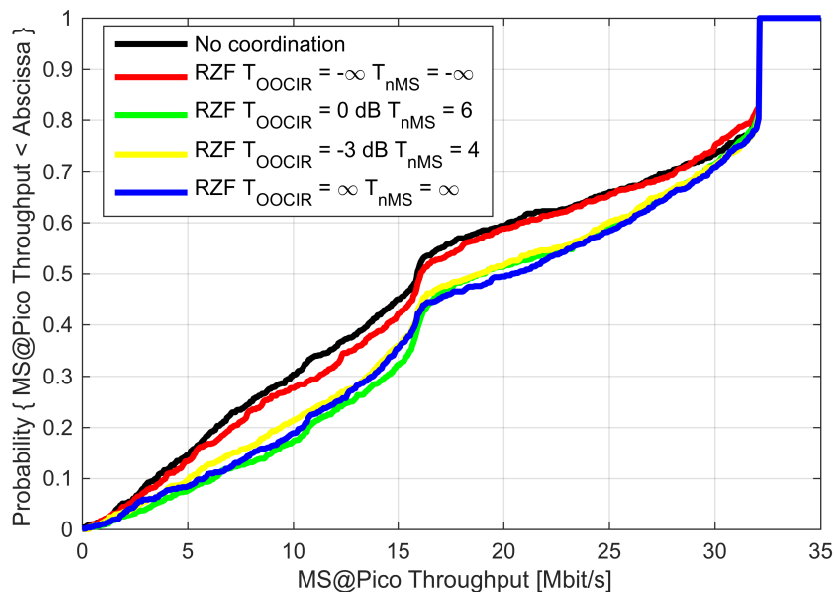


Figure 7.4: Throughput of MSs associated to the PBS in a network large network with 42 MSs (network from Figure 2.2)

Figure 7.5 shows results for the same network with 315 MSs. Significant performance gains are now obtained for coordinated scheduling with MRT precoding only ($T_{OOCIR} = T_{nMS} = -\infty$). This is due to ability of the coordinated scheduling algorithm to project the effect of a precoder for an MMS onto the performance of a PMS as described in Section 4.2. The mean throughput of the PMSs in this case increases by 19%. Additional gains from calculating more precoders are only present for an exhaustive search ($T_{OOCIR} = T_{nMS} = \infty$), which achieves 29% mean throughput gain compared to the uncoordinated case.

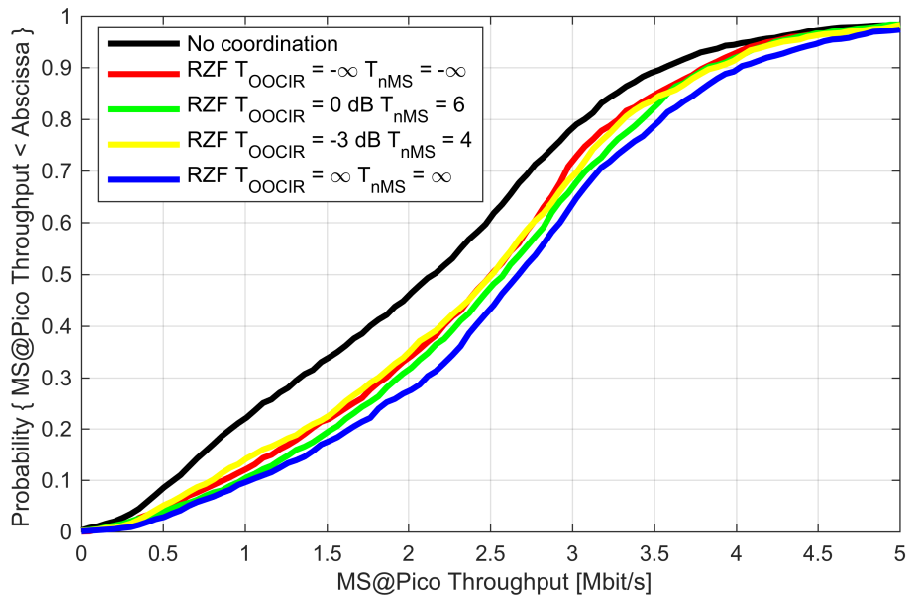


Figure 7.5: Throughput of MS associated to the PBS in a network large network with 315 MSs (network from Figure 2.2)

Comparing Figure 7.4 and 7.5 shows the adaptability of HRSH: In the network conditions with a low number of MSs substantial gains from interference suppressing precoders can be achieved. These gains are also to a large extent realized by HRSH. For a higher number of MSs, where low gains from calculating additional precoders are possible, HRSH tends towards applying MRT precoding only, which is desired for complexity reasons.

As already stated, the previously investigated network (depicted in Figure 2.2) is characterised by a relatively low OOCI at the PMSs, enabling the performance gains from CBF, especially in the case of only 42 MSs. For comparison also the network depicted in Figure 7.6 was simulated. Here the PBSs are located at the edges of the coverage areas of the MBSs, making it likely that PMSs receive interference from multiple MBSs. A higher OOCIR and thus an expected lower gain from coordination is the result.

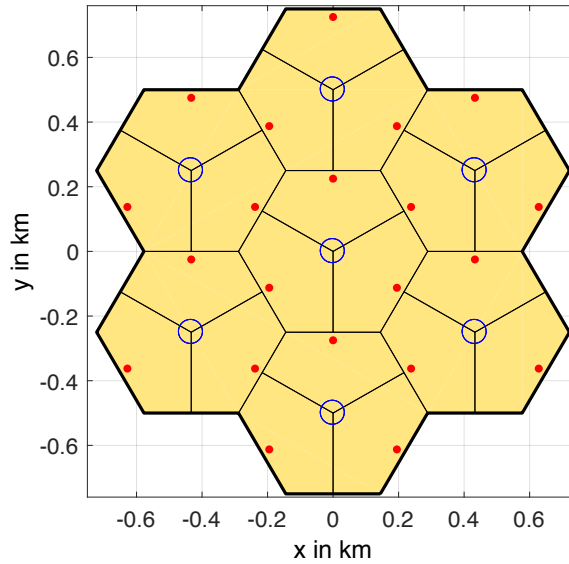


Figure 7.6: Heterogeneous Network with higher Out of Cluster Interference

Figure 7.7 again shows the result for 42 MSs. Performance gains from coordination can be seen, especially for the case when all precoders are calculated ($T_{OOCIR} = T_{nMS} = \infty$). Here the mean throughput of the PMS increases by 7%. The influence of the OOCI can be seen from the fact for the network of Figure 2.2 this gain was 13%.

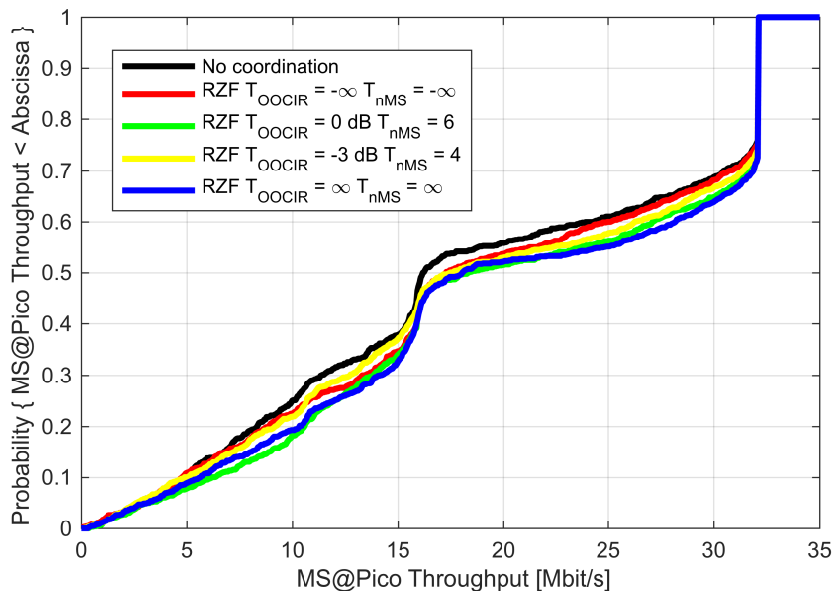


Figure 7.7: Throughput of MSs associated to the PBS in a network large network with 42 MSs (network from Figure 7.6)

Figure 7.8 shows the results for the case of 315 MSs. Similar to the previous network, the huge number of MSs enables gains for precoding based on MRT precoding only ($T_{OOCIR} = T_{nMS} = -\infty$). The mean throughput of the PMSs increases by 3%. Creating additional precoders is not of value in this scenario. For the previous network, 19%

($T_{OOClR} = T_{nMS} = -\infty$) to 29% ($T_{OOClR} = T_{nMS} = \infty$) gain were possible, which again highlights the influence of OOCI.

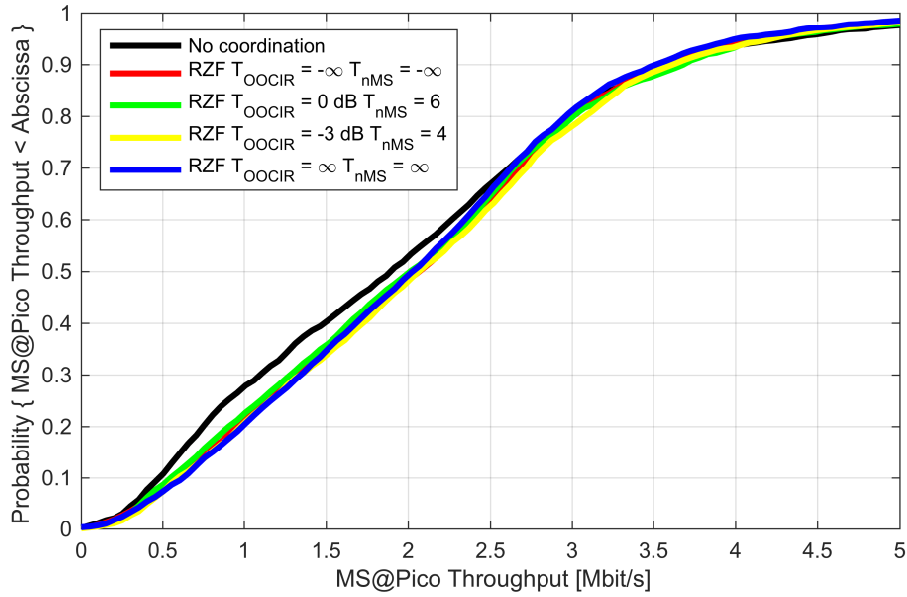


Figure 7.8: Throughput of MS associated to the PBS in a network large network with 315 MSs (network from Figure 7.6)

In summary, the results show that a high level of OOCI prohibits gains from CBF. This could limit the applicability to selected area, e.g. to the centre of the MBS coverage areas. For lower levels of OOCI, substantial gains are possible. The source of the achievable gains differs, depending on the number of MSs: For a low a number of MSs, gains can be achieved when calculating interference suppressing precoders (black versus green curve in Figure 7.4). For a high number of MSs, gains can be achieved by calculating MRT precoders only (black versus red curve in Figure 7.5).

The analysis in Chapter 5 and the simulation results in this section show two main influencing factors for the performance of Coordinated Beamforming (CBF). The detailed understanding and description of the factors is a main contribution of Chapter 5. It was also shown that these have the potential to heavily affect the achievable performance gains. For example, calculating interference suppressing precoders in the two-cell deployment with three MSs considered for Figure 7.1, resulted in a mean throughput gain for the PMSs of 57%. The same principle leads to a gain of only 8% for the larger deployment considered for Figure 7.5.

The influence of the performance limiting factors can also be used to better interpret existing results from the literature: The work presented in [30] is based on ideal assumptions for gains from ZF: Two BSs with two MSs are considered. In accordance with the

results presented above this can lead to high performance gains, especially at low OOCI. OOCI is not explicitly covered in [30], as BSs that are not part of the coordination are not present. However, there are results with different noise levels (e.g. Figure 2 in [30]). A high noise level or a low Signal to Noise Ratio (SNR) causes similar effects as a high OOCI. Accordingly, Figure 2 in [30] shows high gains in spectral efficiency (which can be mapped to throughput gains) at high SNRs, e.g. more than 100% gain at 25 dB SNR. [46] provides simulation results for a network with three and with 21 BSs, with one MS per BS. In the case of three BSs (no OOCI), significant performance gains are obtained (an increase in spectral efficiency from approximately 6.5 bit/second/Hertz (bps/Hz) to approximately 8 bps/Hz (Figure 2 in [46])). For a network with 21 BSs the gains deteriorate to almost zero (see also Figure 2 in [46]).

7.4 Complexity

As described in Section 6.1, the complexity of the scheduling process is an important factor. Corresponding to the complexity definition provided there, the number of potential scheduling decisions that were needed to achieve the results in Section 7.3 were evaluated and the corresponding results are presented in this section.

Figure 7.9 shows the result for the case of 42 MSs and the network layout with lower OOCI (as depicted in Figure 2.2). HRSB in this case reduces the number of calculations compared to the exhaustive search. However, it is still on a high level compared to MRT precoding only and the uncoordinated case. On the other hand, the increased complexity also achieves the performance gains depicted in Figure 7.4.

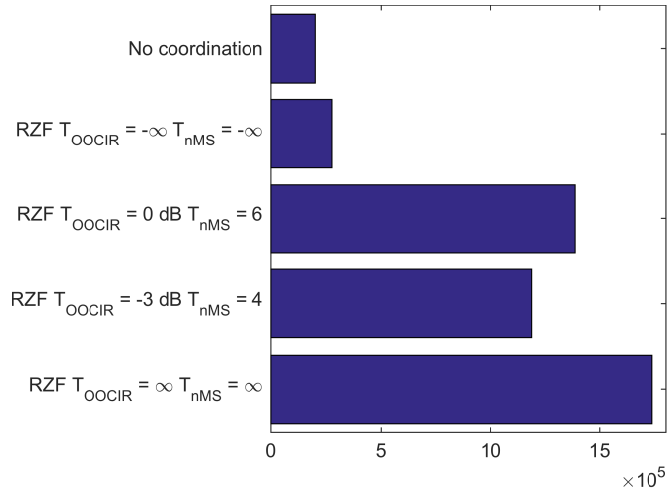


Figure 7.9: Number of transmission parameters calculated for the case of 42 MSs and the network layout depicted in Figure 2.2

Figure 7.10 shows the number of calculations for the case of 315 MSs and the same network layout. Here HRSB significantly reduces the complexity. This also corresponds to the performance results in Figure 7.5 where HRSB limits the complexity as the thresholds (especially T_{nMS}) are often exceeded. It achieves a performance similar to MRT precoding only, because calculating additional precoders would only show low gains under these conditions.

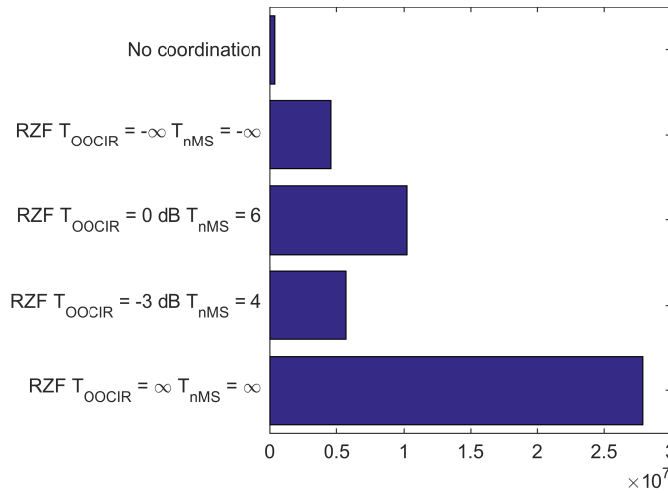


Figure 7.10: Number of transmission parameters calculated for the case of 315 MSs and the network layout depicted in Figure 2.2

For the performance results in Figures 7.7 and 7.8, obtained using the network layout with higher OOCI in Figure 7.6, the complexity considerations are depicted in Figures 7.9 and 7.10, with very similar results.

In summary, a relatively strict restriction of the algorithm (e.g. in terms of selecting $T_{nMS} = 4$) provides a good compromise between complexity and performance. This is especially relevant for the case of a high OOCI, where the potential for performance gains is limited.

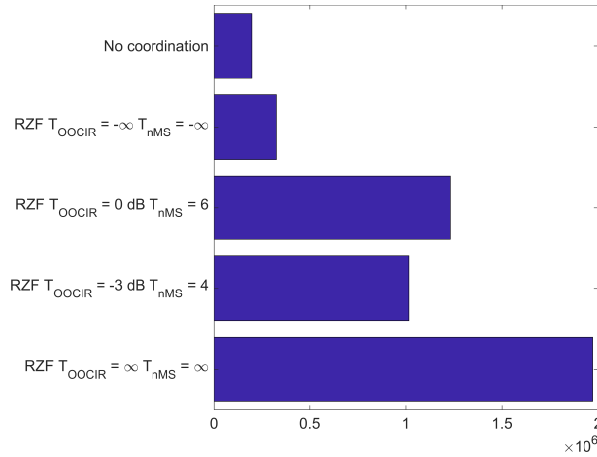


Figure 7.11: Number of transmission parameters calculated for the case of 42 MSs and the network layout depicted in Figure 7.6

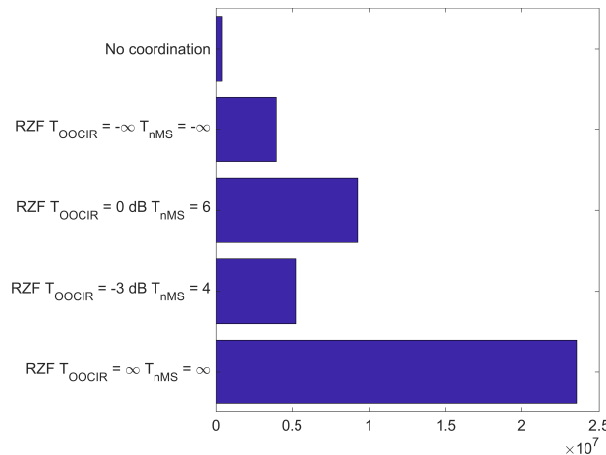


Figure 7.12: Number of transmission parameters calculated for the case of 315 MSs and the network layout depicted in Figure 7.6

7.5 Applicability of the results to other precoding and scheduling algorithms and other traffic models

The results shown in this section were generated using the HetNet RZF algorithm. However, the conclusions drawn here can also be interpreted in a broader way. The effect of

OOCI affects all kinds of coordination schemes, as also emphasized in [6] and [47]. Also, the general considerations depicted in Figure 5.1 are not bound to the usage of a certain precoding algorithm. Similarly, the impact of the number of MSs has a general background: The more MSs there are in a system, the more degrees of freedom the scheduler has in allocating the radio resources and setting corresponding precoders (even if only Maximum Ratio Transmission (MRT) is applied).

For systems with limited channel state information (e.g. Long Term Evolution Advanced (LTE-A) Frequency Division Duplex (FDD) systems), a flexible feedback from the MSs as standardized in LTE-Advanced [89] can be applied. In it, the BSs send out precoded pilot data and the MSs report on the effect these precoders cause. This might limit the performance of CBF (e.g. a ZF precoder is hard to find using this approach), but still enable a limited operation.

The simulations described here make use of the full buffer traffic model. With respect to interference, this is a worst-case scenario: All BSs in the system transmit at any time using all Physical Resource Blocks (PRBs). In a non-fully loaded system, the following effects can occur, which are not part of the simulation used here:

- The number of active MSs constantly changes, as individual MSs become inactive at times of no traffic demand.
- Also a BS can become inactive if there is no demand at any of its attached MSs.
- BSs might also make use of only parts of the PRBs, in the case there is a low demand by the connected MSs.
- Strong imbalances in the traffic load can occur, e.g. a very high load in one BS and a low load in second BS.

This is expected to cause the following effects to the performance and / or HRSF itself:

- For the configuration parameter T_{nMS} , only the number of active MSs should be taken into account. Inactive users are not part of the scheduling process.
- In general, a reduced traffic load (compared to a full buffer case) leads to reduced interference. There can be situations where this causes a lower OOCI: If, for example, a cooperation cluster (i.e. an MBS and its cooperating PBS) is fully loaded, but surrounding BSs currently experience a low load, the level of OOCI is low. Along with the principles described in Section 5.1, this will lead to a improved gain

from coordination. HRSH is able to detect such situations via the Out of Cluster Interference Ratio (OOCIR).

- In situations where the BSs use only parts of the system bandwidth due to a low load, the OOCI can drastically vary per subband, e.g. if a strong interferer is only active at half of the system bandwidth. However, such situations can also happen in a fully loaded system due to a frequency selective radio channel. It is therefore required to always measure the OOCIR per subband.
- For conditions with a heavy imbalance in the MS assignment, e.g. one MS being served by an MBS and ten MSs being served by the cooperating PBS, an additional benefit in the scheduling (as described in Section 4.2) is expected: In such a scenario, the MMS is expected to achieve a much higher throughput than the PMSs, as it does not have to share the PRBs of the MBS, whereas ten PMSs have to share the PRBs of the PBS. Due to its high throughput in the past, the proportional fair metric of the MMS (Equation 4.46 in Section 4.2) will therefore be lower than the ones of the PMSs. As a result, the proportional fair metric of a pair of one MMS and one PMS (Equation 4.47 in Section 4.2) will be dominated by the proportional fair metric of the PMS. If the conditions in terms of OOCIR allow, the scheduler will then prefer interference suppression in terms of selecting a low value of the control parameter λ_1 and thus improve the performance of the PMSs even if this might be at the cost of the MMS.

7.6 Summary

This chapter provided results of SLSs and analysed the behaviour of HRSH. It was shown that CBF can provide significant gains in a heterogeneous network, which can however be significantly impacted by OOCI. With respect to HRSH, it was shown that the algorithm achieves a performance close to an exhaustive search with a limited computational complexity.

The results also can be used to provide further insights with respect to the first and the third objective defined as part of the research problem (Section 2.7). As stated in Section 2.7, the first objective is to determine and describe the factors that influence the performance of CBF. Chapter 5 determined these factors, which can now be complemented with detailed simulation results, fulfilling all requirements defined in Section 2.7. The simula-

tion results show especially the strong effect of the OOCI: For the network in Figure 2.2, which is characterized by a low OOCI, significant performance gains could be achieved, whereas for the network in Figure 7.6 there are low gains. In contrast, the number of MSs has a different effect: It does not prohibit gains, but changes the underlying effect: For a low number of MSs, gains can be leveraged with interference-suppressing precoders, whereas for a high number MRT precoding is sufficient.

Also the third objective was addressed by the SLSs. It is to design a computational efficient implementation of the scheduling process for CBF in a heterogeneous network. The simulation results in Section 7.4 show that HRSH significantly decreases the computational efficiency, whereas the performance is close to an exhaustive search.

Chapter 8

Conclusions and Future Work

This work shows that in order to fulfil the growing traffic demand in wireless networks, Coordinated Beamforming is a suitable mean to be applied in heterogeneous network to increase the network capacity.

It contributed an answer to the question "Under which conditions can Coordinated Beamforming provide substantial performance gains in a large-scale heterogeneous network?": Two main performance limiting factors, namely Out of Cluster Interference and the number of mobile stations were identified and the corresponding dependencies were described, which was then verified by detailed simulations.

In addition to this first contribution, also two new algorithms, named (1) HetNet Relaxed Zero Forcing (RZF) and (2) HetNet RZF Scheduling Heuristic (HRSH) were contributed by this Thesis. HRSH was designed using the knowledge of the performance limiting knowledge, a new scheduling heuristic was developed in order to provide an efficient implementation.

The simulation results showed that Coordinated Beamforming is capable of achieving an improved throughput at the mobile stations connected to a low power base station, thus improving the network capacity, subject to the aforementioned factors which limit the available gains.

In the future, this work can be extended in different directions:

- Section 4.1 described that in this work Relaxed Zero Forcing precoding was used to reveal the full set of available precoding options to the scheduling algorithm. Using a precoding approach that itself optimizes the precoding on the basis of certain parameters (such as Signal to Leakage and Noise Ratio precoding) would reduce

the complexity of the scheduling and the precoding, but restrict the flexibility of the scheduling. A potential solution could be a flexible precoding heuristic that, based on the actual conditions proposes a limited set of potential selected precoders to the scheduling algorithm.

- The work could be extended into the direction of Interference Alignment to also benefit from interference mitigation at the receiver. This would especially require the design of non-iterative Interference Alignment schemes that can cope with a high level of out of cluster interference.
- It would be possible to extend the static cooperation cluster of a fixed assignment of one pico base station to one macro base station. Due to the propagation conditions (e.g. fading), it can be the case that a mobile station attached to a pico base station is interfered more by a second macro base station than the cooperating one. In this case it would be beneficial to flexibly adapt the cooperation cluster on a per mobile station basis.
- Interesting insights could be gained by performing simulations in a not fully loaded system, i.e. with a detailed traffic model. The reduced out of cluster interference due to inactive neighbouring base stations should lead to higher performance gains.
- A load adaptive heuristic could be created: In case there is a high load in the pico base station (e.g. to be measured by the active number of mobile stations), it is more important to reduce interference at the pico mobile stations than for situations with a low load.
- With respect to Out of Cluster Interference (OOCI), it might be possible to design new types of antennas that physically limit the problem, such that less power of a macro base station leaks into surrounding cells.
- In the direction of 5G, Massive Multiple Input Multiple Output (MIMO) [92] and Ultra-Dense Networks [93] networks are under discussion. Massive MIMO increases the number antennas at the base stations to the order of hundreds and therefore strongly improves their beamforming capabilities. Ultra-dense networks on the other hand increase the number of small cells by order of magnitudes. If an ultra-dense network should ever be deployed using the same frequency band as a massive

MIMO base station, this would most probably require completely new approaches to interference mitigation.

Bibliography

- [1] Cisco Systems. Cisco Visual Networking Index: Global Mobile Data Traffic Forecast Update, 2016-2021 White Paper. Technical report, 2017.
- [2] Ericsson. Ericsson Mobility Report. Technical Report June, 2017.
- [3] Amitabha Ghosh, Nitin Mangalvedhe, Rapeepat Ratasuk, Bishwarup Mondal, Mark Cudak, Eugene Visotsky, Timothy Thomas, Jeffrey Andrews, Ping Xia, Han Jo, Harpreet Dhillon, and Thomas Novlan. Heterogeneous cellular networks: From theory to practice. *IEEE Communications Magazine*, 50(6):54–64, jun 2012.
- [4] Chan-byoung Chae, Insoo Hwang, Robert W. Heath, Jr., and Vahid Tarokh. Interference Aware-Coordinated Beamforming in a Multi-Cell System. *IEEE Transactions on Wireless Communications*, 11(10):3692–3703, oct 2012.
- [5] Hayssam Dahrouj and Wei Yu. Coordinated beamforming for the multicell multi-antenna wireless system. *IEEE Transactions on Wireless Communications*, 9(5):1748–1759, may 2010.
- [6] Angel Lozano, Robert W. Heath, and Jeffrey G. Andrews. Fundamental Limits of Cooperation. *IEEE Transactions on Information Theory*, 59(9):5213–5226, sep 2013.
- [7] Erik Dahlman, editor. *4G: LTE/LTE-Advanced for Mobile Broadband*. Elsevier Academic Press, 2011.
- [8] Li Chen, Wenwen Chen, Bin Wang, Xin Zhang, Hongyang Chen, and Dacheng Yang. System-level simulation methodology and platform for mobile cellular systems. *IEEE Communications Magazine*, 49(7):148–155, jul 2011.

- [9] International Telecommunication Union Radiocommunication Sector. IMT traffic estimates for the years 2020 to 2030. Technical report, International Telecommunication Union, 2015.
- [10] Hossein Falaki, Dimitrios Lymberopoulos, Ratul Mahajan, Srikanth Kandula, and Deborah Estrin. A first look at traffic on smartphones. In *Proceedings of the 10th annual conference on Internet measurement - IMC '10*, page 281, New York, New York, USA, 2010.
- [11] Aamod Khandekar, Naga Bhushan, Ji Tingfang, and Vieri Vanghi. LTE-Advanced: Heterogeneous networks. In *2010 European Wireless Conference (EW)*, pages 978–982. IEEE, 2010.
- [12] Ritesh Madan, Jaber Borran, Ashwin Sampath, Naga Bhushan, Aamod Khandekar, and Tingfang Ji. Cell Association and Interference Coordination in Heterogeneous LTE-A Cellular Networks. *IEEE Journal on Selected Areas in Communications*, 28(9):1479–1489, dec 2010.
- [13] Lu Zhang, Lin Yang, and Tao Yang. Cognitive Interference Management for LTE-A Femtocells with Distributed Carrier Selection. In *2010 IEEE 72nd Vehicular Technology Conference - Fall*, pages 1–5. IEEE, sep 2010.
- [14] ITU-R. Guidelines for evaluation of radio interface technologies for IMT-Advanced. Technical report, 2009.
- [15] Ericsson; ST-Ericsson. 3GPP Standardisation RAN1 Document R1-101752: Considerations on non-CA based heterogeneous deployments, 2010.
- [16] Mahmudur Rahman, Halim Yanikomeroglu, and William Wong. Interference Avoidance with Dynamic Inter-Cell Coordination for Downlink LTE System. In *2009 IEEE Wireless Communications and Networking Conference*, pages 1–6. IEEE, apr 2009.
- [17] R. Pickholtz, D. Schilling, and L. Milstein. Theory of Spread-Spectrum Communications - A Tutorial. *IEEE Transactions on Communications*, 30(5):855–884, may 1982.

- [18] Z. Kotic and N. Sollenberger. Performance and implementation of dynamic frequency hopping in limited-bandwidth cellular systems. *IEEE Transactions on Wireless Communications*, 1(1):28–36, 2002.
- [19] Ke-Lin Du and M. N. S. Swamy. *Wireless Communication Systems*. Cambridge University Press, Cambridge, 1. publ. edition, 2010.
- [20] Moe Rahnema. Overview of the GSM system and protocol architecture. *IEEE Communications Magazine*, 31(4):92–100, apr 1993.
- [21] Nazmus Saquib, Ekram Hossain, and Dong Kim. Fractional frequency reuse for interference management in LTE-advanced hetnets. *IEEE Wireless Communications*, 20(2):113–122, apr 2013.
- [22] Thomas David Novlan, Radha Krishna Ganti, Arunabha Ghosh, and Jeffrey G. Andrews. Analytical Evaluation of Fractional Frequency Reuse for OFDMA Cellular Networks. *IEEE Transactions on Wireless Communications*, 10(12):4294–4305, dec 2011.
- [23] Nageen Himayat, Shilpa Talwar, Anil Rao, and Robert Soni. Interference management for 4G cellular standards. *IEEE Communications Magazine*, 48(8):86–92, aug 2010.
- [24] David Lopez-Perez, Ismail Guvenc, Guillaume de la Roche, Marios Kountouris, Tony Quek, and Jie Zhang. Enhanced intercell interference coordination challenges in heterogeneous networks. *IEEE Wireless Communications*, 18(3):22–30, jun 2011.
- [25] Beatriz Soret, Hua Wang, K. I. Pedersen, and Claudio Rosa. Multicell cooperation for LTE-advanced heterogeneous network scenarios. *IEEE Wireless Communications*, 20(1):27–34, feb 2013.
- [26] A Barbieri, P Gaal, S Geirhofer, T Ji, D Malladi, Y Wei, and F Xue. Coordinated downlink multi-point communications in heterogeneous cellular networks. In *2012 Information Theory and Applications Workshop*, pages 7–16. IEEE, feb 2012.
- [27] J.G. Andrews. Modulation, coding and signal processing for wireless communications - Interference cancellation for cellular systems: a contemporary overview. *IEEE Wireless Communications*, 12(2):19–29, apr 2005.

- [28] Eugene Visotsky and U. Madhow. Space-time transmit precoding with imperfect feedback. *IEEE Transactions on Information Theory*, 47(6):2632–2639, 2001.
- [29] Shyamnath Gollakota, Samuel David Perli, and Dina Katabi. Interference alignment and cancellation. *ACM SIGCOMM Computer Communication Review*, 39(4):159, aug 2009.
- [30] Chan-byoung Chae, Insoo Hwang, Robert W Heath, and Vahid Tarokh. Jointly optimized two-cell MIMO systems. In *2011 IEEE GLOBECOM Workshops (GC Wkshps)*, pages 421–425. IEEE, dec 2011.
- [31] G. Boudreau, J. Panicker, and S. Vrzic. Interference coordination and cancellation for 4G networks. *IEEE Communications Magazine*, 47(4):74–81, apr 2009.
- [32] Juho Lee, Younsun Kim, Hyojin Lee, Boon Ng, David Mazzaresse, Jianghua Liu, Weimin Xiao, and Yongxing Zhou. Coordinated multipoint transmission and reception in LTE-advanced systems. *IEEE Communications Magazine*, 50(11):44–50, nov 2012.
- [33] Qian Clara Li, Huaning Niu, Apostolos Tolis Papathanassiou, and Geng Wu. 5G Network Capacity: Key Elements and Technologies. *IEEE Vehicular Technology Magazine*, 9(1):71–78, mar 2014.
- [34] Mamoru Sawahashi, Yoshihisa Kishiyama, Akihito Morimoto, Daisuke Nishikawa, and Motohiro Tanno. Coordinated multipoint transmission/reception techniques for LTE-advanced. *IEEE Wireless Communications*, 17(3):26–34, 2010.
- [35] Uk Jang, Hyukmin Son, Jongrok Park, and Sanghoon Lee. CoMP-CSB for ICI Nulling with User Selection. *IEEE Transactions on Wireless Communications*, 10(9):2982–2993, sep 2011.
- [36] Bruno Clerckx, Younsun Kim, Hyojin Lee, Joonyoung Cho, and Juho Lee. Coordinated multi-point transmission in heterogeneous networks: A distributed antenna system approach. In *2011 IEEE 54th International Midwest Symposium on Circuits and Systems (MWSCAS)*, number March 2017, pages 1–4. IEEE, aug 2011.
- [37] Gregory Morozov, Alexei Davydov, and Ilya Bolotin. Performance evaluation of dynamic point selection CoMP scheme in heterogeneous networks with FTP traffic

- model. In *2012 IV International Congress on Ultra Modern Telecommunications and Control Systems*, pages 922–926. IEEE, oct 2012.
- [38] Luca Venturino, Narayan Prasad, and Xiaodong Wang. Coordinated Scheduling and Power Allocation in Downlink Multicell OFDMA Networks. *IEEE Transactions on Vehicular Technology*, 58(6):2835–2848, jul 2009.
- [39] Oscar D. Ramos-Cantor, Jakob Belschner, Ganapati Hegde, and Marius Pesavento. Centralized coordinated scheduling in LTE-Advanced networks. *EURASIP Journal on Wireless Communications and Networking*, 2017(1):122, dec 2017.
- [40] Dragan Samardzija and Howard Huang. Determining backhaul bandwidth requirements for network MIMO. In *European Signal Processing Conference*, number Eusipco, pages 1494–1498, 2009.
- [41] Thorsten Biermann, Luca Scalia, Changsoon Choi, Wolfgang Kellerer, and Holger Karl. How backhaul networks influence the feasibility of coordinated multipoint in cellular networks [Accepted From Open Call]. *IEEE Communications Magazine*, 51(8):168–176, aug 2013.
- [42] Sivarama Venkatesan, Angel Lozano, and Reinaldo Valenzuela. Network MIMO: Overcoming Intercell Interference in Indoor Wireless Systems. In *2007 Conference Record of the Forty-First Asilomar Conference on Signals, Systems and Computers*, pages 83–87. IEEE, nov 2007.
- [43] Howard Huang, Matteo Trivellato, Ari Hottinen, Mansoor Shafi, P. Smith, and Reinaldo Valenzuela. Increasing downlink cellular throughput with limited network MIMO coordination. *IEEE Transactions on Wireless Communications*, 8(6):2983–2989, jun 2009.
- [44] Min Li, Chunshan Liu, Iain B Collings, and Stephen V Hanly. Multicell Coordinated Scheduling with Multiuser ZF Beamforming. In *2014 IEEE International Conference on Communications Workshops (ICC)*, pages 5017–5022, 2014.
- [45] A. Barbieri, P. Gaal, S. Geirhofer, T. Ji, D. Malladi, Y. Wei, and F. Xue. Coordinated downlink multi-point communications in heterogeneous cellular networks. In *2012 Information Theory and Applications Workshop, ITA 2012 - Conference Proceedings*, pages 7–16. IEEE, feb 2012.

- [46] Danish Aziz, Federico Boccardi, and Andreas Weber. System-level performance study of interference alignment in cellular systems with base-station coordination. In *2012 IEEE 23rd International Symposium on Personal, Indoor and Mobile Radio Communications - (PIMRC)*, pages 1155–1160. IEEE, sep 2012.
- [47] George C. Alexandropoulos, Paul Ferrand, Jean-marie Gorce, and Constantinos B. Papadias. Advanced coordinated beamforming for the downlink of future LTE cellular networks. *IEEE Communications Magazine*, 54(7):54–60, jul 2016.
- [48] Mai Vu and Arogyaswami Paulraj. MIMO Wireless Linear Precoding. *IEEE Signal Processing Magazine*, 24(5):86–105, sep 2007.
- [49] F. Boccardi, F. Tosato, and G. Caire. Precoding Schemes for the MIMO-GBC. *2006 International Zurich Seminar on Communications*, pages 10–13, 2006.
- [50] David Gesbert, Marios Kountouris, Robert Heath Jr., Chan-byoung Chae, and Thomas Salzer. Shifting the MIMO Paradigm. *IEEE Signal Processing Magazine*, 24(5):36–46, sep 2007.
- [51] M. Tomlinson. New automatic equaliser employing modulo arithmetic. *Electronics Letters*, 7(5-6):138, 1971.
- [52] H. Harashima and H. Miyakawa. Matched-Transmission Technique for Channels With Intersymbol Interference. *IEEE Transactions on Communications*, 20(4):774–780, aug 1972.
- [53] Max H M Costa. Writing on Dirty Paper. *IEEE Transactions on Information Theory*, 29(3):439–441, 1983.
- [54] Shao-Yu Lien, Shin-Lin Shieh, Yenming Huang, Borching Su, Yung-Lin Hsu, and Hung-Yu Wei. 5G New Radio: Waveform, Frame Structure, Multiple Access, and Initial Access. *IEEE Communications Magazine*, 55(6):64–71, 2017.
- [55] D Tse and P Viswanath. *Fundamentals of Wireless Communication*. Wiley series in telecommunications. Cambridge University Press, 2005.
- [56] Christoph Windpassinger, R.F.H. Fischer, T. Vencel, and J.B. Huber. Precoding in Multiantenna and Multiuser Communications. *IEEE Transactions on Wireless Communications*, 3(4):1305–1316, jul 2004.

- [57] T.K.Y. Lo. Maximum ratio transmission. *IEEE Transactions on Communications*, 47(10):1458–1461, 1999.
- [58] Ya-Feng Liu, Yu-Hong Dai, and Zhi-Quan Luo. Coordinated Beamforming for MISO Interference Channel: Complexity Analysis and Efficient Algorithms. *IEEE Transactions on Signal Processing*, 59(3):1142–1157, mar 2011.
- [59] Mirette Sadek, Alireza Tarighat, and Ali Sayed. A Leakage-Based Precoding Scheme for Downlink Multi-User MIMO Channels. *IEEE Transactions on Wireless Communications*, 6(5):1711–1721, may 2007.
- [60] G Lee, J Park, Y Sung, and M. Yukawa. Coordinated beamforming with relaxed zero forcing. In *2011 International Conference on Wireless Communications and Signal Processing (WCSP)*, pages 1–5. IEEE, nov 2011.
- [61] M. Yukawa. Coordinated Beamforming With Relaxed Zero Forcing: The Sequential Orthogonal Projection Combining Method and Rate Control. *IEEE Transactions on Signal Processing*, 61(12):3100–3112, jun 2013.
- [62] Eduard a Jorswieck, Erik G Larsson, and Danyo Danev. Complete characterization of the pareto boundary for the MISO interference channel. *IEEE Transactions on Signal Processing*, 56(56):5292–5296, 2008.
- [63] Erik G. Larsson and Eduard A. Jorswieck. Competition versus cooperation on the MISO interference channel. *IEEE Journal on Selected Areas in Communications*, 26(26):1059–1069, 2008.
- [64] E.G. Larsson, D. Danev, and E.a. Jorswieck. Asymptotically optimal transmit strategies for the multiple antenna interference channel. *2008 46th Annual Allerton Conference on Communication, Control, and Computing*, 2008.
- [65] Krishna Gomadam, Viveck R. Cadambe, and Syed A. Jafar. Approaching the Capacity of Wireless Networks through Distributed Interference Alignment. In *IEEE GLOBECOM 2008 - 2008 IEEE Global Telecommunications Conference*, pages 1–6. IEEE, 2008.
- [66] Krishna Gomadam, Viveck R. Cadambe, and Syed A. Jafar. A Distributed Numerical Approach to Interference Alignment and Applications to Wireless Interference Networks. *IEEE Transactions on Information Theory*, 57(6):3309–3322, jun 2011.

- [67] Steven W. Peters and Robert W. Heath. Cooperative algorithms for MIMO interference channels. *IEEE Transactions on Vehicular Technology*, 60(1):206–218, 2011.
- [68] Emil Björnson, Mats Bengtsson, and Björn Ottersten. Optimal Multiuser Transmit Beamforming: A Difficult Problem with a Simple Solution Structure. *IEEE Signal Processing Magazine*, 31(4):142–148, apr 2014.
- [69] T.F. Maciel and a. Klein. On the Performance, Complexity, and Fairness of Suboptimal Resource Allocation for Multiuser MIMOOFDMA Systems. *IEEE Transactions on Vehicular Technology*, 59(1):406–419, jan 2010.
- [70] Richard van Nee and Ramjee Prasad. *OFDM for Wireless Multimedia Communications*. Artech House, Inc., Norwood, MA, USA, 1st edition, 2000.
- [71] D Astely, E Dahlman, A. Furuskar, Y Jading, M Lindstrom, and S Parkvall. LTE: the evolution of mobile broadband. *IEEE Communications Magazine*, 47(4):44–51, apr 2009.
- [72] Haiying Zhu and Roshdy Hafez. Scheduling schemes for multimedia service in wireless OFDM systems. *IEEE Wireless Communications*, 14(5):99–105, oct 2007.
- [73] Stefan Schwarz, Christian Mehlhauer, and Markus Rupp. Low complexity approximate maximum throughput scheduling for LTE. In *2010 Conference Record of the Forty Fourth Asilomar Conference on Signals, Systems and Computers*, pages 1563–1569. IEEE, nov 2010.
- [74] Jingxian Wu, Neelesh B Mehta, Andreas F Molisch, and Jin Zhang. Unified Spectral Efficiency Analysis of Cellular Systems with Channel-Aware Schedulers. *IEEE Transactions on Communications*, 59(12):3463–3474, dec 2011.
- [75] Christian Wengerter, Jan Ohlhorst, and A. Golitschek Edler von Elbwart. Fairness and Throughput Analysis for Generalized Proportional Fair Frequency Scheduling in OFDMA. In *2005 IEEE 61st Vehicular Technology Conference*, volume 3, pages 1903–1907. IEEE, 2005.
- [76] Motorola 3GPP TSG RAN1#44bis. R1-060877 Frequency Domain Scheduling for E-UTRA. 2006.
- [77] Volker Pohl, P.H. Nguyen, Volker Jungnickel, and C. von Helmolt. How Often Channel Estimation is Needed in MIMO Systems. In *GLOBECOM '03. IEEE Global*

Telecommunications Conference (IEEE Cat. No.03CH37489), volume 2, pages 814–818. IEEE, 2003.

- [78] Konstantinos Manolakis, Lars Thiele, Christian Oberli, Thomas Haustein, and Volker Jungnickel. Impairment modeling for joint transmission CoMP. In *2011 2nd International Conference on Wireless Communication, Vehicular Technology, Information Theory and Aerospace & Electronic Systems Technology (Wireless VI-TAE)*, pages 1–5. IEEE, feb 2011.
- [79] T.L. Marzetta and B.M. Hochwald. Fast transfer of channel state information in wireless systems. *IEEE Transactions on Signal Processing*, 54(4):1268–1278, apr 2006.
- [80] G Vivier, K Kalliojärvi, R Irmer, A Pollard, K Brüninghaus, H Choi, Y Cho, M Döttling, and Jörn Von Häfen. Winner II Deliverable D6.13.1: WINNER II Test scenarios and calibration cases issue 1. Technical Report 1, 2006.
- [81] 3rd Generation Partnership Project (3GPP). Spatial channel model for Multiple Input Multiple Output (MIMO) simulations (Technical Report 25.996) Version 14.0.0. Technical report, 2017.
- [82] K. Brueninghaus, D. Astely, T. Salzer, S. Visuri, A. Alexiou, S. Karger, and G. Seraji. Link Performance Models for System Level Simulations of Broadband Radio Access Systems. In *2005 IEEE 16th International Symposium on Personal, Indoor and Mobile Radio Communications*, volume 4, pages 2306–2311. IEEE, 2005.
- [83] 3GPP2. cdma2000 Evaluation Methodology. Technical report, 2004.
- [84] Aleksandar Damnjanovic, Juan Montojo, Joonyoung Cho, Hyoungju Ji, Jin Yang, and Pingping Zong. UE’s role in LTE advanced heterogeneous networks. *IEEE Communications Magazine*, 50(2):164–176, feb 2012.
- [85] 3rd Generation Partnership Project (3GPP). Technical Report 36.814 Further advancements for E-UTRA physical layer aspects v 9.0.0. Technical report, 2010.
- [86] 3GPP TSG RAN WG1 Meeting #57bis. Summary on calibration step 1c. Technical report, 2009.
- [87] Jyrki T. J. Penttinen, editor. *The Telecommunications Handbook*. John Wiley & Sons, Ltd, Chichester, UK, feb 2015.

- [88] Martin Sauter. *From GSM to LTE*. John Wiley & Sons, Ltd, Chichester, UK, dec 2010.
- [89] Daewon Lee, Hanbyul Seo, Bruno Clerckx, Eric Hardouin, David Mazzaresse, Satoshi Nagata, and Krishna Sayana. Coordinated multipoint transmission and reception in LTE-advanced: deployment scenarios and operational challenges. *IEEE Communications Magazine*, 50(2):148–155, feb 2012.
- [90] 3rd Generation Partnership Project. TR 36.819 Coordinated multi-point operation for LTE physical layer aspects, version 11.1.0. Technical report, 2011.
- [91] LG Electronics. 3GPP Standardisation RAN1 Document R1-111628: Full Buffer CoMP Evaluation v5, 2011.
- [92] Erik Larsson, Ove Edfors, Fredrik Tufvesson, and Thomas Marzetta. Massive MIMO for next generation wireless systems. *IEEE Communications Magazine*, 52(2):186–195, feb 2014.
- [93] Xiaohu Ge, Song Tu, Guoqiang Mao, Cheng-Xiang Wang, and Tao Han. 5G Ultra-Dense Cellular Networks. *IEEE Wireless Communications*, 23(1):72–79, feb 2016.

Appendix A

Numerical MIMO Examples

A.1 Maximum Ratio Transmission via Singular Value Decomposition

Figure A.1 shows a numeric example for this process in the notation of the programming language MATLAB. A random channel matrix H is generated and then decomposed into U , λ and V . The elements λ_{11} and λ_{22} of the matrix λ show the gains of the parallel Single Input Single Output (SISO) channels. As both elements are non-zero, this channel would support the transmission of two data streams in parallel. However, the gain of the second channel is significantly lower than the one of the first channel. The target is now to transmit the information $s = 5$ via H with a maximal received power. As introduced before, the transmit precoder v_t is selected such that $v_{t1} = v_{11}$ and $v_{t2} = v_{21}$. The norm of the precoder is equal to one which is correct as the precoder is not able to change the transmit power. The receive combining vector u_r is set to $u_{r1} = u_{11}^*$ (the conjugate transpose is represented by $'$ in MATLAB) and $u_{r2} = u_{21}^*$. The execution of $u_r U \lambda V^* v_t s$ models the complete chain of the wireless channel with precoding and receive combining. It can be seen that s is mapped to the first SISO channel as it is received with the gain of the first channel (1.4562). The imaginary part of the result is caused by numerical inaccuracies in the computation.

```

1  >> H = rand(2)+i*rand(2)
2
3  H =
4
5      709.3648e-003 +655.0980e-003i    276.0251e-003 +118.9977e-003i
6      754.6867e-003 +162.6117e-003i    679.7027e-003 +498.3641e-003i
7
8  >> [U,lambda,V]=svd(H)
9
10 U =
11
12     -516.9640e-003 -398.2120e-003i    330.1921e-003 +682.0180e-003i
13     -721.9896e-003 -230.0140e-003i   -467.5766e-003 -455.1887e-003i
14
15
16 lambda =
17
18      1.4562e+000      0.0000e+000
19      0.0000e+000      456.6202e-003
20
21
22 V =
23
24     -830.8281e-003 +          i    556.5292e-003 +          i
25     -546.2457e-003 +106.4910e-003i   -815.4762e-003 +158.9776e-003i
26
27 >> s = 5
28
29 s =
30
31      5.0000e+000
32
33 >> vt = V(:,1)
34
35 vt =
36
37     -830.8281e-003 +          i
38     -546.2457e-003 +106.4910e-003i

```

```

40 >> norm(vt)
41
42 ans =
43
44     1.0000e+000
45
46 >> ur(1)=U(1,1)'
47
48 ur =
49
50     -516.9640e-003 +398.2120e-003i   -531.1763e-003 +552.6761e-003i
51
52 >> ur(2)=U(2,1)
53
54 ur =
55
56     -516.9640e-003 +398.2120e-003i   -721.9896e-003 +230.0140e-003i
57
58 >> ur*U*lambda*V'*vt*s
59
60 ans =
61
62     7.2811e+000 + 69.3889e-018i

```

Figure A.1: Singular Value Decomposition of the Wireless Channel: Example

A.2 Zero Forcing precoding

Figure A.2 gives an example for the Zero Forcing (ZF) precoding algorithm proposed in [4]. The Equations A.1 to A.5 show how the precoders are calculated (eig stands for the calculation of the eigenvectors), for more details the reader is referred to [4].

$$v_1 = \text{eig}(H_{22}^*H_{21}, H_{12}^*H_{11}) \quad (\text{A.1})$$

$$z = H_{22}^*H_{21}v_1 \quad (\text{A.2})$$

$$v_2 = \begin{pmatrix} z_2^* \\ -z_1^* \end{pmatrix} \text{ or } v_2 = \begin{pmatrix} -z_2^* \\ z_1^* \end{pmatrix} \quad (\text{A.3})$$

$$u_1 = (H_{11}v_1)^* \quad (\text{A.4})$$

$$u_2 = (H_{22}v_2)^* \quad (\text{A.5})$$

After generating random channels (lines 1 to 20 in Figure A.2), the eigenvectors of $H_{22}^*H_{21}$ and $H_{12}^*H_{11}$ are generated. The first of the two eigenvectors is selected as the transmit precoder for BS 1 in line 26. It would also be possible to use the second eigenvector with a similar result. The lines 31 to 40 are used to calculate the transmit precoder of BS 2. The lines 41 to 50 make sure that norm of both precoders equals one, such that they do not de- or increase the transmitted power. The receive combining vectors for Maximum Ratio Combining (MRC) are calculated and normalized in the lines 51 to 66. Two arbitrarily chosen signals (+5 and -5) should now be transmitted to the receivers. The lines 75 to 82 show that the interfering channels are as desired nulled out (again small numerical inaccuracies occur). The wanted transmission through H_{11} and H_{22} is still possible, as the lines 83 to 90 show. However, it can be seen here, that the received power (especially for the link between BS 2 and MS 2) is reduced compared to what was possible in the example presented in Figure A.1. As it is pointed out in Section 2.5.2, ZF precoding is able to mitigate interference on the cost of the strength of the intended received signal.

The principle of mitigating the interference can be understood when looking at the lines 91 to 103. The lines 91 to 95 calculate the interfering signal that arrives at the two antennas of MS 1. It was precoded such that after the multiplication with the receive combining vector the two parts sum up destructively (lines 96 to 103). The same happens for the interference at MS 2 (lines 104 to 115).

```

1 >> H11 = rand(2)+i*rand(2)
2 H11 =
3     814.7237e-003 +632.3592e-003i    126.9868e-003 +278.4982e-003i
4     905.7919e-003 + 97.5404e-003i    913.3759e-003 +546.8815e-003i
5
6 >> H22 = rand(2)+i*rand(2)
7 H22 =
8     957.5068e-003 +957.1669e-003i    157.6131e-003 +800.2805e-003i
9     964.8885e-003 +485.3756e-003i    970.5928e-003 +141.8863e-003i
10
11 >> G1 = rand(2)+i*rand(2)
12 G1 =
13     421.7613e-003 +655.7407e-003i    792.2073e-003 +849.1293e-003i
14     915.7355e-003 + 35.7117e-003i    959.4924e-003 +933.9932e-003i
15
16 >> H12 = rand(2)+i*rand(2)
17 H12 =
18     678.7352e-003 +655.4779e-003i    743.1325e-003 +706.0461e-003i
19     757.7401e-003 +171.1867e-003i    392.2270e-003 + 31.8328e-003i
20
21 >> [V,~]=eig(H22'*H21,H12'*H11)
22 V =
23    -766.8897e-003 -233.1103e-003i   -116.9764e-003 -228.0542e-003i
24     329.8925e-003 +267.6605e-003i    873.4331e-003 -126.5669e-003i
25
26 >> v1 = V(:,1)
27 v1 =
28    -766.8897e-003 -233.1103e-003i
29     329.8925e-003 +267.6605e-003i
30
31 >> z = H22'*H21*v1
32 z =
33    -683.1587e-003 +643.5022e-003i
34    -671.7490e-003 +495.6404e-003i
35
36 >> v2 = [z(2)';-z(1)']
37 v2 =
38    -671.7490e-003 -495.6404e-003i
39     683.1587e-003 +643.5022e-003i

```

```

40
41 >> v1 = v1/norm(v1)
42 v1 =
43   -845.3783e-003  -256.9683e-003i
44   363.6559e-003  +295.0547e-003i
45
46 >> v2 = v2/norm(v2)
47 v2 =
48   -534.8030e-003  -394.5968e-003i
49   543.8867e-003  +512.3147e-003i
50
51 >> u1 = (H11*v1)'
52 u1 =
53   -562.2461e-003  +605.1954e-003i  -569.8775e-003  -153.1541e-003i
54
55 >> u1 = u1/norm(u1)
56 u1 =
57   -553.8366e-003  +596.1435e-003i  -561.3539e-003  -150.8634e-003i
58
59 >> u2 = (H22*v2)'
60 u2 =
61   -458.6543e-003  +373.7155e-003i   130.7044e-003  + 65.9032e-003i
62
63 >> u2 = u2/norm(u2)
64 u2 =
65   -752.5460e-003  +613.1808e-003i   214.4558e-003  +108.1319e-003i
66
67 >> s2 = -5
68 s2 =
69   -5.0000e+000
70
71 >> s1 = 5
72 s1 =
73   5.0000e+000
74
75 >> u1*H12*v2*s2
76 ans =
77   -1.2490e-015  +138.7779e-018i
78
79 >> u2*H21*v1*s1

```

```

80 ans =
81     971.4451e-018 -971.4451e-018i
82
83 >> u1*H11*v1*s1
84 ans =
85     5.0759e+000 -138.7779e-018i
86
87 >> u2*H22*v2*s2
88 ans =
89     -3.0474e+000 +832.6673e-018i
90
91 >> y1_interference = H12*v2*s2
92 y1_interference =
93     309.3903e-003 -731.7427e-003i
94     703.3668e-003 +861.4791e-003i
95
96 >> u1(1)*y1_interference(1)
97 ans =
98     264.8720e-003 +589.7070e-003i
99
100 >> u1(2)*y1_interference(2)
101 ans =
102     -264.8720e-003 -589.7070e-003i
103
104 >> y2_interference = H21*v1*s1
105 y2_interference =
106     -752.4599e-003 -600.9645e-003i
107     -3.4581e+000 + 1.7862e+000i
108
109 >> u2(1)*y2_interference(1)
110 ans =
111     934.7606e-003 - 9.1406e-003i
112
113 >> u2(2)*y2_interference(2)
114 ans =
115     -934.7606e-003 + 9.1406e-003i

```

Figure A.2: Precoding with Coordination: Zero Forcing Example

Appendix B

Further Simulation Results

In this chapter the simulation results presented in Section 7.3 are complemented with the corresponding throughput results for the Macro Mobile Stations (MMSs) in Figures B.1 to B.4. The cost of the coordination, as discussed in Sections 4.1 and 5.1 can also be seen here.

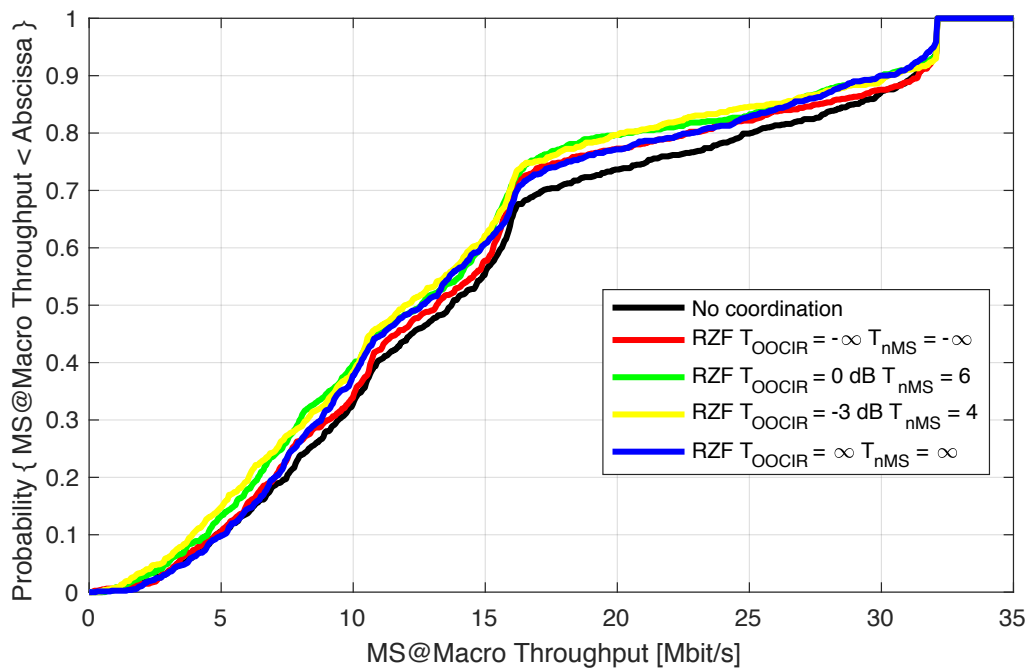


Figure B.1: Throughput of MSs associated to the MBS in a network large network with 42 MSs (network from Figure 2.2)

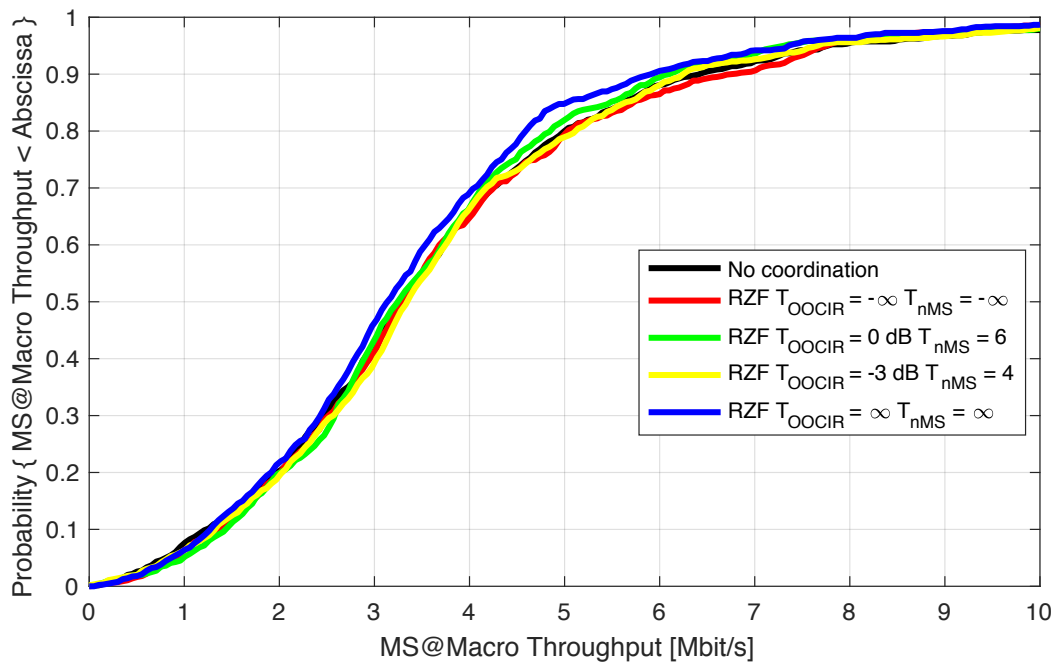


Figure B.2: Throughput of MS associated to the MBS in a network large network with 315 MSs (network from Figure 2.2)

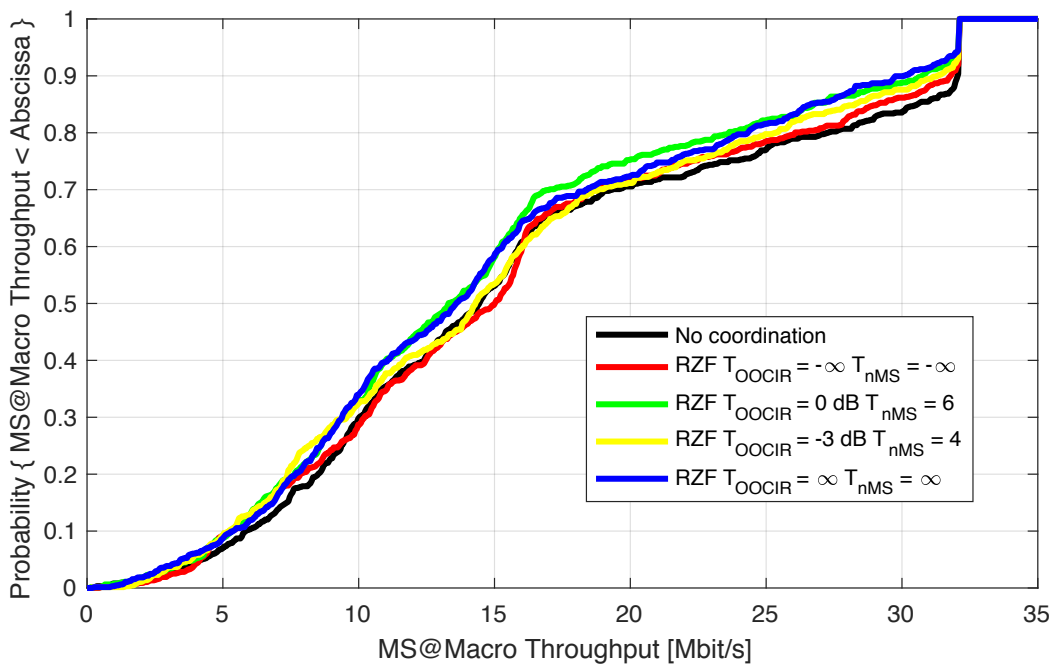


Figure B.3: Throughput of MSs associated to the MBS in a network large network with 42 MSs (network from Figure 7.6)

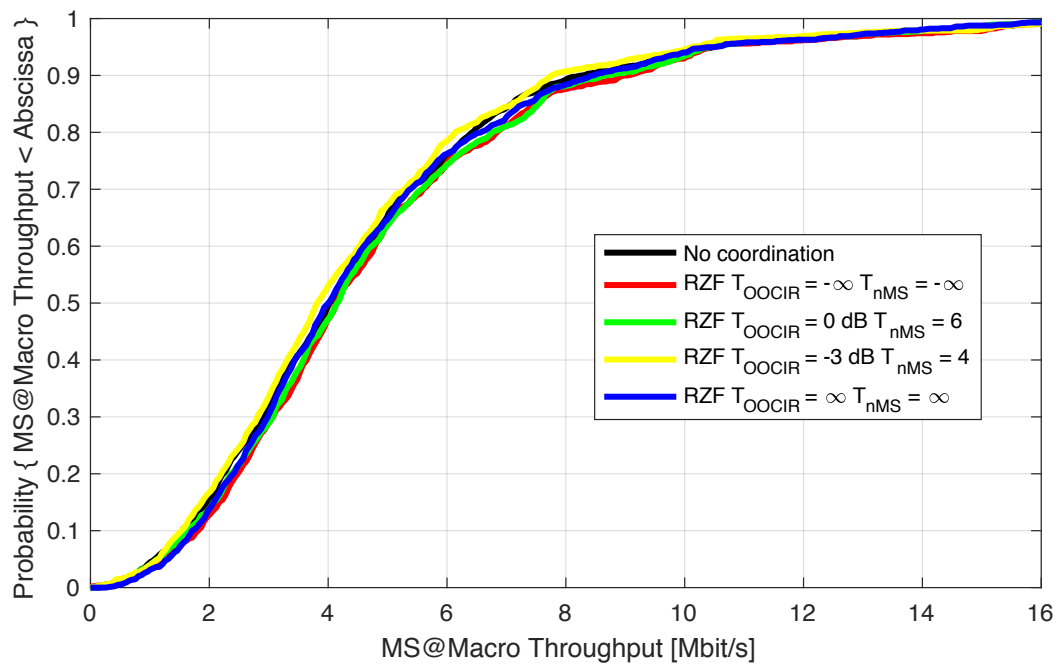


Figure B.4: Throughput of MS associated to the MBS in a network large network with 315 MSs (network from Figure 7.6)